Comparative analysis of transcriptome and sRNAs expression patterns in the *Brachypodium distachyon* - *Magnaporthe oryzae* pathosystem

Dissertation zur Erlangung des Doktorgrades (Dr. rer. nat.) der
Naturwissenschaftlichen
Fachbereiche der Justus-Liebig-Universität Gießen
durchgeführt am Institut für Phytopathologie

vorgelegt von
M. Sc. Silvia Francesca Maria Zanini
Gießen, 2020

1. Gutachter: Prof. Dr. Karl-Heinz Kogel
2. Gutachter: Prof. Dr. Albrecht Bindereif

Selbstständigkeitserklärung

„Ich erkläre: Ich habe die vorgelegte Dissertation selbstständig und ohne unerlaubte fremde Hilfe und nur mit den Hilfen angefertigt, die ich in der Dissertation angegeben habe. Alle Textstellen, die wörtlich oder sinngemäß aus veröffentlichten Schriften entnommen sind, und alle Angaben, die auf mündlichen Auskünften beruhen, sind als solche kenntlich gemacht. Ich stimme einer evtl. Überprüfung meiner Dissertation durch eine Antiplagiat-Software zu. Bei den von mir durchgeführten und in der Dissertation erwähnten Untersuchungen habe ich die Grundsätze guter wissenschaftlicher Praxis, wie sie in der „Satzung der Justus-Liebig- Universität Gießen zur Sicherung guter wissenschaftlicher Praxis“ niedergelegt sind, eingehalten.“

Datum

Unterschrift

Parts of this work are already or will be published.

Talks:

"sRNA-mediated interaction between pathogenic fungus *Magnaporthe oryzae* and cereal model *Brachypodium distachyon"* IS-MPMI XVIII Congress, Glasgow, Scotland (**July 2019**)

"Cross-Kingdom RNAi as a naturally occurring communication strategy in plant - fungi systems" Monogram Conference, Norwich, United Kingdom (**April 2018**)

Publications:

Zanini, S., Šečić, E., Busche, T., Galli, M., Zheng, Y., Kalinowski, J., Kogel, K-H. (**2021**) Comparative Analysis of Transcriptome and sRNAs Expression Patterns in the *Brachypodium distachyon—Magnaporthe oryzae* Pathosystems. International Journal of Molecular Sciences, 22, 650.

Zanini, S., Šečić, E., Buche, T., Kalinowski, J., Kogel, K.H. (**2019**) Discovery of interaction-related sRNAs and their targets in the *Brachypodium distachyon* and *Magnaporthe oryzae* pathosystem. bioRxiv 631945; doi: https://doi.org/10.1101/631945 (preprint)

Šečić, E., **Zanini, S**., Kogel, K.H. (**2019**). Further elucidation of the ARGONAUTE and DICER protein families in the model grass species Brachypodium distachyon. Frontiers in Plant Science, 10, 1332.

Zanini, S., Šečić, E., Jelonek, L. and Kogel, K. H. (**2018**) A Bioinformatics Pipeline for the Analysis and Target Prediction of RNA Effectors in Bidirectional Communication During Plant–Microbe Interactions. *Frontiers in plant science*, **9**.

Abbreviations

AGO = Argonaute

At = *Arabidopsis thaliana*

Bc = *Botrytis cinerea*

Bd = *Brachypodium distachyon*

BG = background

BIC = Biotrophic Interfacial Complex

C = cellular component

ck-sRNA = cross-kingdom small RNA

cDNA = complementary DNA

DCL = dicer-like

DE = differentially expressed

DEG = differentially expressed genes

DGE = differential gene expression

DPI = days post inoculation

dsRNA = double-stranded RNA

endo-sRNA = endogenous small RNA

EV = extracellular vesicle

F = molecular function

FDR = false discovery rate

GO = gene ontology

GOE = gene ontology enrichment

hpRNA = hairpin RNA

h = hours

HIGS = Host-Induced Gene Silencing

KO = Knock-out

miRNA = microRNA

mRNA = messenger RNA

Mo = *Magnaporthe oryzae*

MIAs = monoterpenoid indole alkaloids

MS = Murashige & Skoog Medium

MSA= multiple sequences alignment

nt = nucleotide

NGS = next generation sequencing

Nc = *Neurospora crassa*

OMA = oatmeal agar

P= biological process

PE = paired-end

PR = pathogenesis-related

PTI = pattern-triggered immunity

PTGS = post-transcriptional gene silencing

qRT-PCR = quantitative real-time PCR

RIN = RNA integrity number

RNAi = RNA interference

RdDM = RNA-dependent DNA methylation

RdRPs = RNA-dependent RNA polymerases

RPM = reads per million

SE = single-end

SIGS = Spray-Induced Gene Silencing

sRNA = small RNA

siRNA = small interfering RNA

tasiRNAs = trans-acting siRNA

TGS = transcriptional gene silencing

Vd = *Verticillium dahliae*

WT = wild-type

Table of Contents

1. Introduction

1.1 *Magnaporthe oryzae*

Magnaporthe oryzae (Mo) (anamorph: *Pyricularia grisea*) is a fungal pathogen belonging to the Ascomycota division, with a fully sequenced genome of 41.03 Mb that encodes 12,593 genes. Mo is the causal agent of rice blast, one of the most devastating and widespread diseases of cultivated rice, reducing yields up to 30% annually (Dean et al., 2012; Donofrio et al., 2014; Fisher et al., 2012). Members of the Magnaporthe genus can infect a variety of cereals additional to rice, including barley, rye, and wheat, making it a major threat to global food security (Sesma & Osbourn, 2004; Wilson & Talbot, 2009). Currently, blast management strategies rely on a combination of fungicide applications (e.g. azoles), development of resistant cultivars, and agronomic practices such as removal of crop residues, water management and crop/land rotation (Nalley et al., 2016; Asibi et al., 2019).

1.1.1 Mo life cycle and blast disease

Mo can reproduce both asexually and sexually, with ascospores (sexual spores) being produced and released after the successful mating of compatible (opposite) mating type strains and the formation of perithecia (Fig. 1; Dean et al., 2005). The foliar infection process begins with the adhesion and germination of Mo asexual spores (macroconidia) on the host surface and the development of a specialized penetration structure called appressorium, which bypasses the need for natural openings or wounds on the leaf cuticle to establish the infection. Appressoria are able to rupture leaf cuticle due to the mechanical force generated by the osmotic pressure (estimated at 8.0 MPa) accumulated within the fungal infection structure and exerted via the penetration peg (Howard et al., 1991). In the early stages of infection Mo behaves as a biotroph, forming a Biotrophic Interfacial Complex (BIC) between the primary invasive hyphae (derived from the penetration peg) and the infected host cell, where it secretes small molecules (effectors) to modulate the interaction (Osés-Ruiz & Talbot, 2017; Talbot, 1995). Afterwards, the fungus creates secondary hyphae and spreads to neighboring cells, undertaking a lifestyle

change and switching to a necrotrophic growth, with the appearance of the characteristic blast lesions on host leaves (Wilson and Talbot, 2009).

Additional to leaves, Mo is able to infect all aerial parts of rice including nodes, panicles and necks, and has been shown to colonize and produce necrotic lesions on both rice and barley roots (Sesma & Osbourn, 2004). Furthermore, *Mo* infections also have been established in the grass *B. distachyon* (Routledge et al., 2004; Parker et al., 2008).

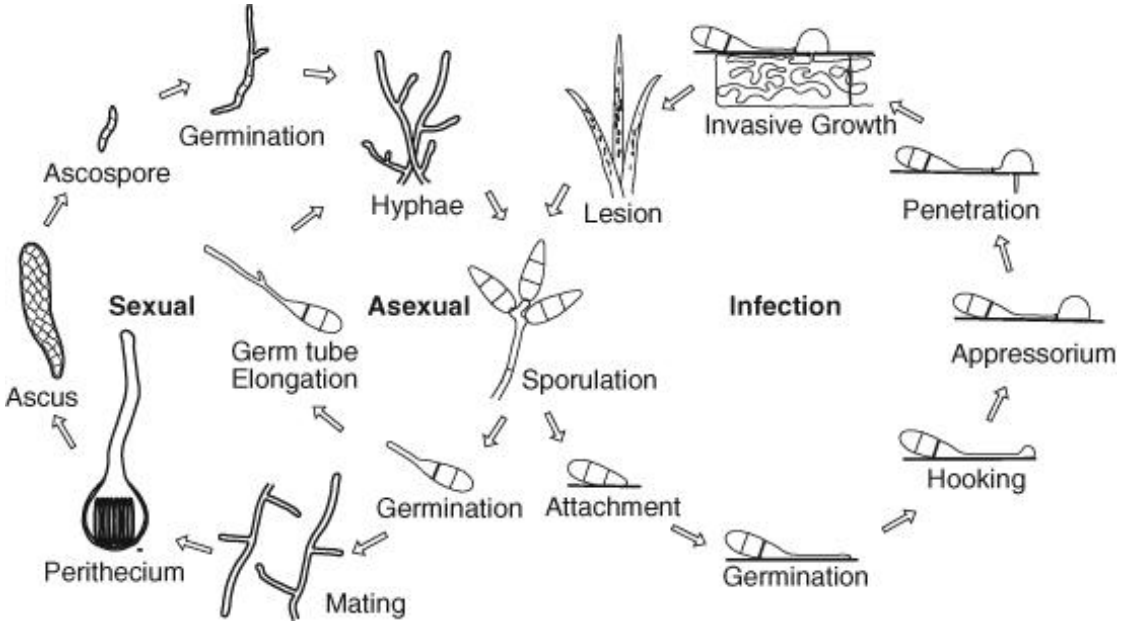

Figure 1. Life cycle of *Magnaporthe oryzae* (from Dean et al., 2005)

1.2 *Brachypodium distachyon*

Since early 2000s *Brachypodium distachyon* (Bd) has been proposed as a model for grasses, as it is preferable for research over more complex crops such as wheat (*Triticum aestivum*, with an estimated total genome size of 17 Gb) and barley (*Hordeum vulgare*, with haploid genome size of 5.3 Gb). Bd has a smaller genome (272 Mb in Bd21-3 v1.0 assembly) with low genome complexity, a short life cycle, simple growth requirements and a vast T-DNA insertion library available (Fitzgerald et al., 2015; Vogel et al., 2006; Brutnell et al., 2015).

Additional to its relevance for bioenergy research, Bd serves as a model for food crop studies due to the large number of pathogen of rice, wheat and barley that are able to infect Bd, including Fusarium spp. (Peraldi et al., 2011), *Puccinia striiformis* (Draper et al., 2001) and, as mentioned above, *Magnaporthe oryzae* (Routledge et al., 2004).

1.3 RNAi interference

Small (s)RNAs such as small interfering (si)RNAs, and micro (mi)RNAs are systemic signals that modulate distal gene regulation and epigenetic events in response to biotic and abiotic environmental cues in plants (Molnar et al., 2010; Borges & Martienssen, 2015; Kehr & Kragler, 2018). Particularly, sRNA-mediated gene silencing is one of the main defense mechanisms against viral attack and damaging effects of transposons. The action of sRNAs rests upon their role in RNA interference (RNAi), a conserved mechanism of gene regulation in eukaryotes at the transcriptional (TGS or transcriptional gene silencing) and post-transcriptional (PTGS or post-transcriptional gene silencing) levels (Fire et al., 1998; Vaucheret & Fagard, 2001; Castel & Martienssen, 2013). In plants, the trigger for RNAi is either endogenous or exogenous (e.g. viral) double-stranded (ds)RNA or hairpin (hp)RNA that is processed into short 20 to 24 nucleotide (nt) double-stranded sRNAs by DICER-like (DCL) enzymes (Fig. 2) (Hamilton & Baulcombe 1999; Baulcombe 2004). These sRNAs are incorporated into an RNA-induced silencing complex (RISC), containing an RNAse III-type endonucleolytic ARGONAUTE (AGO) protein to target complementary RNAs for degradation/inhibition or epigenetic modification by RNA-dependent DNA methylation (RdDM), histone modification and chromatin remodeling. Additionally, secondary sRNAs are generated in plants by RNA-dependent RNA polymerases (RdRPs) (Castel & Martienssen, 2013; Vaucheret et al., 2004).

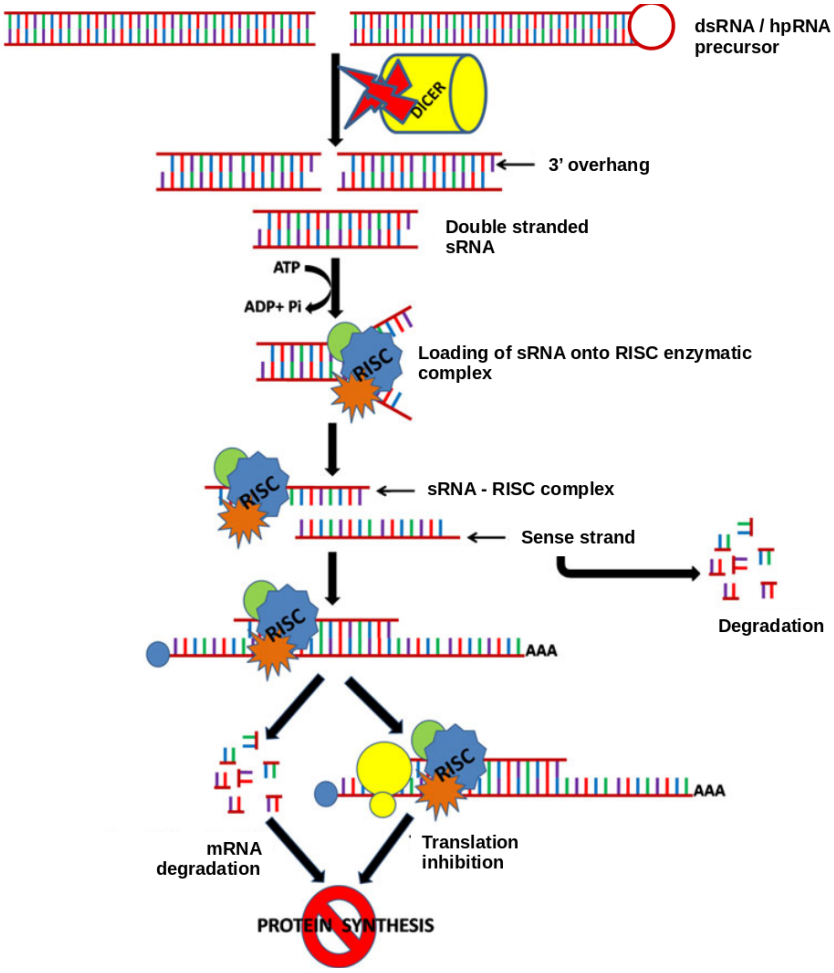

Figure 2. RNAi mechanism: post transcriptional gene silencing (modified from Jagtap et al., 2011)

1.3.1 RNAi in rice blast

The genome of Mo encodes a complete RNAi machinery, comprised of two *DCL* genes, three *AGO* genes, and three *RdRP* genes (Kadotani et al., 2003; Murphy et al., 2008; Raman et al., 2017). Knock-out (KO) of RNAi pathway components were shown to severely affected the sRNA species produced by Mo and their accumulation in axenic culture, with deletion of *MoDCL2*, *MoRdRP2*, and *MoAGO3* genes reducing sRNA expression levels (Raman et al., 2017), suggesting that MoDCL2, MoRdRP2 and MoAGO3 are required for the biogenesis and function of sRNAs. In particular, MoDCL2, but not MoDCL1, was found to be necessary for siRNA production from dsRNA precursor molecules. Of note, loss of MoAGO3 and MoRdRP1 function reduced

both sRNAs and fungal virulence on barley leaves. Transcriptome analysis of RNAi Mo KO mutants also confirmed that these genes play an important role in the regulation of Mo pathogenicity. *Moago3* and *Mordrp1* had the highest amount of differentially expressed genes (DEG) compared to the other KO mutants analyzed and similar expression patterns among each other, with 3 genes known to be involved in Mo pathogenicity downregulated in both datasets (MGG_01662, MGG_02329 and MGG_02378) (Raman et al., 2017).

sRNA-mediated alterations of TGS and PTGS have been detected *in vitro* both during starvation/different nutrient availability, and *in planta* during the different stages of rice leaf infection (Raman et al., 2013). Additionally, Mo sRNAs were found to differentially accumulate in mycelia and appressoria (Nunes et al., 2011), further supporting the notion that Mo sRNAs regulate fungal developmental processes, growth and virulence.

1.3.2 RNAi in Brachypodium

Similarly to Mo, endogenous sRNAs expression is subject to change also in *B. distachyon*, where miRNAs have been proven to vary during exposure to abiotic stresses and between vegetative and reproductive tissues (Wei et al., 2009), pointing to operable RNAi-based regulatory mechanisms in the model grass (Wang et al., 2015). Up to date, 328 Bd miRNA precursor sequences have been identified and deposited in the miRBase database, corresponding to 536 mature Bd miRNAs with predicted regulatory functions in cold stress response (Zhang et al., 2009), heat stress (Franke et al., 2018), drought stress (Bertolini et al., 2013) and morphological alterations (Jeong et al., 2013).

While the knowledge about the Bd RNAi machinery is not comprehensive and there are currently no RNAi KO studies in this organism, our recent work confirmed and characterized *in silico* the major components of *Bd*'s RNAi machinery, resulting in 16 BdAGO-like and six BdDCL candidates and suggesting that the RNAi machinery follows the trend that cereals have extended families of key enzymes involved in RNAi (Šečić et al., 2019). In particular, phylogenetic analysis of BdAGOs identified five proteins grouping with AtAGO1, the Argonaute protein proven to be involved in Arabidopsis sRNA-mediated cross-kingdom communication with *Botrytis cinerea* (Weiberg et al., 2013).

1.3.3 ck-RNAi

Consistent with the exchange of RNAs during animal-parasitic interactions (Buck et al., 2014; LaMonte et al., 2012; Garcia-Silva et al., 2014), recent reports suggest that sRNAs are also transported in host plant – pathogen interactions (Weiberg et al., 2013; Zhang et al., 2016; Wang et al., 2017a, 2017b). First hints for a transfer of RNA between species of different kingdoms and the action of sRNA effectors in plants, termed cross-kingdom (ck)-RNAi, came from studies that showed delivery of artificially designed sRNA from plants into interacting microbes. Such plant-mediated RNAi, termed host-induced gene silencing (HIGS, Nowara et al., 2010), includes i. formation of dsRNA from hairpin or inverted promoter constructs, ii. dsRNA processing into sRNA and iii. its transfer into the interacting microbe. Since then, HIGS has emerged as a promising strategy for crop protection against viruses, fungi, oomycetes, nematodes, and insects (Koch and Kogel 2014; Cai et al., 2018a; Gaffar and Koch 2019). The broad applicability of the HIGS technique suggests the presence of an evolutionarily-conserved mechanism of cross-kingdom trafficking of sRNAs in plant systems. Consistent with this view, the plant-pathogenic fungus *Verticillium dahliae* (*Vd*) contained plant miRNAs when recovered from infected cotton samples, indicating that host-derived sRNAs were transmitted into the pathogen during infection (Zhang et al., 2016). Two of those cotton miRNAs, miR166 and miR159, target the fungal genes *Ca2+-DEPENDENT CYSTEINE PROTEASE CALPAIN* (*VdClp-1*) and *ISOTRICHODERMIN C-15 HYDROXYLASE* (*VdHiC-15*), respectively, which are known to contribute to fungal virulence.

Similarly, *Arabidopsis* cells secrete vesicles to deliver sRNAs into grey mold fungal pathogen *Botrytis cinerea* (*Bc*) (Cai et al., 2018b). These sRNA-containing vesicles accumulate at the infection sites and are taken up by the fungal cells, where they cause silencing of fungal genes critical for pathogenicity. Consistent with the bidirectional move of sRNAs in plant-microbe interactions, *Bc* also produces sRNA effectors that down-regulate *Arabidopsis* and tomato genes involved in immunity (Weiberg et al., 2013). Some of these sRNAs, for example *Bc*-siR37, downregulate a large set of host immunity genes to enhance *Bc* pathogenicity (Wang et al., 2017b).

A recently discussed sRNA transfer mechanism in plant host - microbe interactions involves extracellular vesicles (EVs), derived from multivesicular bodies (MVBs; An et al., 2006a, 2006b). These lipid compartments traffic proteins, lipids and metabolites

between cells. Their content is enriched in stress response proteins and lipids and displays antifungal activity (Rutter and Innes 2017). Consistent with the finding for animal EVs (Buck et al., 2014), plant EVs also contain sRNAs such as miRNAs, tasiRNAs and heterochromatic sRNAs derived from intergenic regions (Cai et al., 2018b; Baldrich et al., 2019).

1.4 Workflow to find and characterize sRNA mediated plant-microbe interactions

1.4.1 Sequencing setup

Identification and confirmation of interaction-related sRNAs starts with the preparation of suitable biological samples. When planning which and how many samples to sequence, control samples of uninfected plants and, when possible, axenic cultures of the microbe should be included in order to verify the infection-related upregulation/induction of the candidate sRNAs in both organisms. Sequencing depth, number of replicates and type of libraries are all experiment-specific and highly variable depending on the aim of the study and the resources available. For example, for adequate statistical power in the data analysis, a minimum of three biological replicates is required (Love et al., 2014) and, while for mRNA it is usually recommended to explore the option of longer read length or paired-end (PE) sequencing, single-end (SE) short reads are perfectly suitable for sRNAseq. Regardless of the specific datasets, some measures have to be taken to ensure the removal of unwanted fragments that would overweight the sequences of interest. In particular, size selection prior to sRNA sequencing is required to avoid sequencing longer fragments that would not be the focus of the study. Subsequent analysis of the derived datasets is the critical point towards discovery of candidate sRNAs. Acquisition of the raw reads is the first step of the bioinformatics analysis and is immediately followed by quality check. FastQC (Andrews, 2010) is the most frequently used program for this task, as it is recommended by Illumina for the analysis of Illumina NGS data and it is compatible also with PacBio and 454 datasets. Alternatively, programs such as NGS-QC can be used for the analysis of data obtained from several sequencing platforms (Dai et al., 2010). With these, the overall quality of the sequencing can be assessed, in particular the sequence quality, GC content, N content, and

overrepresented sequences. While there are no universal cutoffs for some of these tests, as the values vary based on the organisms and the sequencing setups, similar results should be obtained throughout the same kind of datasets both for “failed” k-mer and duplication tests.

When analyzing sRNA datasets, a test that will most likely fail is the adapter content test: given that the fragments sequenced (usually 18-35 nt) are often shorter than the read length (36 bp), the machine is bound to read into the adapter. There are a number of software programs designed to do the necessary trimming, such as Cutadapt or FASTX-Toolkit (Martin, 2011). At this point of the analysis, low quality reads/bases should be removed, as well as adapters and PCR artifacts.

1.4.2 Reads mapping and target prediction

Trimmed reads can now be mapped with short read un-gapped mappers such as Bowtie (Langmead, 2010) and SOAP (Li et al., 2008) to reference genomes and transcriptomes; by this way one gains information on the origin of the potential ck-sRNA and its localization in the respective genome. The workflow, summarized in Figure 3, can be used to identify either the sRNAs originating from the plant or the ones originating from the microorganism by deciding at the beginning which is the organism of origin and which is the target, and then repeating the analysis with the roles inverted to have information on the bidirectional ck-sRNAs. Given that it is crucial to find the sRNAs from the “source” organism that target the interacting organism, this alignment step includes the removal of reads that align to both organisms. In particular, sRNAs are kept only if *i.* they align 100% to the source organism’s genome, and *ii.* have at least 2 mismatches to the target organism’s genome or transcriptome. As an additional step, the removal of sequences aligning 100% to the source organism’s transcriptome can be done in order to select exclusively sRNAs originating from non-coding regions, removing short sequences derived from mRNA degradation. After the alignments, sRNAs can be additionally filtered based on their presence in the sample of the pure source organism as they are expected to be either upregulated in the sample from the interacting organisms compared to the control (pure organism), or present exclusively in that sample (Weiberg et al., 2013).

The remaining sequences can be further analyzed for target prediction. There are various software platforms available for small interfering RNA (siRNA) and micro RNA (miRNA) detection, originally tailored for mammal sRNAs. While these can be customized for plant and microbe studies, two well established tools are designed specifically for plants: psRNATarget and TAPIR (Dai et al., 2011; Bonnet et al., 2010). Both are comparable regarding sRNA identification rates at their default settings and are widely used in plant miRNA analysis and discovery research, making them the best options for this analysis. While TAPIR offers a standalone and an online version, psRNATarget is only available online, making it less convenient for automatized workflows. On the other hand, psRNATarget provides more options for customizing settings and parameters of the prediction, making it more adaptable to different organisms and systems. Both programs work by aligning sRNA sequences to the target transcriptome and assigning penalties for mismatches, gaps and G:U pairs, in particular in the seed region (between positions 2 and 12 of the sRNA for TAPIR and 2-13 for psRNATarget), which is critical for target recognition. The resulting score is between 0 and 5, and can be decreased from the default value to further reduce the risk of false positives. Additionally, TAPIR separately scores the free energy ratio, represented by the free energy of the predicted sRNA:target duplex divided by the free energy of the corresponding duplex having a perfect complementarity (Bonnet et al., 2010). In this case, the minimal value cutoff suggested is 0.7 (range between 0 and 1).

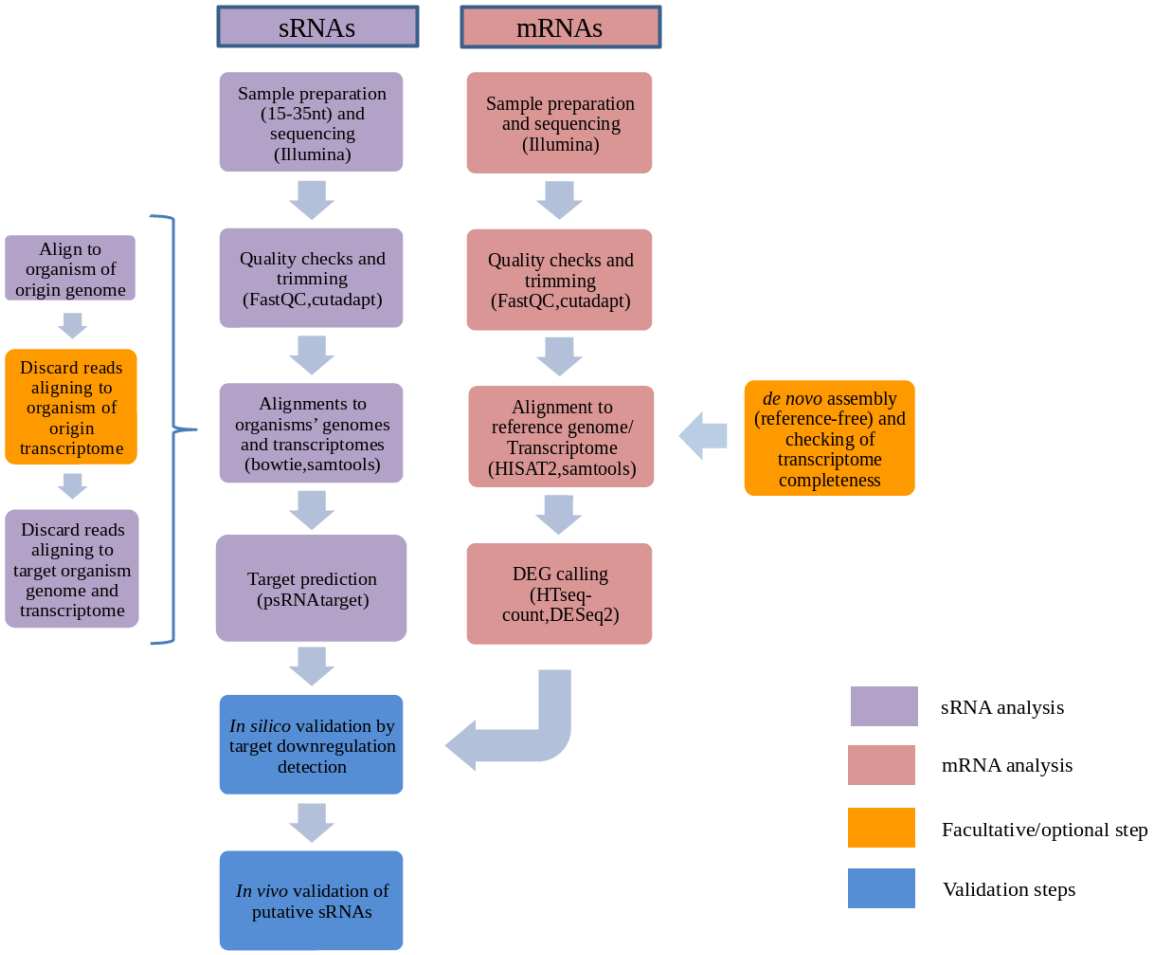

Figure 3. Sequencing/analysis workflow (Published in Zanini et al., 2018)

1.4.3 Candidate ck-sRNA validation

The first validation step of candidate ck-sRNAs is the confirmation of corresponding target gene downregulation in the sample from colonized tissue. Plant and microbial mRNA levels can be checked by mRNA sequencing analysis from the same biological samples the sRNA was obtained from. Since the library preparation for sRNA libraries is based on size separation and excision of a specific nucleotide length interval, the longer RNA fraction from the same samples can be used to prepare mRNA libraries. Read length and sequencing depth selected can vary depending on the experimental design and resources available, but the mRNA sequences are primarily obtained from the large RNA fraction after polyA affinity selection, as more than 90% of total RNA is comprised of

ribosomal RNA (Conesa et al., 2016). In bacterial samples or in samples with low RNA integrity number (RIN) values, where polyA selection would not be effective, rRNA depletion can be done instead. Since there is a multitude of RNAseq tools available, the experimental design and the availability of published reference data are the main factors in deciding on a pipeline (Conesa et al., 2016). Quality check and trimming of sequencing artifacts are necessary steps at the beginning of the analysis, following the similar principle as in sRNA analysis, namely the use of FastQC (Andrews, 2010) and cutadapt (Martin, 2011). If reference sequences for the organisms involved are available, the mapping of RNAseq reads can be done as a straight forward strategy (see below). Depending on available -omics data for the organisms in question, mapping of reads can be done to the reference genome or transcriptome. Without available reference sequences, *de novo* assembly (reference-free) of the transcriptome can be computed from all RNAseq datasets, usually with a De Bruijn graph-based assembler like Trinity (Grabherr et al., 2011), SOAPdenovoTrans (Xie et al., 2014), Oases (Schulz et al., 2012), or Trans-AbySS (Robertson et al., 2010). Functional annotation and orthologue search can then be performed with common platforms such as BLAST (Altschul et al., 1990) and ENSEMBL (Zerbino et al., 2018) or transcriptome annotation tools like Trinotate (github, http://trinotate.github.io/) and FunctionAnnotator (Chen et al., 2017). Transcriptome completeness can be checked with Busco (Simão et al., 2015). These tools can also be used in case of unsatisfactory annotation of available reference genome or transcriptome.

Spliced alignment to the reference genome is done by mappers that take into account the introns in the genome. TopHat/TopHat2 (Trapnell et al., 2009; Kim et al., 2013) are gapped mappers developed to detect novel splice-sites. They were superseded by a new mapper called HISAT2 (Kim et al., 2015) that is more accurate and much more efficient. Another option is Spliced Transcripts Alignment to a Reference (STAR), which also allows for fast and precise mapping with known and novel splice-sites (Dobin et al., 2013). Correction for exon sizes specific to the respective plant and microbe organism in question are needed, since typically the programs use default settings for the human genome. Un-gapped mappers, such as Bowtie (Langmead, 2010), can be used to map against a reference transcriptome if no novel transcript discovery is needed. However, since the goal of the analysis is to discover a high number of transcripts, including those with a low level of expression, and since organisms in question often are not sufficiently

annotated, the gapped mapping on a genome followed by quality control is the recommended strategy. The quality of the mapping can be checked by programs such as Picard (Picard tools, github), RseQC (Wang et al., 2012) and Qualimap (Garcia-Alcalde et al., 2012). Percentage of mapped reads, multi-mapping reads (mapping to the several identical regions) and the uniformity of read coverage are relevant parameters to assess sequencing quality at this point (Conesa et al., 2016).

The first step for differential gene expression (DGE) is determining transcript abundances using program packages like Cufflinks (Trapnell et al., 2010) or htseq-count (Anders et al., 2015). DGE analysis can be done by a variety of programs, including DeSeq (Anders and Huber, 2010), Deseq2 (Love et al., 2014), edgeR (Robinson et al., 2010) and voom (Law et al., 2014). Low replicate numbers of transcripts and outliers among the replicates can complicate the DGE analysis. Thus, a powerful analytical method proves crucial to determine when the fold change in transcripts between the control and treated sample is different. The programs differ in statistical distributions they use for analysis of data and how they treat the variability among the replications, but a comparison study claims DeSeq2 and edgeR have an advantage when it comes to smaller number of replicates (below 12) (Schurch et al., 2016).

The results of this target prediction and analysis pipeline can be visualized at several levels and by a variety of programs, some of which focus on sRNA-mRNA duplex conformation structure and others on a broader representation of cross-kingdom effects between genomes. ReadXplorer (Hilker et al., 2014) and Integrative Genomics Viewer (IGV) (Thorvaldsdóttir et al., 2013) are used for different types of presentation of sequencing data, and in this case specifically for visualization of mapped reads on the reference genome. miRPlant (An et al., 2014), a tool for prediction of miRNAs from NGS data, provides the visual presentation of the predicted miRNA in the precursor hairpin structure and with the indication of where the mature fragment is. CummerBund (Goff et al., 2013) is commonly used after the Cufflinks package for visualization of differentially expressed genes in different types of plots. The software package Circos (Krzywinski et al., 2009) is a good choice for circular visualization of entire genomes, transcriptomes, sRNA candidates and the range of silencing downregulation effects.

1.5 Aim of the thesis

Because only a few studies have been published since the landmark paper of Weiberg et al., (2013), the abundance and role of sRNA effectors in host-microbe interactions is unclear and their involvement is even challenged for certain pathosystems (Kettles et al., 2018). Therefore, after establishing and characterizing the interaction of *Magnaporthe oryzae* (Mo) with *Brachypodium distachyon* (Bd) I sought preliminary hints for cross-kingdom RNAi in this cereal pathosystem.

I explored the role of Mo and Bd sRNAs in the Mo-Bd interaction based on data generated by parallel sRNA and mRNA deep sequencing of infected leaf and root material and compared it to data derived from control samples (uninfected plant samples and fungal axenic culture). Following the previously published bioinformatics pipeline reported in Chapter 1.4 (Zanini et al., 2018) for characterization of sRNA effectors and their targets, I report and discuss first indication of bidirectional ck-RNAi in a grass pathosystems.

Overall, this work includes the *in silico* characterization of MoDCL and MoAGO proteins to complement our work on Brachypodium RNAi machinery (Šečić et al., 2019), transcriptomic analysis of both interacting organisms and the detection and characterization of putative infection related sRNAs, both for endogenous and cross-kingdom functions.

2. Material and Methods

2.1 AGOs and DCLs protein analysis and 3D structure modeling

Known Argonaute and Dicer-like protein sequences were downloaded from the NCBI database and analyzed following the workflow utilized for *B. distachyon* AGOs and DCLs (Šečić et al., 2019). The phylogenetic analysis and tree rendering were done by the Phylogeny.fr web server (Dereeper et al., 2008; Dereeper et al., 2010). Multiple sequence alignment of AGO PIWI domains (MSA) was done using Clustal Omega (Sievers et al., 2011; Goujon et al., 2010) and visualized with the Mview multiple alignment viewer (Brown et al., 1998). Protein domains were identified by using Simple Modular Architecture Research Tool (SMART) including PFAM domains in the search (Schultz et al., 1998; Letunic and Bork, 2017) and visualized with the Illustrator for Biological Sequences (IBS) online illustrator (Liu et al., 2015). Prediction of protein location was done using the plant subcellular localization integrative predictor (PSI; Liu et al., 2013), and prediction of the interactome was done using the STRING database (Szklarczyk et al., 2019), excluding text mining as indication of putative interaction. Finally, AGOs and DCLs aa sequences were utilized for predicting the proteins' 3D structure utilizing SWISS-MODEL (Waterhouse et al., 2018). Predictions were selected for further validations based on the GMQE and QMEAN Z-score values (Benkert et al., 2011). PROCHECK (Morris et al., 1992; Laskowski et al., 1993) and WHATCHECK (Hooft et al., 1996) were used to check the stereochemical quality of the selected structures and calculate the Ramachandran Z-score (Ramachandran et al., 1963). Open-Source PyMOL (The Py-MOL Molecular Graphics System Version 2.4.0a0) was used for visualization of the predicted structures (Schrödinger, 2010).

2.2 Sample preparation from *Mo-Bd* interactions

Magnaporthe oryzae (*Mo* 70-15; Raman et al., 2013) was grown on oatmeal agar (OMA) for two weeks at 26°C with 16 h light/8 h dark cycles both for sampling of mycelium and conidia production. Samples from axenic cultures were collected by scraping a mixture of mycelia and spores from three plates, followed by immediate freezing in liquid nitrogen. For root inoculation, sterilized seeds (3% NaClO for 15 min, followed by three

times 5 min washes in sterile water) of *Brachypodium distachyon* genotype *Bd21-3* (Vogel & Hill, 2008) were vernalized in the dark at 4°C for two days on half strength MS (Murashige & Skoog, 1962) medium and then moved to a 16 h light/8 h dark cycle at 22°C/18°C. Roots of one-week-old seedlings were dip-inoculated in 1 ml of conidia solution (250,000 conidia/ml in 0.002% Tween water) for 3 h, transplanted in a (2:1) mixture of vermiculite (Deutsche Vermiculite GmbH) and Oil-Dri (Damolin, Mettmann, Germany) and grown for additional 4 days before harvesting. Control roots were mock-inoculated with 1 ml of Tween water solution. For leaf inoculation, third leaves of three-week-old *Bd21-3* were detached and drop-inoculated with 10 µl of conidia solution (50,000 conidia/ml in 0.002% Tween water) on 1% agar plates. Control leaves were mock-inoculated with Tween water. Leaves were collected for sequencing at 2 DPI (days post inoculation) and 4 DPI.

2.3 RNA extraction, library preparation and sequencing

Three roots or two leaves, respectively, were pooled per sample for RNA extraction and for each condition three pooled biological samples were prepared. Frozen tissue stored at -80°C was ground in liquid nitrogen using mortar and pestle. Total RNA was isolated with ZymoBIOMICS TM RNA Mini Kit (Zymo Research, USA) according to the manufacturer's instructions. Quantity and integrity of the RNA were assessed with DropSense16/Xpose (BIOKÉ, Netherlands) and Bioanalyzer 2100 (Agilent, Germany), respectively. Purification of small and large RNAs into separate fractions was carried out using RNA Clean & Concentrator TM -5 (Zymo Research) and concentration and quality of the fractions were checked again. Fifty ng of small RNA (17 to 200 nt) were used for cDNA library preparation with TruSeq® Small RNA Library Prep (Illumina, USA) and 1.5 µg of large RNA were used for cDNA library preparation with TruSeq® Stranded mRNA (Illumina). Constructed cDNA libraries of sRNAs were further size selected with BluePippin (Sage Science, USA) for fragments between 140 and 160 nt in length (15-35 nt without adapters). Quality of polyA mRNA libraries was assessed using the Fragment AnalyzerTM Automated CE System (Advanced Analytical Technologies, Austria). The Illumina HiSeq1500 sequencing platform was used to sequence the Illumina TruSeq® Small RNA libraries single end with 35 nt read length and the Illumina TruSeq® Stranded mRNA libraries (paired-end [PE] sequencing, 70 nt) of all samples.

2.4 mRNA analysis

Paired end sequenced cDNA reads of Illumina TruSeq® Stranded mRNA libraries were analyzed through the quality check in FastQC and alignment in the junction mapper HISAT2 (Kim et al., 2015). *Magnaporthe oryzae* MG8 release 38 (Yates et al., 2020) and *Brachypodium distachyon* Bd21-3 v1.1 (DOE-JGI, http://phytozome.jgi.doe.gov/) assemblies were utilized throughout this study. Htseq-count (Anders et al., 2014) and DESeq2 (Love et al., 2014) were then used for differential gene expression calling (DGE) between the infected and control sample genes. Heatmaps for selected DEG were obtained with the pheatmap package for R (Kolde & Kolde, 2015). Gene Ontology Enrichment (GOE) analysis on DEG was done with AgriGO v2 (Du et al., 2010).

2.5 sRNA analysis

The single end sequenced cDNA reads of Illumina TruSeq® Small RNA libraries were analyzed starting with quality check with FastQC (Andrews, 2010) and trimming of adapter artifacts with cutadapt (Martin, 2011). The alignment of the reads to reference genomes and transcriptomes of Bd and Mo was done using the short read aligner Bowtie (Langmead et al., 2009). Reads with a 100% alignment to the genome of the organism of origin were selected, alongside the reads with at least two mismatches in the alignment to the target organism genome. Venn diagrams for sRNA and target overlaps were obtained with the VennDiagram package for R (Chen and Boutros, 2011).

2.6 Identification of endo-sRNA

To identify interaction-related Bd sRNAs with endogenous function, both infected and control datasets were analyzed with ShortStack (Johnson et al., 2016) to identify potential miRNA generating loci. Genomic coordinates and corresponding RPM (reads per million) of the identified clusters were compared between infected and control datasets to select clusters exclusively present or increased during infection. Both potential precursors and mature miRNAs deriving from these clusters were compared to known miRNA sequences, obtained from miRBase (Griffiths-Jones et al., 2006). Confirmed known miRNAs were further analyzed and the target prediction software

psRNATarget was used with default settings to identify their potential target transcripts (Dai & Zhao, 2011). The structure of miRNA generating clusters was visualized with strucVis (version 0.4, Michael J. Axtell).

2.7 Identification of ck-sRNA effectors

Bioinformatics analysis of ck-sRNAs effectors was done as described in the introduction chapter 1.4 (Zanini et al., 2018). Only sRNA reads of 20-22 nt length originating from non-coding regions and with a higher count in the organism of origin control datasets compared to the infected ones were analyzed further for ck-sRNA effector identification by the target prediction software psRNATarget used with customized settings (Dai & Zhao, 2011).

2.8 sRNA target confirmation

Expression levels obtained for each gene were used as confirmation of downregulation of predicted targets from the psRNATarget software. GOE analysis on the confirmed targets was carried out with AgriGO v2 (Du et al., 2010). PHI-base, a collection of experimentally verified pathogenicity/virulence genes from fungal and microbial pathogens (Baldwin et al., 2006), was used to gather information regarding phenotype and virulence of fungal mutants carrying a mutation in the identified Mo gene targets.

3. Results

3.1 Protein prediction

Magnaporthe oryzae genome encodes three putative AGO and two DCL proteins, previously identified by domain search and phylogeny with known *Neurospora crassa* (Nc) RNAi machinery genes (Murphy et al., 2008; Kadotani et al., 2004; Raman et al., 2017). The corresponding protein sequences were obtained from NCBI; XP_003714515.1 (MGG_01541T0, MoDCL1), XP_003715365.1 (MGG_12357T0, MoDCL2), XP_003716704.1 (MGG_14873T0, MoAGO1), XP_003717504.1 (MGG_13617T0, MoAGO2) and XP_003714217.1 (MGG_01294T0, MoAGO3) and were included in a new phylogenetic tree to confirm these findings (Fig. 4A-B). Functional domains prediction was carried out with Simple Modular Architecture Research Tool (SMART) in order to assess the conservation of key AGO and DCL domains. As shown in Figure 5A, all 3 AGOs have conserved domain structures, with five characteristic domains: the N terminal domain, DUF1785, PAZ, L2 and PIWI (Tab. 1). Additionally, a closer look at the MoAGO PIWI domains by MSA confirmed the conservation of the DEDD catalytic tetrade and the QF-V motif (Fig. 6). Similarly, four conserved domains required for the successful cleavage of dsRNAs were found in both MoDCLs: DEXDc, HELICc, Dicer-dimer and RIBOc (Fig. 5B, Tab. 1).

PSI-predictor was utilized to assess MoAGOs and MoDCLs subcellular localizations: MoDCL1, MoAGO1 and MoAGO3 were predicted to primarily localize in the nucleus, while MoDCL2 and MoAGO2 in the cytosol. MoAGO1 and MoAGO2 also had secondary predicted localizations, the first in the cytosol and the second in plastids (Tab 2).

Protein interaction analysis with STRING did not highlight any known physical interactions for MoAGO and MoDCL proteins, but putative homologs were found to either interact or co-express with several proteins in other species (Tab 3A-B). In particular, all MoAGOs were predicted to interact with the two MoDCL proteins, a U5 small nuclear ribonucleoprotein component (MGG_13500) and a cell cycle control protein cwf14 (MGG_06309). Interactions with a Pumilio-family RNA binding repeat protein (MGG_03158), ATP-dependent RNA helicase DED1 (MGG_02762), high-

affinity glucose transporter (MGG_13651) and four uncharacterized proteins were predicted exclusively for AGO1.

In addition to the interaction with the AGO proteins, both DCL1 and 2 were predicted to interact with ATP-dependent DNA helicase MPH1 (MGG_04429), 30S ribosomal protein S16 (MGG_02598), a WD domain-containing protein (MGG_06727), and three uncharacterized proteins.

Next, 3D protein structure modeling was attempted for both DCL and AGO aa sequences with SWISS-MODEL. While no acceptable QMEAN Z-scores (>-4) values were obtained for either DCLs and AGO2 models, two models for AGO1 (model 1 based on hAGO1, GMQE= 0.52 QMEAN= -3.98 and model 3, based on hAGO2, GMQE= 0.51 QMEAN = -3.31) and model 6 for AGO3 (based on hAGO4 template, GMQE =0.46 QMEAN =-3.50) passed the first quality check and were further validated with PROCHECK and WHATCHECK. Model 1 of AGO1 had a higher percentage of residues in the core region of the Ramachandran plot (88.4%) and a better Ramachandran Z-score (-1.808) compared to model 3 (87.6% and -1.531 Z-score), while the AGO3 model scored 86.7% and -2.088, respectively. As a result, model 1 of AGO1 and model 6 of AGO3 were selected as the best models and visualized with PyMOL (Fig. 7A-B).

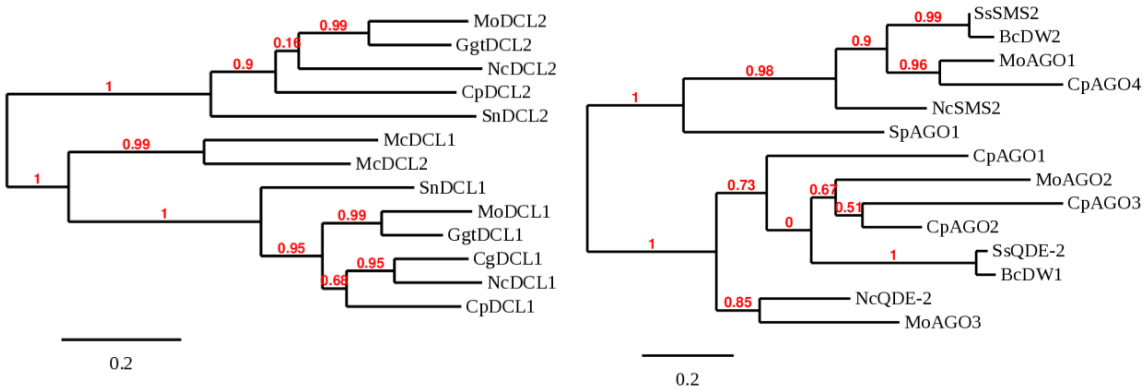

Figure 4. Phylogram of (A) MoDCL and (B) MoAGO protein sequences. Branch support values are displayed, the scale bar defines the branch length.

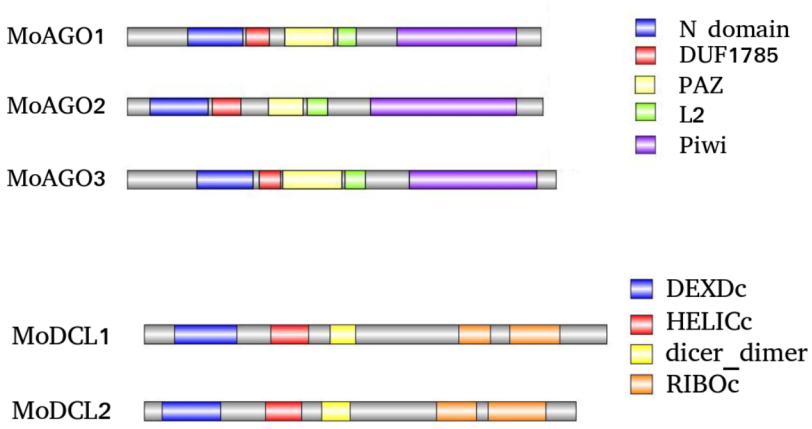

Figure 5. Visual representation of domain structure of (A) MoAGO and (B) MoDCL proteins. Domains were identified by SMART and PFAM search and represented with IBS illustrator. Displayed domains of AGOs: N-domain, DUF1785, PAZ, L2, PIWI. Sequence with no domain predicted is colored in grey. Displayed domains of DCLs: DEXDc, HELICc, dicer_dimer and RIBOc.

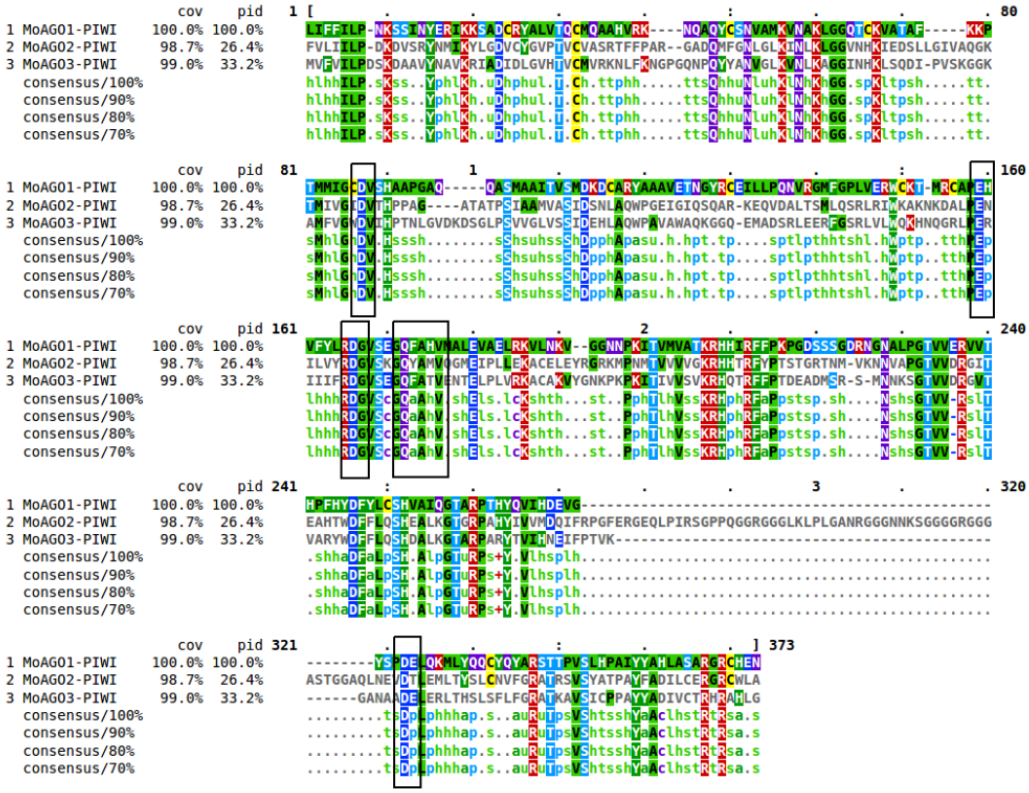

Figure 6. Multiple sequence alignment of the PIWI domain of MoAGO proteins. Sequences were selected based on SMART domain identification, aligned with Clustal Omega and visualized with Mview. The catalytic tetrad DEDD and the QF-V motifs are boxed.

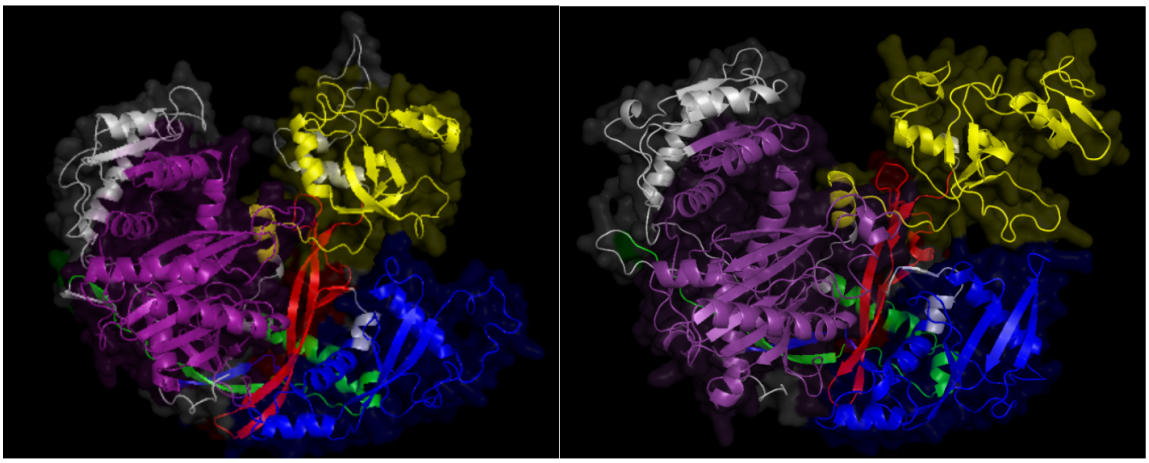

Figure 7. 3D structure predictions for (A) MoAGO1 and (B) MoAGO3. Structures were modeled with Swiss Prot and visualized by PyMOL. Blue = N-domain, red = DUF1785, yellow = PAZ, green = L2, purple = PIWI, the rest of the sequence with no domain predicted is colored in grey.

Table 1. Domain structures and coordinates (with corresponding pvalues in brackets) of MoAGOs and MoDCLs as detected by SMART+PFAM search.

Protein	N domain	DUF1785	PAZ	L2	PIWI
MoAGO1	150-287 (8.2e-16)	296-354 (5.54e-10)	392-515 (1.5e-15)	524-570 (4.3e-14)	672-970 (9.69e-100)
MoAGO2	56-200 (3.6e-19)	211-283 (4.36e-17)	352-439 (1.9e-9)	448-497 (9.7e-10)	606-969 (6.62e-84)
MoAGO3	172-314 (2.3e-14)	328-383 (5.09e-9)	387-534 (4.1e-8)	543-592 (8.8e-15)	702-1020 (1.4e-96)

Protein	DEXDc	HELICc	Dicer_dimer	RIBOc	RIBOc
MoDCL1	104-317 (6.29e-19)	436-565 (4.3e-19)	639-726 (8.4e-20)	1083-1190 (3.4e-19)	1258-1429 (4.73e-20)
MoDCL2	61-262 (3.17e-15)	415-541 (9.7e-18)	609-709 (4e-22)	1004-1142 (2.3e-14)	1183-1381 (3.99e-18)

Table 2. MoAGOs and MoDCLs protein localization prediction results by PSI. Scores range from 0 to 1 and represent the likelihood of detecting the protein in the identified sublocalization, with corresponding pvalues.

Protein	Name	Gene	Sublocalization	Score	Pvalue
XP_003714515.1	MoDCL1	MGG_01541	Nuclear	0.799	0
XP_003715365.1	MoDCL2	MGG_12357	Cytosol	0.565	0
XP_003716704.1	MoAGO1	MGG_14873	Nuclear	0.556	1.7435e-227
			Cytosol	0.329	1.5233e-100
XP_003717504.1	MoAGO2	MGG_13617	Cytosol	0.516	0
			Plastid	0.236	2.5706e-294
XP_003714217.1	MoAGO3	MGG_01294	Nuclear	0.747	0

Table 3. Prediction of protein interactome for MoDCLs and MoAGOs with STRING. The score is the combination of experimental and coexpression scores from STRING prediction.

Interacting protein	Protein description	DCL1 score	DCL2 score
MGG_01294	Argonaute 3	0.664	0.517
MGG_04429	ATP-dependent DNA helicase MPH1	0.515	0.515
MGG_11029	Argonaute 1	0.664	0.512
MGG_13617	Argonaute 2	0.664	0.512
MGG_02598	30S ribosomal protein S16	0.463	0.463
MGG_09464	Uncharacterized protein	0.457	0.457
MGG_06727	WD domain-containing protein	0.45	0.45
MGG_06468	Uncharacterized protein	0.439	0.439
MGG_09301	Uncharacterized protein	0.416	0.416
MGG_04741	Small nuclear ribonucleoprotein Sm D1	0.503	
MGG_09464	Uncharacterized protein	0.457	
MGG_07168	Uncharacterized protein		0.551

Interacting protein	Protein description	AGO1 score	AGO2 score	AGO3 score
DCL1	Dicer-like protein 1	0.664	0.664	0.664
DCL2	Dicer-like protein 2	0.512	0.512	0.517
MGG_13500	U5 small nuclear ribonucleoprotein component	0.685	0.506	0.506
MGG_06309	Cell cycle control protein cwf14	0.685	0.506	0.506
MGG_05172	Uncharacterized protein	0.688		
MGG_03158	Pumilio-family RNA binding repeat protein	0.656		
MGG_02762	ATP-dependent RNA helicase DED1	0.64		
MGG_13651	High-affinity glucose transporter	0.614		
MGG_06873	Uncharacterized protein	0.611		
MGG_13734	Uncharacterized protein	0.611		
MGG_15299	Uncharacterized protein	0.611		

3.2 mRNA sequencing

TruSeq® Stranded mRNA libraries were produced from *i.* Mo axenic culture, *ii. Mo*-infected and mock-treated Bd roots (at 4 DPI), and *iii. Mo*-infected and mock-treated Bd leaves (at 2 DPI and 4 DPI) (Fig. 8). These time points were selected to assess expression pattern changes between both the biotrophic and necrotrophic phase of leaf infections of the hemibiotrophic Mo (Wilson and Talbot 2009). At 2 DPI a total of 233 genes were differentially expressed in *B. distachyon* (224 upregulated and 9 downregulated), compared to 4,978 at 4 DPI (3,023 upregulated and 1,955 downregulated) and 128 during root infection (89 upregulated and 39 down-regulated) (Fig. 9-10, Tab. 4). Minor overlaps were observed comparing downregulated Bd genes between the setups, with only two shared between the foliar infections, and five between the necrotrophic phase and the root setup (Fig. 11A). Among the upregulated genes, the highest overlap was recorded between the leaf samples, sharing 134 DEG, compared to 16 and 72 between root with biotrophic and necrotrophic phase, respectively. Interestingly, 15 Bd genes were found to be upregulated in all setups, including ABC transporter (BdiBd21-3.3G0465100.1), anthranilate synthase component II (BdiBd21-3.5G0159100.1), protein kinase xa21 (BdiBd21-3.3G0144800.1), and secologanin synthase-like (BdiBd21-

3.2G0563800.1) (Tab. 5). In total, 2,135 Mo genes were DE during the foliar biotrophic phase (1,041 upregulated and 1,094 downregulated), compared to the necrotrophic phase (3,186, of which 1,710 were upregulated and 1,476 down-regulated) and 1,000 during root infection (673 upregulated and 327 downregulated) (Fig. 9-10, Tab. 4). Some 498 downregulated and 346 upregulated genes were shared between the foliar infections, 172 (downregulated) and 220 (upregulated) between root infection and the foliar infection at the biotrophic stage, while between the necrotrophic phase and the root infection 203 downregulated and 498 upregulated were shared. Overall, 142 genes were significantly downregulated in all setups, while 168 were consistently upregulated in all samples (Fig. 12A-B).

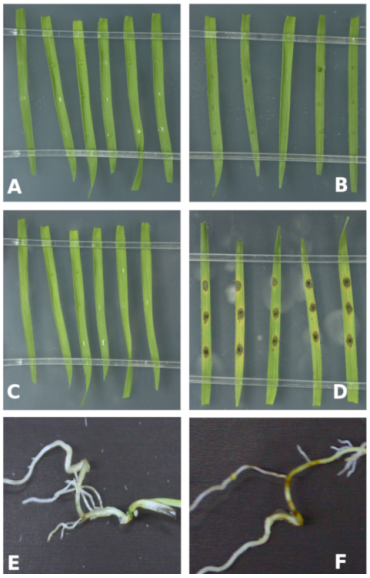

Figure 8. The interaction of *Brachypodium distachyon* and *Magnaporthe oryzae*. (A,D) Detached 21-day-old Bd leaves were drop-inoculated with 10 µl of Mo conidia solution (50,000 spores/ml) and kept for 2 (B) and 4 days (D) at high humidity. Controls were mock-inoculated (A,C). **(E,F)** Roots of seven-day-old Bd were inoculated with 1 ml of spore solution (250,000 spores/ml) and kept for 4 days under high humidity at 16 h light/8 h dark cycle at 22°C/18°C (F). Mock-treated control roots (E).

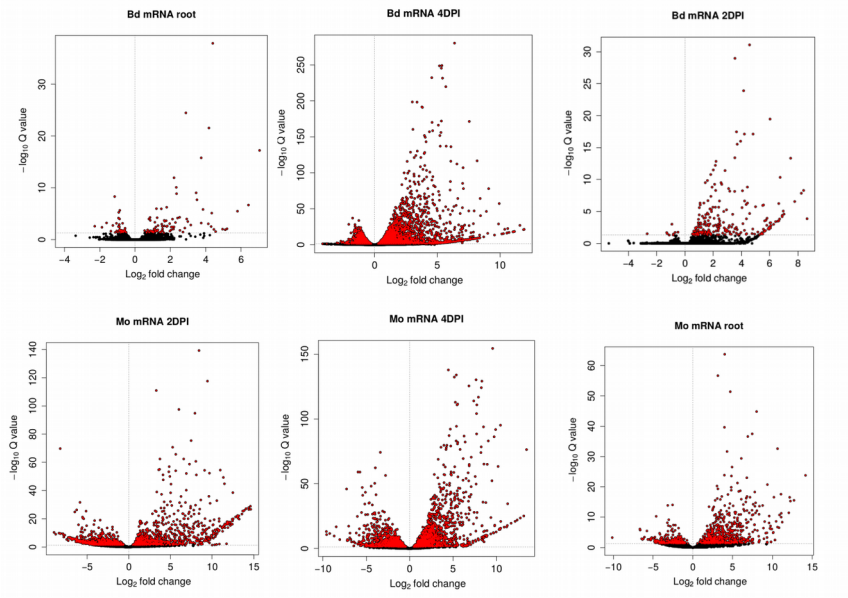

Figure 9. Volcano plots of DESeq2 results based on mRNAseq analysis of *M. oryzae*-infected leaves and roots of *B. distachyon* vs. control. Differentially expressed genes (DEGs) are highlighted in red with significant adjusted p-values (padj < 0.05).

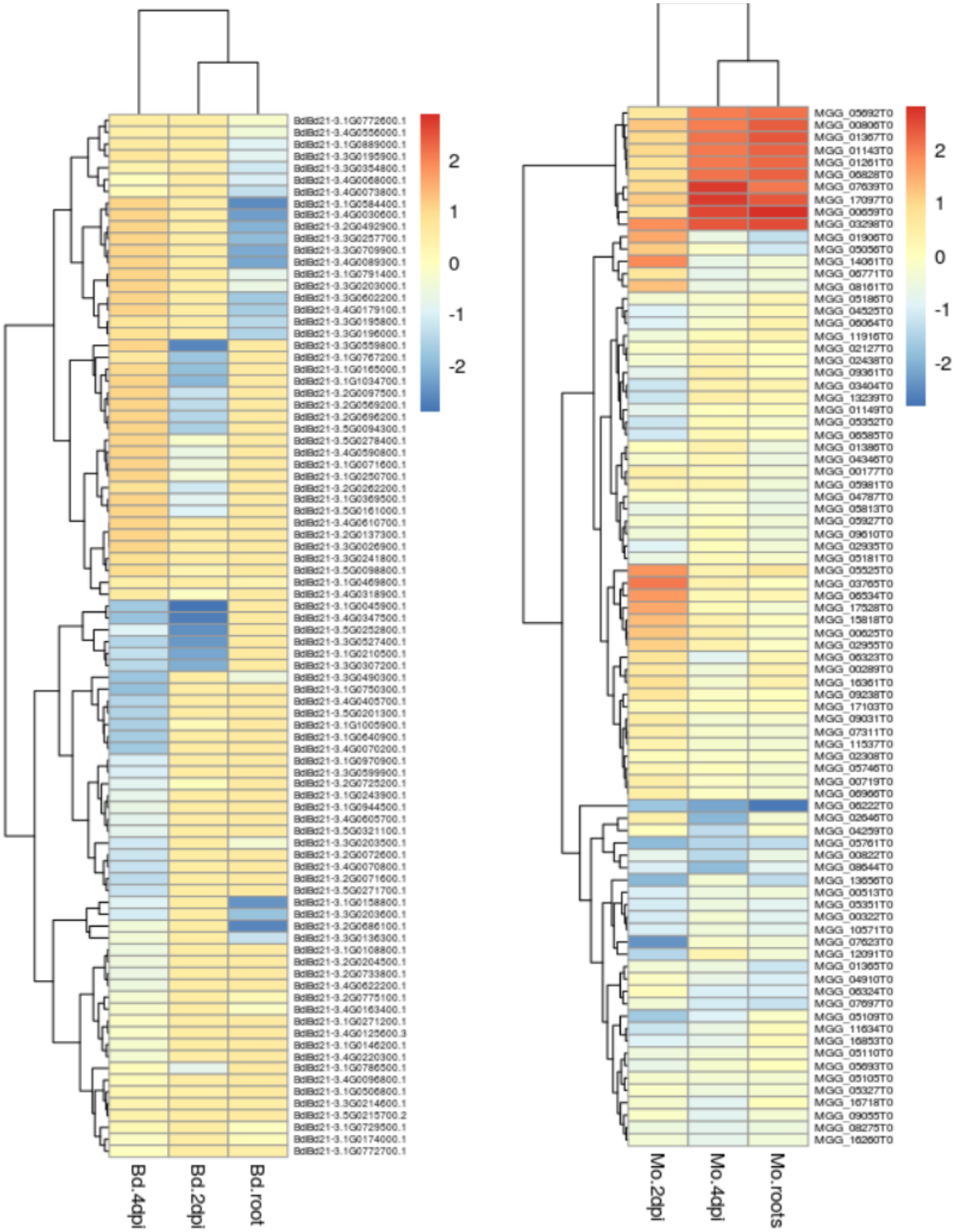

Figure 10. Heatmap for Mo and Bd DEG calling with DESeq2. Heatmap of expression levels (logFC) of the top Bd (A) and Mo (B) mRNAs in all 3 setups (leaf 2 DPI, leaf 4 DPI and root). Color gradient from red to blue indicative of log2FC of corresponding transcript as shown in the legend.

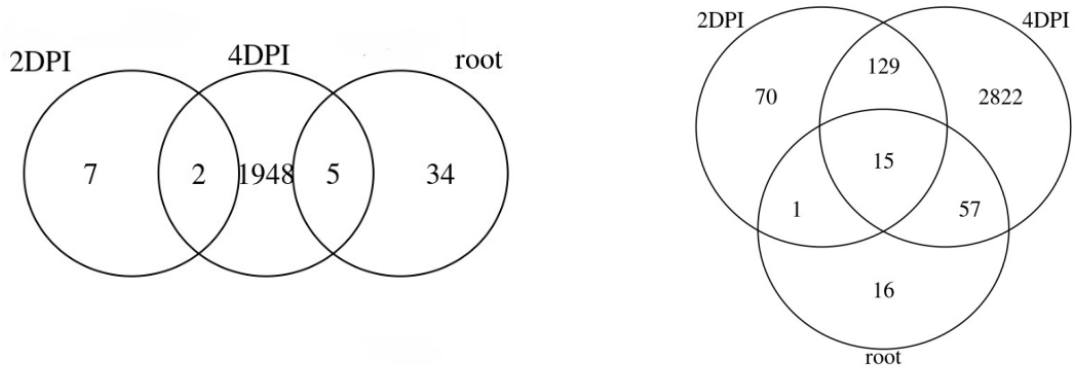

Figure 11. Venn diagram of DE Bd genes.

Significantly (A) downregulated (FC < 0 padj < 0.05) and (B) upregulated (FC > 0 padj < 0.05) Bd genes shared between setups: Leaf biotrophic phase (“2 DPI”) Leaf necrotrophic phase (“4 DPI”), and root (“root”). Transcript downregulation was calculated from mRNAseq data with DESeq2.

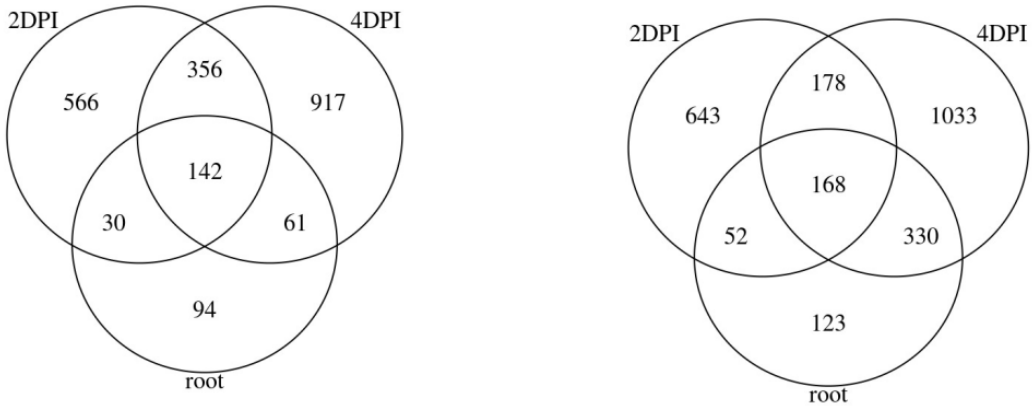

Figure 12. Venn diagram of DE Mo genes.

Significantly (A) downregulated (FC < 0 padj < 0.05) and (B) upregulated (FC > 0 padj < 0.05) Mo genes shared between setups: Leaf biotrophic phase (“2 DPI”) Leaf necrotrophic phase (“4 DPI”), and root (“root”). Transcript downregulation was calculated from mRNAseq data with DESeq2.

Table 4. Total numbers of significantly (padj < 0.05) up- or down-regulated genes in *Brachypodium distachyon – Magnaporthe oryzae* interaction Overview of DESeq2 results. DESeq2 test for differential expression based on negative binomial distribution

Setup	Total Mo genes (up)	Total Mo genes (down)	Total Bd genes (up)	Total Bd genes (down)
Leaf 2 DPI	1041	1094	224	9
Leaf 4 DPI	1710	1476	3023	1955
Root	673	327	89	39

Table 5. Selected significantly (padj < 0.05) differentially expressed (DE) Bd defense related genes during Mo foliar infection (2DPI, 4DPI) and root infection

Gene	Description	LogFC 2DPI	LogFC 4DPI	LogFC Root
BdiBd21-3.3G0465100	abc transporter a family member 2-like	1.146	3.384	0.785
BdiBd21-3.3G0464900	abc transporter a family member 7-like		2.638	0.712
BdiBd21-3.2G0605400	abc transporter b family member 4-like	2.154	5.082	
BdiBd21-3.2G0605600	abc transporter b family member 4-like		0.782	
BdiBd21-3.2G0550500	pleiotropic drug resistance protein 3-like	1.777	6.823	1.513
BdiBd21-3.3G0610700	e3 ubiquitin-protein ligase el5-like	2.936	2.895	
BdiBd21-3.5G0159100	anthranilate synthase component ii	0.760	2.749	0.875
BdiBd21-3.2G0371400	beta-glucosidase 22-like		0.479	0.846
BdiBd21-3.3G0344500	chitinase 1		2.703	
BdiBd21-3.2G0371800	cytochrome p450 71c4		1.319	2.118
BdiBd21-3.2G0281400	disease resistance protein		1.155	
BdiBd21-3.1G0952300	disease resistance response		2.073	
BdiBd21-3.3G0144800	protein kinase xa21	1.770	2.414	1.238

BdiBd21-3.2G0545400	lrr receptor-like serine threonine-protein kinase gso1		1.585	1.794
BdiBd21-3.2G0632400	receptor-like protein kinase hsl1-like		3.146	
BdiBd21-3.2G0663500	receptor-like serine threonine-protein kinase sd1-8-like		3.321	
BdiBd21-3.4G0554000	putative wall-associated receptor kinase-like 16	1.923	-0.753	
BdiBd21-3.1G0713100	proton-coupled amino acid transporter 3-like	0.847	1.969	0.969
BdiBd21-3.2G0114800	pathogenesis related protein	1.341	1.251	
BdiBd21-3.1G0165000	pathogenesis-related protein 1	6.055	8.194	
BdiBd21-3.4G0068000	pathogenesis-related protein 10		3.466	3.745
BdiBd21-3.4G0043000	pathogenesis-related protein 5		2.905	
BdiBd21-3.1G0772600	pathogenesis-related protein class i		5.287	4.465
BdiBd21-3.1G0772700	pathogenesis-related protein prb1-2-like		3.406	6.423
BdiBd21-3.3G0422200	pr3-like 1		2.628	
BdiBd21-3.3G0639500	pr3-like 2		3.963	
BdiBd21-3.4G0025400	pr5-like		1.371	
BdiBd21-3.2G0600500	pr5-like		2.275	
BdiBd21-3.1G0875700	Pathogenesis-related protein Bet v I family		2.135	
BdiBd21-3.1G0054700	nac1 transcription factor		2.487	
BdiBd21-3.3G0652700	myb-related protein myb4-like		3.334	
BdiBd21-3.2G0688100	probable wrky transcription factor 33-like		2.685	
BdiBd21-3.2G0615100	probable wrky transcription factor 51-like	1.448	3.438	
BdiBd21-3.3G0669400	ethylene-responsive transcription factor 1a-like		2.158	

BdiBd21-3.1G0780100	transcription factor jungbrunnen 1-like		2.303	1.266
BdiBd21-3.4G0171000	multicopper oxidase family expressed	4.354	9.932	2.349
BdiBd21-3.4G0387000	cationic peroxidase spc4-like	3.166	3.718	
BdiBd21-3.1G0233800	peroxidase		1.493	
BdiBd21-3.1G0233900	peroxidase		2.107	
BdiBd21-3.2G0563800	secologanin synthase-like	0.571	0.540	1.078
BdiBd21-3.5G0045900	udp-glycosyltransferase 74f2-like	0.875	1.790	

3.3 GOE analysis and defense-related genes expression in Bd in response to Mo infections

Gene Ontology Enrichment Analysis (GOE) was carried out on all DEG identified from the mRNAseq data analysis with AgriGO v2. In all 3 datasets GO:0003824 (catalytic activity), GO:0016491 (oxidoreductase activity) and GO:0044710 (single-organism metabolic process) were enriched, while GO:0044699 (single-organism process) was found enriched in both the 2 DPI and the root subsets, and GO:0046906 (tetrapyrrole binding) in both foliar datasets (Tab. 6). At 4 DPI, corresponding to the necrotrophic infection stage, the highest amount of GO terms enriched was recorded among all samples, in particular those related to various cellular metabolic processes (Fig. 13).
Consistent with the extensive metabolic reprogramming highlighted in the GOE analysis, the highest number of overall DEG was observed during the foliar necrotrophic phase, in particular a significant upregulation of known Bd defense response genes and transcription factors (Tab. 5).

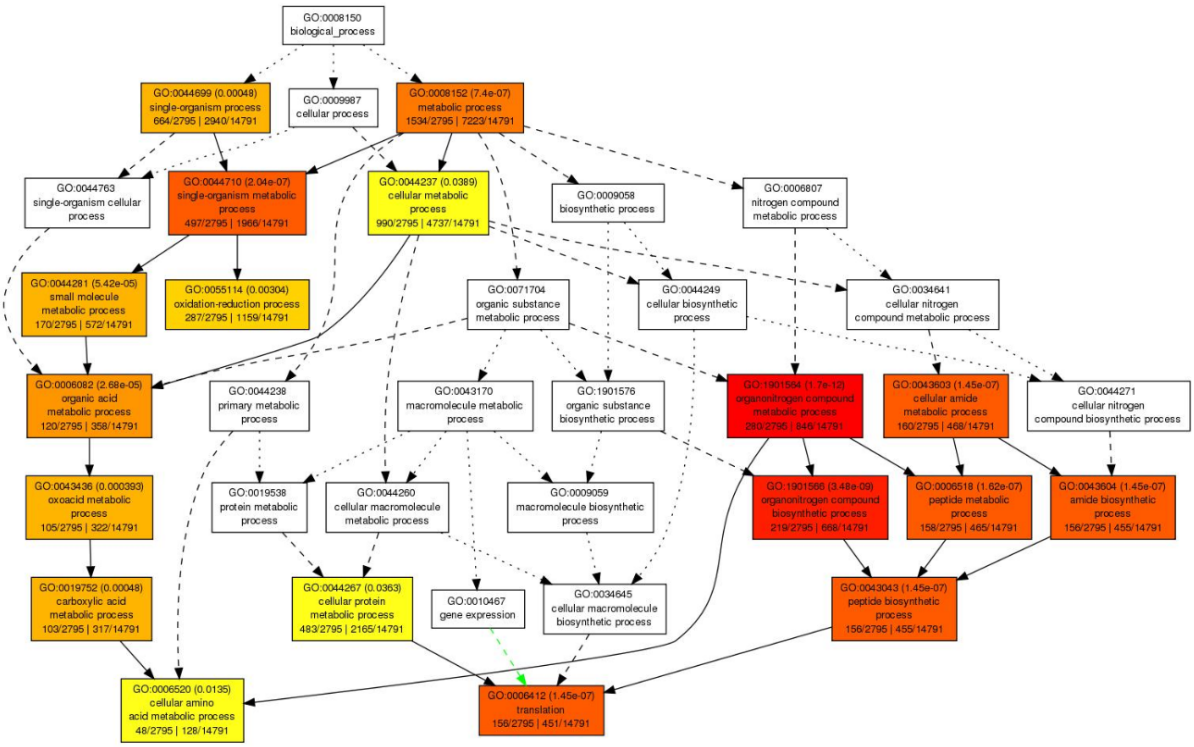

Figure 13. Results of gene ontology enrichment (GOE) analysis for significantly DE Bd genes in the 4 DPI leaf setup. GOE analysis done with AgriGO v2.

Table 6. Selection of significantly enriched Bd GO terms from 2DPI, 4DPI and root Bd DEG datasets. GO terms and GOE analysis was done with AgriGO v2 against the pre-compiled Bd reference, after transforming Bd21-3 IDs to Bd21 ones. Abbreviations: O= ontology, P= biological process, F = molecular function, C = cellular component, BG = background, FDR = false discovery rate.

Setup	GO term	O	Description	Input list	BG/Ref	p-value	FDR
4DPI	GO:1901564	P	organonitrogen compound metabolic process	280	846	6.30E-16	1.70E-12
4DPI	GO:0006412	P	translation	156	451	1.90E-10	1.50E-07
4DPI	GO:0043603	P	cellular amide metabolic process	160	468	2.20E-10	1.50E-07
4DPI	GO:0043043	P	peptide biosynthetic process	156	455	3.20E-10	1.50E-07
4DPI	GO:0008152	P	metabolic process	1534	7223	2.50E-09	7.40E-07
4DPI	GO:0006082	P	organic acid metabolic process	120	358	9.90E-08	2.70E-05
4DPI	GO:0044281	P	small molecule metabolic process	170	572	2.20E-07	5.40E-05
4DPI	GO:0043436	P	oxoacid metabolic process	105	322	1.70E-06	3.90E-04
4DPI	GO:0044699	P	single-organism process	664	2940	2.40E-06	4.80E-04
4DPI	GO:0055114	P	oxidation-reduction process	287	1159	1.70E-05	3.00E-03
4DPI	GO:0044267	P	cellular protein metabolic process	483	2165	2.30E-04	3.60E-02
4DPI	GO:0003735	F	structural constituent of ribosome	127	312	2.30E-12	1.70E-09
4DPI	GO:0005198	F	structural molecule activity	133	330	1.20E-12	1.70E-09
4DPI	GO:0003824	F	catalytic activity	1408	6501	2.40E-10	1.20E-07
4DPI	GO:0016491	F	oxidoreductase activity	318	1274	3.20E-06	1.20E-03
4DPI	GO:0035639	F	purine ribonucleoside triphosphate binding	376	1608	6.00E-05	1.50E-02
4DPI	GO:0005737	C	cytoplasm	239	793	2.30E-10	3.00E-08

4DPI	GO:0043228	C	non-membrane-bounded organelle	156	547	5.00E-06	3.80E-04
2DPI	GO:0055114	P	oxidation-reduction process	30	1159	5.70E-08	2.10E-05
2DPI	GO:0044710	P	single-organism metabolic process	40	1966	1.40E-07	2.50E-05
2DPI	GO:0044699	P	single-organism process	46	2940	1.90E-05	2.30E-03
2DPI	GO:0005506	F	iron ion binding	20	313	7.20E-12	1.50E-09
2DPI	GO:0016705	F	oxidoreductase activity, acting on paired donors	19	301	3.10E-11	3.10E-09
2DPI	GO:0020037	F	heme binding	21	438	3.30E-10	2.20E-08
2DPI	GO:0003824	F	catalytic activity	91	6501	5.70E-10	2.30E-08
2DPI	GO:0046906	F	tetrapyrrole binding	21	452	5.70E-10	2.30E-08
2DPI	GO:0016491	F	oxidoreductase activity	30	1274	4.30E-07	1.40E-05
2DPI	GO:0043167	F	ion binding	31	1701	4.70E-05	1.40E-03
2DPI	GO:0043169	F	cation binding	29	1601	9.90E-05	2.00E-03
Root	GO:0006979	P	response to oxidative stress	8	169	4.80E-06	8.70E-04
Root	GO:0044710	P	single-organism metabolic process	25	1966	2.70E-05	1.00E-03
Root	GO:0044264	P	cellular polysaccharide metabolic process	5	61	2.70E-05	1.00E-03
Root	GO:0006950	P	response to stress	11	473	5.30E-05	1.60E-03
Root	GO:0005976	P	polysaccharide metabolic process	5	73	6.20E-05	1.60E-03
Root	GO:0055114	P	oxidation-reduction process	17	1159	1.40E-04	3.20E-03
Root	GO:0044262	P	cellular carbohydrate metabolic process	5	108	3.50E-04	7.10E-03
Root	GO:0016684	F	oxidoreductase activity, acting on peroxide as acceptor	8	174	5.90E-06	2.90E-04
Root	GO:0020037	F	heme binding	12	438	4.70E-06	2.90E-04

Root	GO:0003824	F	catalytic activity	56	6501	2.40E-06	2.90E-04
Root	GO:0046906	F	tetrapyrrole binding	12	452	6.50E-06	2.90E-04
Root	GO:0004601	F	peroxidase activity	8	171	5.20E-06	2.90E-04
Root	GO:0016830	F	carbon-carbon lyase activity	5	72	5.80E-05	1.90E-03
Root	GO:0016491	F	oxidoreductase activity	18	1274	1.40E-04	3.90E-03
Root	GO:0016829	F	lyase activity	6	174	4.10E-04	1.00E-02
Root	GO:0016798	F	hydrolase activity, acting on glycosyl bonds	8	371	9.70E-04	2.20E-02

3.4 GOE analysis and infection-related genes expression in Mo during Bd infection

Significantly upregulated and downregulated genes from all three setups were subjected to GOE analysis to evaluate the enrichment of GO terms in the datasets. At 4 DPI the only term significantly enriched was GO:0044408 (growth or development of symbiont on or near host) while at 2 DPI terms related to developmental processes (GO:0032502, GO:0048856, GO:0007275, GO:0043581) were found enriched (Tab. 7). Interestingly, the highest number of enriched GO terms was observed in the root infection dataset, with most significantly enriched terms relating to the interaction with host (GO:0052047, GO:0044046, GO:0052048, GO:0052051, GO:0052211) (Fig. 14).

Overall, a plethora of infection-related and proliferation-related genes were found significantly upregulated in all datasets (Tab. 8).

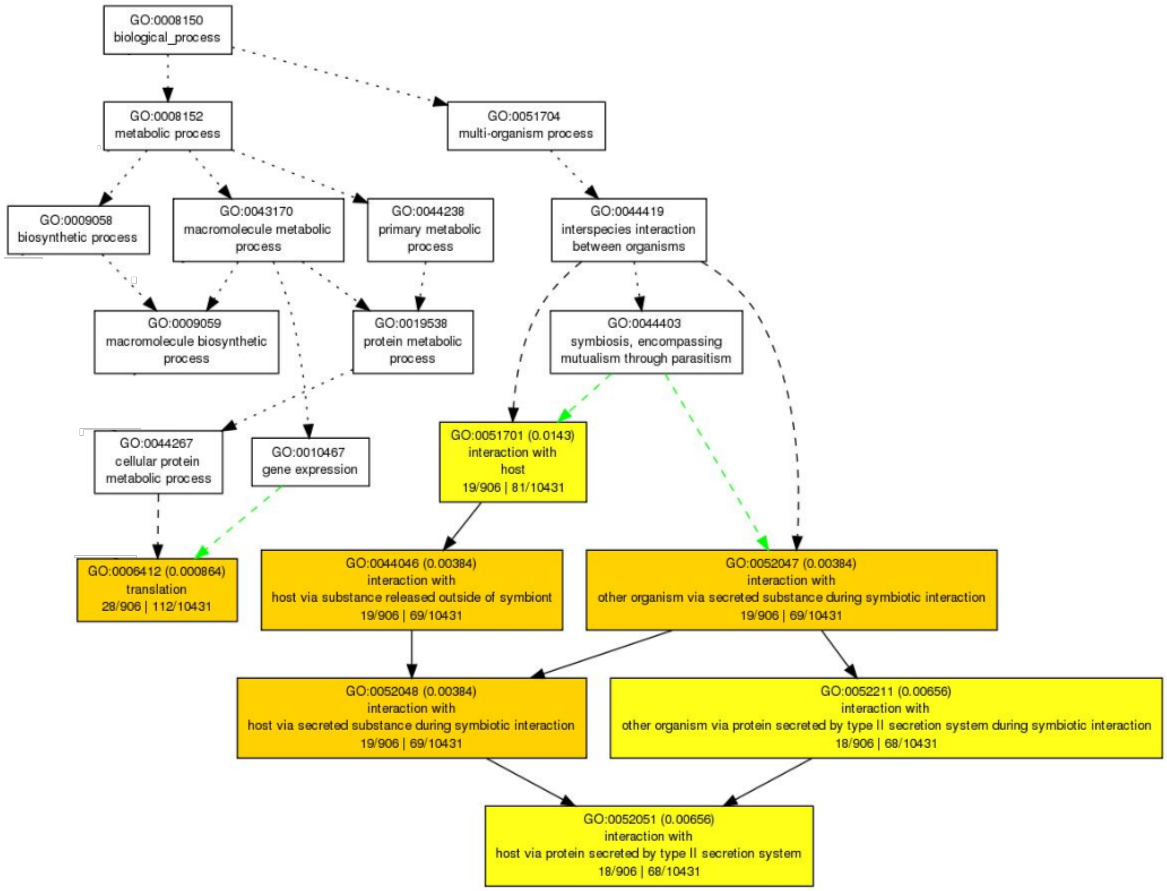

Figure 14. Results of gene ontology enrichment (GOE) analysis for significantly DE Mo genes in the root setup. GOE analysis done with AgriGO v2.

Table 7. Selection of significantly enriched Mo GO terms from 2DPI, 4DPI and root Mo DEG datasets. GO terms and GOE analysis was done with AgriGO v2 against the pre-compiled Mo reference. Abbreviations: P= biological process, F = molecular function, C = cellular component, BG = background, FDR = false discovery rate.

Setup	GO term	O	Description	Input list	BG/ Ref	p-value	FDR
Root	GO:0044408	P	growth or development of symbiont on or near host	198	1478	1.80E-09	6.50E-07
Root	GO:0006412	P	translation	28	112	4.70E-06	8.60E-04
Root	GO:0052047	P	interaction with other organism via secreted substance during symbiotic interaction	19	69	5.20E-05	3.80E-03
Root	GO:0052051	P	interaction with host via protein secreted by type II secretion system	18	68	1.20E-04	6.60E-03
Root	GO:0052211	P	interaction with other organism via protein secreted by type II secretion system	18	68	1.20E-04	6.60E-03
Root	GO:0051701	P	interaction with host	19	81	3.10E-04	1.40E-02
Root	GO:0003735	F	structural constituent of ribosome	17	65	2.20E-04	2.40E-02
Root	GO:0005198	F	structural molecule activity	17	71	5.20E-04	2.80E-02
2DPI	GO:0032502	P	developmental process	263	1048	8.50E-07	6.60E-04
2DPI	GO:0048856	P	anatomical structure development	245	989	4.80E-06	1.90E-03
2DPI	GO:0032501	P	multicellular organismal process	233	951	1.60E-05	3.10E-03
2DPI	GO:0007275	P	multicellular organismal development	233	950	1.50E-05	3.10E-03
2DPI	GO:0043581	P	mycelium development	230	941	2.10E-05	3.30E-03
2DPI	GO:0034641	P	cellular nitrogen compound metabolic process	38	90	2.80E-05	3.70E-03
4DPI	GO:0044408	P	growth or development of symbiont on or near host	521	1478	1.80E-08	1.50E-05

Table 8. Selected significantly (padj < 0.05) upregulated Mo pathogenicity / virulence related genes during Bd foliar infection (2DPI, 4DPI) and root infection.

Gene stable ID	Gene description	Log2FC 2DPI	Log2FC 4DPI	Log2FC root
MGG_00750	Cytochrome b-245 heavychain subunit beta	2.230	2.119	2.799
MGG_01081	Peroxin 14/17		1.053	
MGG_01092	Homocitrate synthase	1.347		
MGG_01748	Putative protease		1.284	
MGG_02074	Potassium/sodium efflux P-type ATPase		1.278	2.548
MGG_02986	DNA polymerase zeta catalytic subunit			2.459
MGG_03356	Ricin B lectin:Parallel beta-helix		7.080	5.062
MGG_04202	MAS3 protein	2.265		2.749
MGG_04212	L-ornithine 5-monooxygenase (L-ornithine N(5)-oxygenase)	2.815	3.465	3.167
MGG_04301	Pwl2 protein (PWL2) gene	8.533		
MGG_04545	Cytochrome c peroxidase, mitochondrial	3.265	0.947	
MGG_05078	Potassium/sodium efflux P-type ATPase		2.064	
MGG_06011	S-(Hydroxymethyl)glutathione dehydrogenase		2.533	
MGG_06648	Hsp70 (LHS1) gene	1.247		
MGG_06847	Annexin A7		0.995	
MGG_06951	CAAX prenyl protease 1	1.148		
MGG_07514	3-oxoacyl-[acyl-carrier-protein] reductase		1.486	
MGG_07971	Calcium-transporting ATPase 1		1.801	
MGG_08315	1-phosphatidylinositol-4,5-bisphosphate phosphodiesterase delta-1	8.831	7.938	
MGG_08409	Cellulose-growth-specific protein		3.783	
MGG_09022	Transmembrane CFEM domain-containing protein	5.414	7.421	7.876
MGG_09263	GAL4 domain containing protein		1.120	
MGG_09559	Autophagy-related protein 9		1.067	
MGG_09956	PRO41 protein	1.932	1.913	2.623
MGG_10097	Intracellular hyphae protein 1	5.423		
MGG_10510	Ribonuclease T2	3.901		
MGG_10702	Putative MFS monocarboxylate transporter		3.229	
MGG_10730	Potassium/sodium efflux P-type ATPase		4.748	
MGG_11882	Sensor protein zRas		1.598	3.148
MGG_11899	SH3 domain-containing protein	1.934	1.524	

MGG_14517	Developmental regulator flbA		1.566
MGG_14767	Non-ribosomal peptide synthetase		3.961
MGG_15140	Tyrosine-protein phosphatase pmp1		1.095
MGG_15370	Metalloproteinase	11.859	
MGG_15868	Argininosuccinate synthase	1.080	
MGG_15972	AVR-pik/pikm/pikp	14.633	6.326

3.5 Interaction-related sRNAs in the Mo-Bd pathosystem

To establish the role of sRNAs in the interaction between *Magnaporthe oryzae* (Mo 70-15) and *Brachypodium distachyon* (Bd21-3), we isolated sRNA fractions from the same biological material utilized for mRNA sequencing (roots, leaves and axenic mycelium) and after cDNA library preparation performed high throughput next generation sequencing (NGS) (Fig. 8). Before sequencing, multiplexed sRNA libraries were size selected for 15 to 35 nt (140-160 nt including TruSeq adapters). Single end sequencing on Illumina HiSeq1500 platform generated between 22 million (mil) and 38 mil reads each (Tab. 9, Fig. 15). Quality check of raw reads was performed with FastQC, adapters were removed with cutadapt and reads were size selected between 18 to 32 nt. The organism of origin of the trimmed reads was predicted by mapping via Bowtie alignments to both Bd and Mo genomes (Zerbino et al., 2018, Bd21-3 v1.1 DOE-JGI, http://phytozome.jgi.doe.gov/). Ambiguous reads that could not be assigned to the organism of origin with high confidence were excluded to avoid miscalling. As expected, most reads in *Mo*-infected plant samples were assigned to Bd (with 100% match) and not to the fungus (with at least two nucleotide mismatches) (Tab. 9). Size distribution of genome matched unique sRNA reads followed a similar trend throughout samples, with the Mo reads showing a peak between 20-22 nt and Bd reads at 24 nt (Fig. 16). In order to further investigate the sRNAs potentially playing a role in the *Mo-Bd* interaction, fungal unique sRNA reads were compared among samples from Mo axenic culture and Mo-infected leaves and roots and classified as shared or exclusive between samples (Fig. 17). Some 5,708 Mo sRNAs were identified in Bd-infected roots tissue of which 3,263 (57.15%) were found exclusively in the infected sample and not in the axenic culture. Moreover, 7,215 Mo sRNAs (exclusively found in infected samples: 4,399 [60.97%])

were identified in Bd-infected leaf tissue during the biotrophic phase and 63,017 (exclusively found in infected samples: 46,212 [73.33%]) in Bd-infected leaf tissue during the necrotrophic phase.

Equally, unique Bd sRNA reads were compared in root and leaf samples from *Mo*-infected and mock-treated *Bd21-3* (Fig. 17). We found a large number of Bd sRNAs in *Mo*-infected plant tissues: 597,158 Bd sRNAs in Mo-infected roots of which 346,259 (77.92%) were solely found in infected, but not in non-infected roots; 571,644 in leaves during biotrophic interaction (2 DPI) of which 326,657 (72.24%) were solely found in infected leaves; and 415,469 during the necrotrophic interaction (4 DPI) of which 265,172 (69.06%) were solely found in infected leaves. This data suggests that most unique sRNAs from both interacting organisms are expressed exclusively during the interaction and thus are potentially of relevance for the outcome of the disease. We selected unique sRNAs that *i.* were either found exclusively in infected plant tissues or *ii.* showed higher numbers in the infected tissue as compared to mock-infected tissue and axenic culture. Interestingly, the size distribution of these induced sRNA reads did not highlight a change in length preference compared to the total unique reads (Fig. 16).

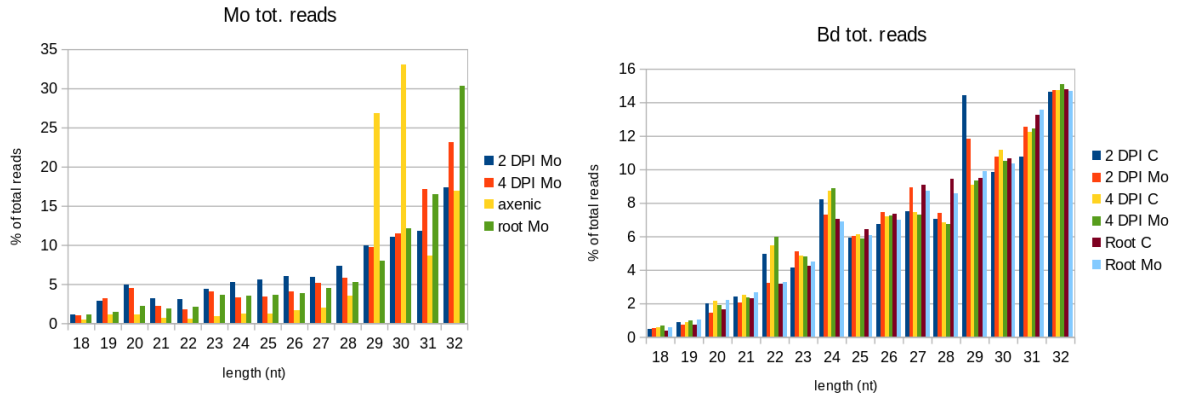

Figure 15. Size distribution of total filtered reads. Raw sequences were trimmed and assigned to the organism of origin by alignment with Bowtie: reads were attributed to one organism or the other only if they aligned with no mismatches to its genome and had a minimum of two mismatches to the interacting organism.

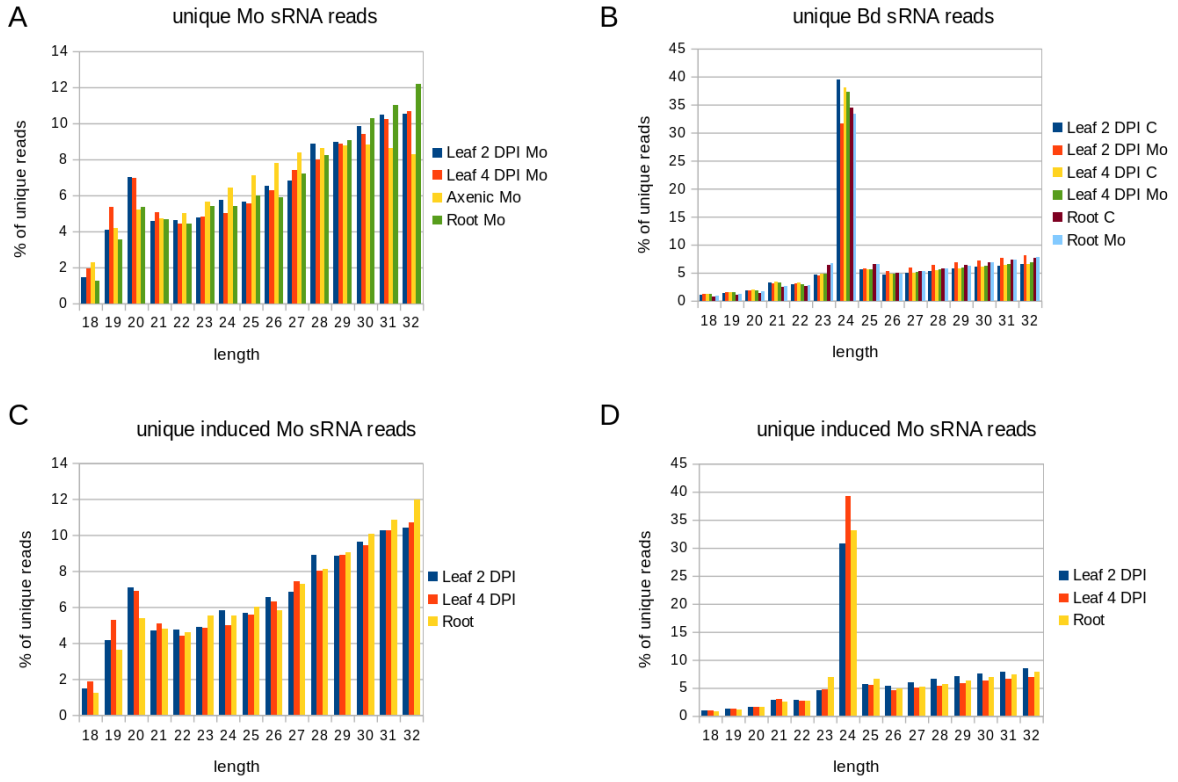

Figure 16. Size distribution of unique sRNA reads in the interaction of *B. distachyon* and *M. oryzae*.

(A,B) Relative size distribution (in percentage) of unique filtered sRNA reads assigned to Mo (A) or Bd (B) in the interaction of *M. oryzae* (*Mo* 70-15) and *B. distachyon* (*Bd21-3*). Reads were assigned to either Mo or Bd only if aligning 100% to the organism of origin genome and

had at least two mismatches to the interacting organism genome. **(C,D)** Relative size distribution of unique filtered sRNA reads assigned to Mo (C) or Bd (D) and induced or increased in infected samples compared to controls (axenic fungal cultures and non-inoculated plants, respectively). Samples for sRNA sequencing by Illumina HiSeq1500 were taken from different setups: leaves (leaf 2 DPI, 4 DPI) and roots (roots 4 DPI).

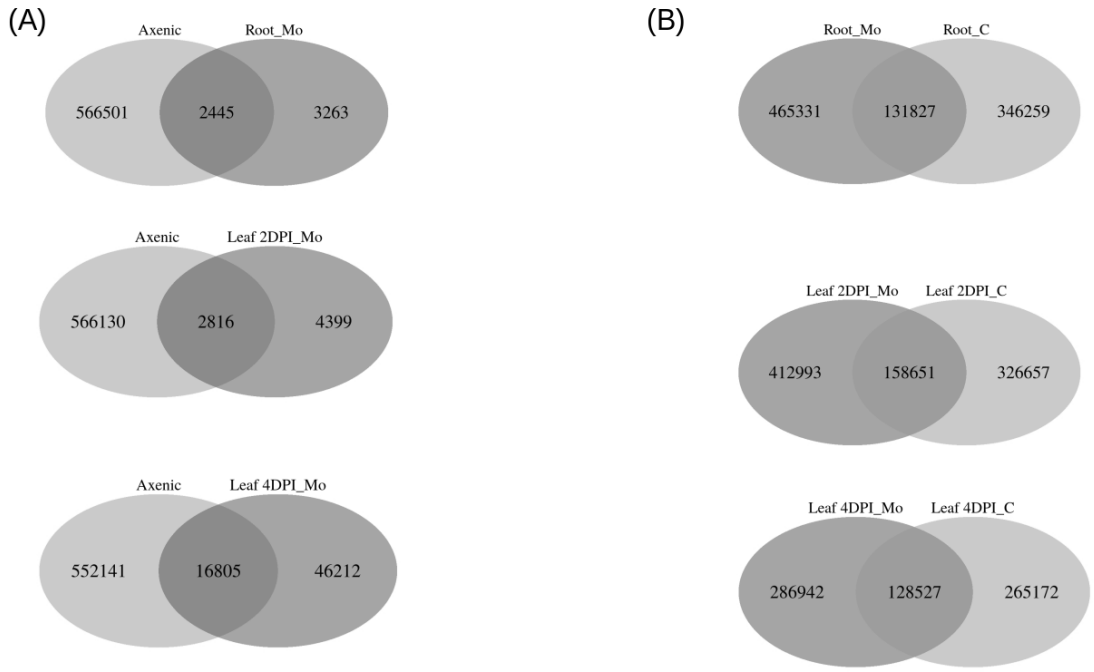

Figure 17. Venn diagrams of unique filtered Mo and Bd reads. (A) Venn diagram of Mo sRNA reads (18-32 nt) in axenic culture and Mo-infected Bd leaves (2 DPI, 4 DPI) and roots (4 DPI). **(B)** Venn diagram of Bd sRNA reads (18-32 nt) in mock-inoculated, non-infected and Mo-infected Bd leaves.

Table 9. Overview of total sRNA and mRNA reads in the *Brachypodium distachyon* – *Magnaporthe oryzae* interaction. Total (tot.) reads sRNA: total number of raw sRNA reads per sample. Total sRNA reads Bd/ Total sRNA reads Mo: total number of sRNA reads aligned without mismatches to organism of origin genome that have at least 2 mismatches to the interacting organism genome. Total reads mRNA: total number of raw mRNA reads per sample.

Sample	Tot. reads sRNA	Tot. sRNA reads *Bd*	Tot. sRNA reads *Mo*	Tot. mRNA reads (millions)
2 DPI leaves con	28 435 036	18 691 859		59.5
2 DPI leaves *Mo*	35 544 788	25 844 498	62 709	59.3
4 DPI leaves con	21 846 438	15 214 694		105
4 DPI leaves *Mo*	26 376 527	15 623 561	827 678	82.8
Roots con	33 722 475	23 139 570		47.8
Roots *Mo*	37 697 368	26 378 677	96 506	44.9
Axenic culture *Mo*	26 407 359		13 721 649	65

3.6 Prediction of plant endo-sRNA (miRNAs) candidates

Filtered Bd sRNA reads were analyzed with Shortstack 3.8.5 to identify infection-dependent upregulation of potential miRNAs. The program identified 14 putative miRNA-generating loci in the 2 DPI infected sample, 15 at 4 DPI and 16 in the root setup (Tab. 10). Matching clusters in the control samples were identified via their genomic coordinates, and numbers of total reads per cluster were compared between colonized and control samples to select exclusively induced or upregulated miRNA loci. The selected clusters' sequences were then aligned to known Bd miRNA stem loop precursors sequences obtained from the miRBase database: three known miRNAs were induced/upreg at 2 DPI, six at 4 DPI and four in the root setup. Target prediction for these miRNAs was done with psRNATarget and the results were merged with the DEG info to assess target downregulation (Tab. 10). Structures of the miRNA precursors with downregulated targets are shown in Figure 18.

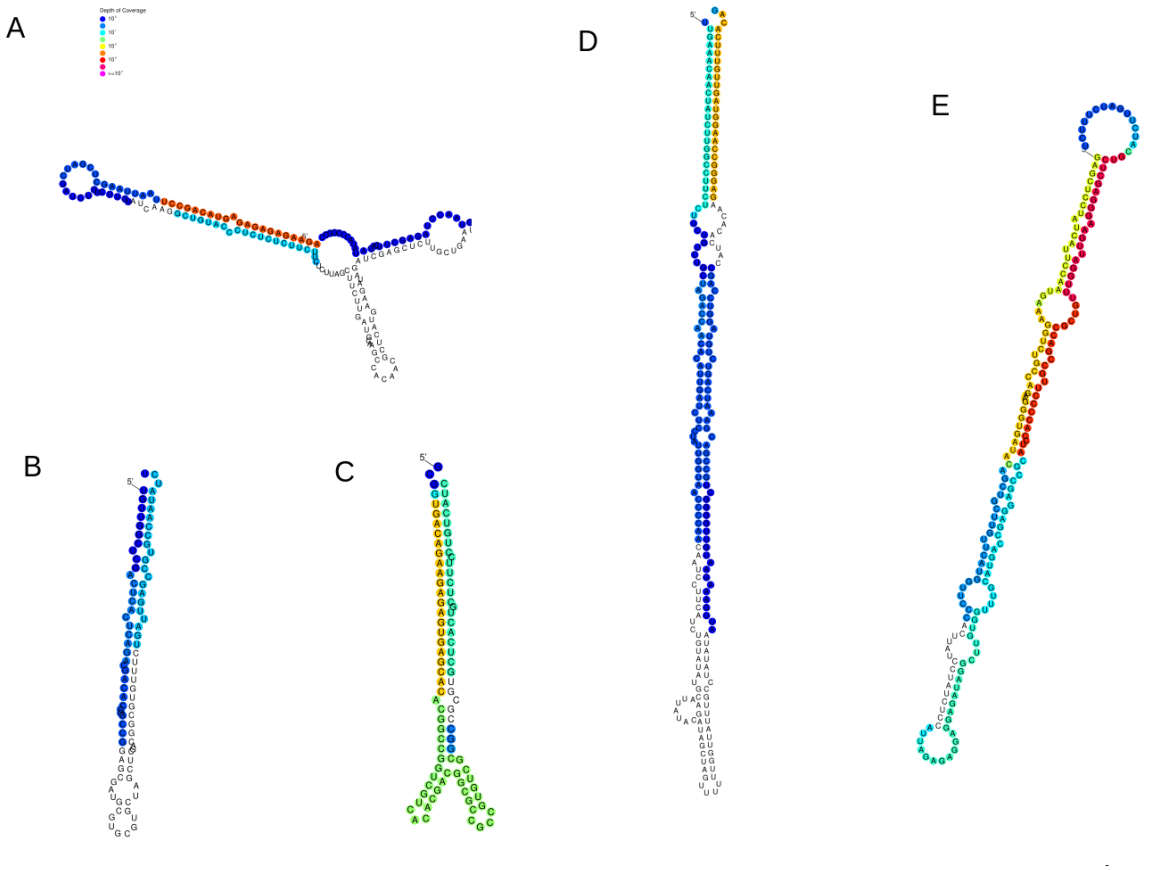

Figure 18. Visual representation of the identified upregulated Bd clusters (miRNA precursors) structures: (A) cluster_7470, (B) cluster_3162, (C) cluster_7744, (D) cluster_2384, (E) cluster_3312.

Table 10. Bd miRNA identification and target prediction. miRNA-generating clusters were identified with Shortstack in all datasets. Genomic coordinates were used to detect and compare the same loci in infected and control samples, and only clusters exclusive or increased in the infected samples were analyzed for potential endogenous targeting. Clusters and mature miRNAs were compared to known miRNA/miRNA precursor from miRBase. Abbreviations: RPM = reads per million , N = no target detected downregulated.

Setup	Cluster number	miRNA	Cluster RPM	Mature mirna name	Target ID	logFC target
4DPI	7744	Bdi-MIR156h	13.79	MIR156h-5p	BdiBd21-3.1G0011700.1	-1.077
					BdiBd21-3.2G0498600.1	-0.930
	3312	Bdi-MIR159b	184.31	miR159b-3p.1	BdiBd21-3.3G0746500.1	-0.939
					BdiBd21-3.3G0778600.1	-0.688
					BdiBd21-3.3G0284600.1	-0.665
				miR159b-3p.2	BdiBd21-3.1G0594400.1	-1.159
					BdiBd21-3.4G0303000.1	-0.821
					BdiBd21-3.2G0800600.1	-0.615
				miR159b-5p.1	BdiBd21-3.4G0504100.1	-0.863
					BdiBd21-3.1G0611900.1	-0.680
				miR159b-5p.2	BdiBd21-3.1G0671500.1	-1.344
					BdiBd21-3.1G0865400.1	-0.966
					BdiBd21-3.3G0647400.1	-0.853
					BdiBd21-3.1G0519500.1	-0.664
	3162	Bdi-MIR171d	0.58	MIR171d-3p	BdiBd21-3.1G0317900.1	-1.313
					BdiBd21-3.1G0415900.1	-0.860
					BdiBd21-3.5G0099800.1	-0.747
	7470	Bdi-MIR529	30.80	MIR529-5p	BdiBd21-3.2G0404400.1	-0.917
					BdiBd21-3.4G0016700.1	-0.705
					BdiBd21-3.1G0442400.1	-0.704
					BdiBd21-3.3G0636800.1	-0.656
					BdiBd21-3.1G0775400.1	-0.621
					BdiBd21-3.1G0775400.1	-0.621
	2384	Bdi-miR7723a	13.02	miR7723a-3p	BdiBd21-3.3G0613900.1	-0.724
	10592	Bdi-MIR156d	8.31	MIR156d-5p	N	
Root	8229		2.87	MIR156i-5p	N	

		Bdi-MIR156i		MIR156i -3p	N
	5121	Bdi-MIR168	310.27	MIR168-5p	N
	9081	Bdi-MIR156d	1.15	miR156d-5p	N
	4330	bdi-MIR9484	3.90	MIR9484	N
2DPI	3086	Bdi-miR159b	118.27	miR159b-3p.2	N
				miR159b-3p.1	N
	3421	Bdi-MIR531	15.03	MIR531	N
	6495	Bdi-MIR156b	2.61	miR156b-3p	N
	7687	Bdi-miR9481b	19.12	miR9481b -5p	N
				miR9481b-3p	N

3.7 Prediction of fungal ck-sRNA effector candidates

sRNAs that were either exclusively produced or increased in the *Mo-Bd* interaction (and with a read count of at least 5 rpm in the infected samples) were further investigated. As anticipated from the work on the *Botrytis cinerea - Arabidopsis thaliana*/*Solanum lycopersicum* pathosystems (Weiberg et al., 2013), differentially expressed 20-22 nt long sRNAs originating from non-coding regions of the Mo genome are candidate sRNA effectors that potentially target Bd genes (Fig. 19). Target prediction was carried out using psRNATarget with modified settings and a default score cut-off of 5.0. Some 604 fungal sRNAs were predicted to target 25,106 Bd mRNAs in the biotrophic phase of leaf infection (2 DPI), while fewer sRNA effector candidates (546 and 394, respectively) were predicted for the necrotrophic phase (4 DPI) and the root setup corresponding to 25,415 and 17,335 mRNA targets (Tab. 11). Of note, the ratio between predicted targets and sRNAs was comparable between biological samples, with the 4 DPI leaf sample having the highest (on average 46.5 predicted targets per sRNA) compared to 44 and 41.6 for root and 2 DPI leaf samples, respectively.

As a first indication of a direct interaction between the predicted fungal sRNA and Bd mRNAs during *Bd-Mo* infection, we combined the target prediction data with the DEG

information derived from the concomitant mRNA sequencing. This strategy allowed for the confirmation of target downregulation in presence of the predicted sRNAs, which further selects for potential sRNA effectors. Of the identified downregulated Bd transcripts, five were predicted to be plant targets of Mo ck-sRNAs in the 2 DPI sample, 1128 in the 4 DPI sample, and 10 in the root sample (Tab. 11, Fig. 20).

The predicted Mo sRNA / Bd mRNAs duplexes included genes for transcription factors such as *transcriptional regulator algH* (BdiBd21-3.1G0488800.1) *myb-related protein Zm38* (BdiBd21-3.3G0559800.1) and *NIGTH1* (BdiBd21-3.2G0063400.1), aquaporin transporters (BdiBd21-3.2G0400800.1, BdiBd21-3.5G0237900.1, BdiBd21-3.2G0803500.1, BdiBd21-3.1G0591400.1), as well as RNA helicases (BdiBd21-3.3G0787100.1, BdiBd21-3.1G0041600.1, BdiBd21-3.5G0124000.1, BdiBd21-3.1G0277900.1), including the putative *BdDCL3b* (BdiBd21-3.2G0305700). Additionally, putative resistance genes *RGA3* (BdiBd21-3.2G0771500.1) *RGA4* (BdiBd21-3.3G0396200.1) and *RPP13-like protein 3* (BdiBd21-3.3G0776700.1) were predicted targets during the necrotrophic foliar phase (Tab. 12).

A GO enrichment (GOE) analysis was carried out with AgriGOv2 to detect over-represented features in the dataset from the 4 DPI leaf setup, which covers the necrotrophic growth phase of *Mo*. In particular, generic GO terms associated with metabolic processes (GO:1901564, GO:0043603, GO:0006518), translation (GO:0006412) and RNA processing (GO:0006396, GO:0034470, GO:0006364) were enriched (Fig. 21, Tab. 13).

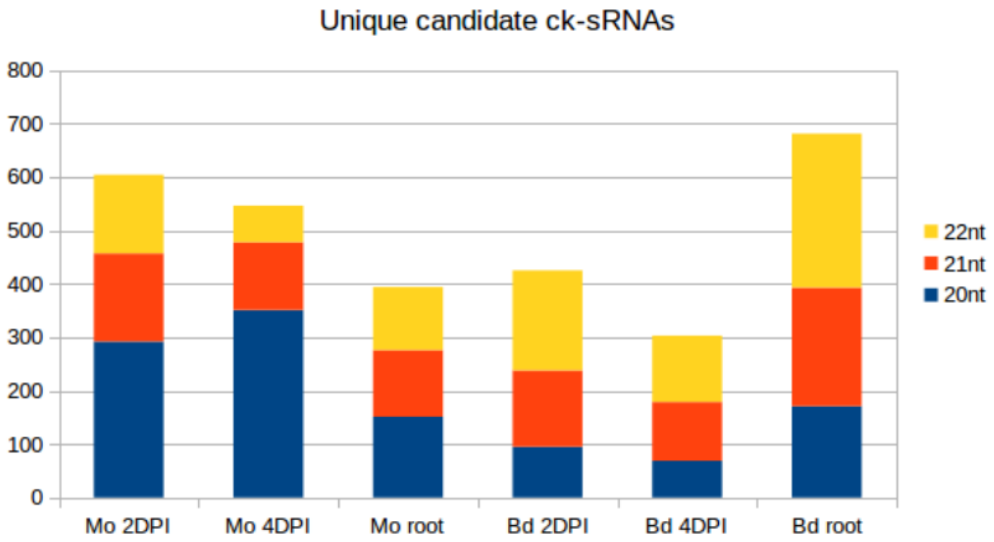

Figure 19. size composition of unique candidate ck-sRNAs in Bd and Mo. The number of unique reads is reported on the y axis ,color code: blue = 20 nt , red = 21nt, yellow = 22nt.

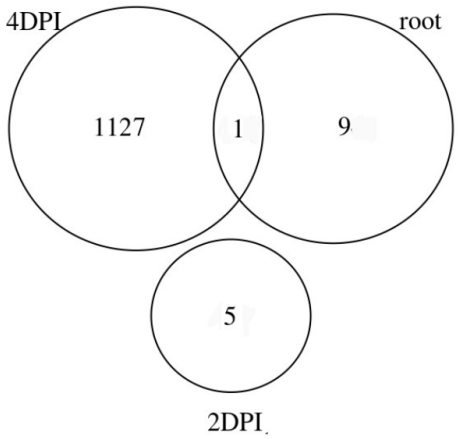

Figure 20. Venn diagram of downregulation Bd targets. Significantly downregulated (FC < 0 padj < 0.05) Bd mRNA targets with complementarity to Mo ck-sRNAs shared between setups: Leaf biotrophic phase (“2 DPI”) Leaf necrotrophic phase (“4 DPI”), and root (“root”). Transcript downregulation was assessed from mRNAseq data with DESeq2.

Table 11. Overview of the number of ck-sRNAs candidates (20-22nt) and their corresponding target mRNAs after target downregulation confirmation (FC < 0, padj < 0.05).

	Setup	Number of ck-sRNA candidates	Number of ck-sRNA candidates with down-regulated targets	Number of targets predicted	Number of targets downregulated	
Mo ck-sRNAs	2DPI	604	7	25106	5	**Bd mRNAs**
	4DPI	546	490	25415	1128	
	roots	394	14	17335	10	
Bd ck-sRNAs	2DPI	424	314	4621	484	**Mo mRNAs**
	4DPI	302	236	4431	527	
	roots	681	263	6730	183	

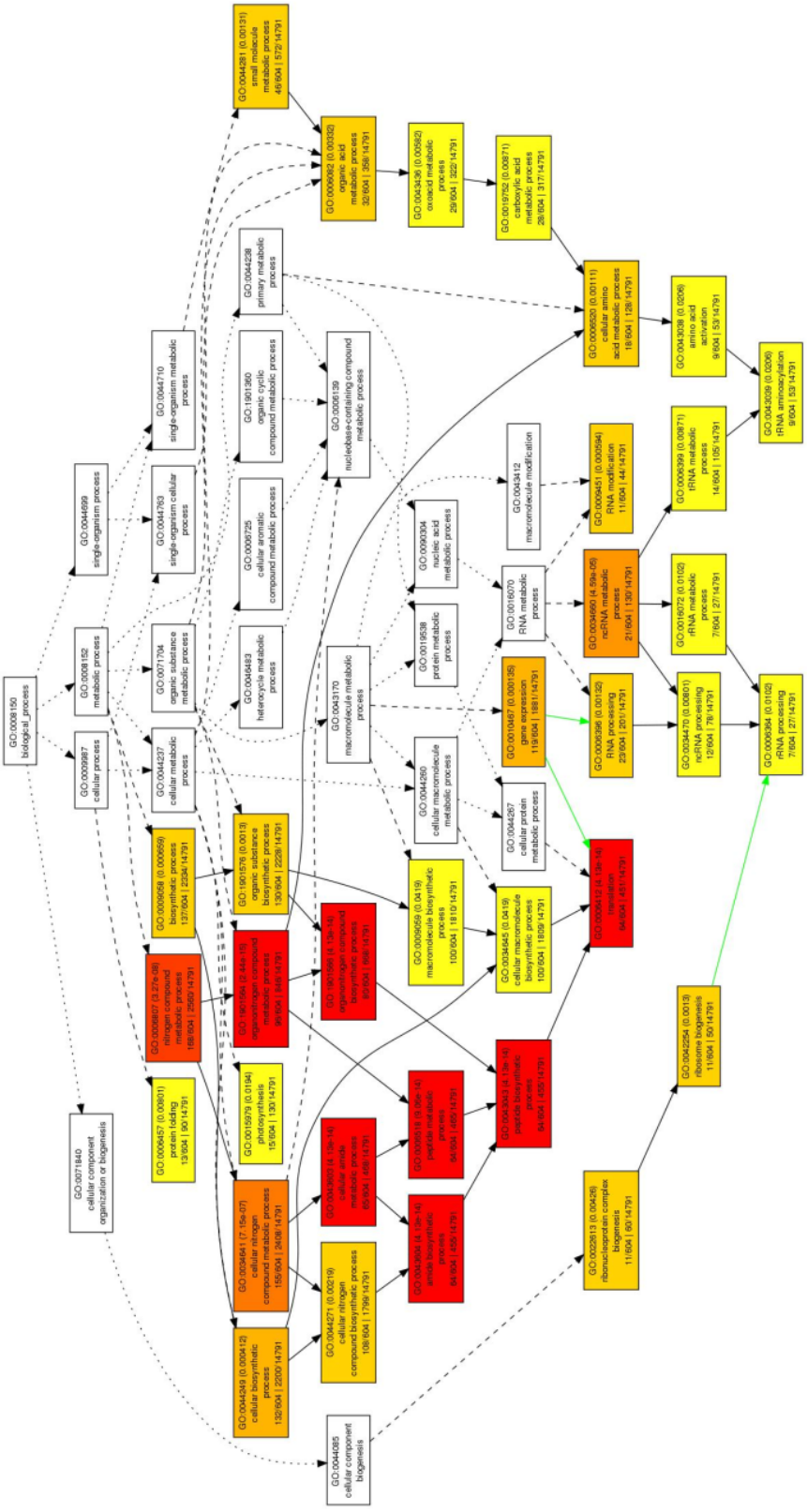

Figure 21. Results of gene ontology enrichment (GOE) analysis for significantly downregulated Bd mRNA targets in the 4 DPI leaf setup. GOE analysis done with AgriGO v2.

Table 12. Selection of *Mo* sRNA / *Bd* mRNA duplexes from the three different setups (leaf 2DPI , leaf 4DPI and root). Abbreviations: RPM = reads per million, I = infected sample, LogRPM = log(RPM I / RPM C), FC = fold change

Setup	sRNA	RPM I	Log RPM	Target	Log FC	Padj	Description
2DPI	TTTCGACGCTG CCCTGACTT	31.9	0.00	BdiBd21-3.4G0610700.1	-1.25	3.04 E-02	probable apyrase 3
2DPI	GGTTATCATCG TCCCAGCCC	15.9	0.00	BdiBd21-3.4G0347500.1	-0.70	1.91 E-02	abscisic stress-ripening protein 3
4DPI	TGGCAGCGGCG CAGGATCTCG	8.5	1.54	BdiBd21-3.5G0309700.1	-1.39	9.87 E-24	ABC transporter B family member 19
4DPI	CAATCGTTGTC TGGCATTGA	83.4	3.03	BdiBd21-3.4G0207200.1	-0.72	2.07 E-09	ABC transporter F family member 5
4DPI	TTGTGTCCAAG CGTTCTGAAA	13.3	1.90	BdiBd21-3.2G0019400.1	-0.88	7.53 E-12	ABC transporter G family member 7
4DPI	TGATTAAGGAG AAGCGGGGG	6.0	4.37	BdiBd21-3.5G0286800.1	-0.95	3.04 E-05	auxin-responsive protein SAUR71
4DPI	TCGCTTTGGCG GCGCGCCGGC	27.8	2.13	BdiBd21-3.1G0937800.1	-1.15	2.60 E-05	cytochrome P450 94B3
4DPI	TCGCACTTCGC GGCGTTGGCG	16.9	2.40	BdiBd21-3.3G0497100.1	-1.11	1.06 E-11	cytokinin dehydrogenase 11
4DPI	TACCGTCGTAG TCTTAACCA	8.5	2.95	BdiBd21-3.1G0041600.1	-1.05	6.26 E-14	DEAD-box ATP-dependent RNA helicase 3
4DPI	AGGGGCTACGA TCTTTGAGAA	18.1	4.26	BdiBd21-3.3G0787100.1	-1.13	2.67 E-10	DexH-box ATP-dependent RNA helicase DExH15
4DPI	TTTCGAGATTG GAAACGGCT	12.1	1.54	BdiBd21-3.2G0305700.1	-0.69	1.79 E-02	Dicer homolog 3b
4DPI	TCGGCGAACGC GACGGGGAA	7.2	3.05	BdiBd21-3.4G0276900.1	-0.93	1.73 E-04	exosome complex component RRP43
4DPI	TAGATCGGTTG GTGTCGGGC	109.9	3.55	BdiBd21-3.1G0507400.1	-0.66	2.46 E-03	GATA transcription factor 21
4DPI	TGACTTTGAGG GTGGCGGGCG	7.2	6.64	BdiBd21-3.5G0103600.1	-0.76	1.24 E-05	nadh-ubiquinone oxidoreductase 39 kda subunit-related
4DPI	TCGGACTAGCG GCAGCGGGT	36.2	3.64	BdiBd21-3.1G0915800.1	-1.10	1.81 E-10	nuclear transcription factor Y subunit C-2
4DPI	TGGGCGGCGGT CATTTCGGC	6.0	2.47	BdiBd21-3.3G0739100.1	-1.86	5.92 E-03	peroxidase 1
4DPI	AGAAGAATTTC ATGCCGGCCAG	8.5	4.86	BdiBd21-3.1G0796400.1	-0.71	3.75 E-03	peroxidase 50

4DPI	CCGGCATGAAA TTCTTCTCGAA	7.2	2.83	BdiBd21-3.1G0093800.1	-0.99	6.95 E-13	photosystem I reaction center subunit III, chloroplastic
4DPI	TAGTAGGGCTG CAAGATCTA	10.9	2.76	BdiBd21-3.5G0116500.1	-0.91	8.39 E-07	photosystem I subunit PsaO
4DPI	TGGCTGTGAAT TCGGCGAGGG	59.2	2.05	BdiBd21-3.5G0237900.1	-0.62	3.16 E-03	probable aquaporin PIP1-2
4DPI	CCAATCGTTGT CTGGCATTGA	105.1	3.75	BdiBd21-3.2G0771500.1	-1.33	3.53 E-02	putative disease resistance protein RGA3
4DPI	TTTCGGATAGA GGCACCCAA	10.9	2.05	BdiBd21-3.3G0396200.1	-0.54	4.20 E-03	putative disease resistance protein RGA4
4DPI	TGCTGCAGCAA CGCTCCGGC	12.1	6.37	BdiBd21-3.4G0303000.1	-0.82	1.18 E-02	receptor protein-tyrosine kinase CEPR2
4DPI	TAGACCGCCTG ACTAAGATG	10.9	2.36	BdiBd21-3.2G0051100.1	-0.90	4.27 E-04	receptor-like protein kinase 5
4DPI	TATCGTCGCGC AGTTGGTCG	7.2	4.31	BdiBd21-3.3G0461000.1	-0.56	2.00 E-02	RNA exonuclease 4
4DPI	TCATTTCGGCG CGGGCTTGT	7.2	3.31	BdiBd21-3.3G0657400.1	-0.53	4.86 E-02	serine carboxypeptidase-like 34
4DPI	TGAGCCGGGG GTATAATCGG	6.0	1.13	BdiBd21-3.4G0029600.1	-0.65	6.06 E-05	stress-induced-phosphoprotein 1
4DPI	TGATTCGGCGG CAGGTCTGGC	14.5	2.24	BdiBd21-3.1G0170300.1	-1.17	1.74 E-02	transcription factor bHLH25
4DPI	TCGGTTTCGGC TTCTGGGGT	10.9	2.47	BdiBd21-3.2G0063400.1	-1.19	3.33 E-02	transcription factor NIGTH1
4DPI	TAAATAATTGG TTGGGGGAG	30.2	2.53	BdiBd21-3.3G0714200.1	-0.96	5.59 E-07	translation initiation factor IF3-4, chloroplastic
4DPI	TAAATACCGTC CCGGCAAGG	9.7	3.88	BdiBd21-3.4G0018600.1	-0.66	2.80 E-02	wall-associated receptor kinase 5
4DPI	TGACGGAGCTC GGCCTGGAA	45.9	2.14	BdiBd21-3.5G0304000.1	-0.90	1.35 E-03	Wound-induced protein
Root	ATCGTCCTAGA CTAGTTGGA	10.4	0.00	BdiBd21-3.2G0492900.1	-1.37	2.36 E-02	peroxidase 30-like
Root	GCATATTGCAG TGTCGGCGGCA	10.4	0.00	BdiBd21-3.2G0521700.1	-0.80	3.87 E-02	vacuolar cation/proton exchanger 1a
Root	TAGGGTGGCCT GAATTATAGT	10.4	6.15	BdiBd21-3.2G0378400.1	-0.74	3.45 E-02	glycine-rich cell wall structural protein 1

Table 13. Selection of significantly enriched Bd GO terms from 4DPI Mo-ck-sRNAs Bd target dataset. GO terms and GOE analysis was done with AgriGO v2 against the pre-compiled Bd reference, after transforming Bd21-3 IDs to Bd21 ones. Abbreviations: P= biological process, F = molecular function, C = cellular component, BG = background, FDR = false discovery rate

GO term	O	Description	Input list	BG/ Ref	p-value	FDR
GO:1901564	P	organonitrogen compound metabolic process	96	846	2.40E-18	2.40E-15
GO:0043043	P	peptide biosynthetic process	64	455	2.50E-16	4.10E-14
GO:1901566	P	organonitrogen compound biosynthetic process	80	668	1.50E-16	4.10E-14
GO:0043603	P	cellular amide metabolic process	65	468	2.50E-16	4.10E-14
GO:0006412	P	translation	64	451	1.70E-16	4.10E-14
GO:0006807	P	nitrogen compound metabolic process	168	2560	2.60E-10	3.30E-08
GO:0034660	P	ncRNA metabolic process	21	130	4.60E-07	4.60E-05
GO:0010467	P	gene expression	119	1881	1.50E-06	1.40E-04
GO:0009451	P	RNA modification	11	44	7.70E-06	5.90E-04
GO:0009058	P	biosynthetic process	137	2334	9.20E-06	6.60E-04
GO:0006520	P	cellular amino acid metabolic process	18	128	1.70E-05	1.10E-03
GO:0042254	P	ribosome biogenesis	11	50	2.20E-05	1.30E-03
GO:1901576	P	organic substance biosynthetic process	130	2228	2.20E-05	1.30E-03
GO:0044281	P	small molecule metabolic process	46	572	2.30E-05	1.30E-03
GO:0006396	P	RNA processing	23	201	2.50E-05	1.30E-03
GO:0044271	P	cellular nitrogen compound biosynthetic process	108	1799	4.40E-05	2.20E-03
GO:0006082	P	organic acid metabolic process	32	358	6.90E-05	3.30E-03
GO:0022613	P	ribonucleoprotein complex biogenesis	11	60	9.30E-05	4.30E-03

GO:0043436	P	oxoacid metabolic process	29	322	1.30E-04	5.80E-03
GO:0034470	P	ncRNA processing	12	78	2.00E-04	8.00E-03
GO:0006457	P	protein folding	13	90	1.90E-04	8.00E-03
GO:0019752	P	carboxylic acid metabolic process	28	317	2.30E-04	8.70E-03
GO:0006399	P	tRNA metabolic process	14	105	2.30E-04	8.70E-03
GO:0016072	P	rRNA metabolic process	7	27	2.90E-04	1.00E-02
GO:0015979	P	photosynthesis	15	130	5.80E-04	1.90E-02
GO:0043039	P	tRNA aminoacylation	9	53	6.60E-04	2.10E-02
GO:0034645	P	cellular macromolecule biosynthetic process	100	1809	1.40E-03	4.20E-02
GO:0005198	F	structural molecule activity	52	330	3.30E-15	9.70E-13
GO:0003735	F	structural constituent of ribosome	51	312	1.70E-15	9.70E-13
GO:0003723	F	RNA binding	48	322	2.50E-13	5.00E-11
GO:0003676	F	nucleic acid binding	119	1815	2.60E-07	3.80E-05
GO:0019843	F	rRNA binding	11	30	3.30E-07	4.00E-05
GO:1901363	F	heterocyclic compound binding	224	4215	4.90E-06	4.10E-04
GO:0016874	F	ligase activity	18	127	1.50E-05	1.10E-03
GO:0016741	F	transferase activity, transferring one-carbon groups	23	224	1.10E-04	6.80E-03
GO:1990904	C	ribonucleoprotein complex	53	363	2.80E-14	1.70E-12
GO:0042651	C	thylakoid membrane	7	34	9.70E-04	1.00E-02
GO:0009654	C	photosystem II oxygen evolving complex	5	23	4.20E-03	4.30E-02
GO:0019898	C	extrinsic component of membrane	5	24	5.00E-03	4.80E-02

3.8 Prediction of plant sRNA effector candidates

Given that plant-derived sRNAs can move into fungal pathogens during plant colonization (Zhang et al., 2016; Cai et al., 2018b), we further explore 20-22 nt sRNAs that i. originate from the non-coding regions of the Bd genome and ii. show a higher read count in the *Mo*-infected compared to non-infected samples (Fig. 19). Target prediction for Bd sRNAs in the Mo transcriptome resulted in 424, 302 and 681 Bd sRNA candidates for the 2 DPI and 4 DPI leaf and root setups, respectively (Tab. 11). The average number of Mo predicted targets per Bd sRNA candidate was the highest at 4 DPI (14.7), compared to 2 DPI (10.9) and root setup (9.9 targets predicted per Bd ck-sRNA). Target downregulation confirmation further reduced the candidate Mo ck-sRNAs to 314, 236 and 263 (2 DPI, 4 DPI and root, respectively), corresponding to 484 targets downregulated during the leaf biotrophic phase, 527 in the necrotrophic and finally 183 in the root setup (Tab. 11).

In the leaf setups, GOE analysis on the Mo targets of Bd ck-sRNAs only highlighted significant differential representation in GO terms at 2 DPI for cellular nitrogen compound metabolic and biosynthetic processes (GO:0034641, GO:0044271) and at 4 DPI for transporters activity (GO:0034641, GO:0044271). The root setup instead showed higher diversity in molecular processes related terms, in particular regarding developmental (GO:0032502, GO:0043581) and metabolic (GO:0008152, GO:0044238, GO:0044237, GO:0019538) processes (Fig. 22, Tab. 14).

Confirmed downregulated Mo targets include cell wall related genes such as *chitin deacetylase 1* (MGG_05023), cell wall protein MGG_09460 and virulence genes such as *CAP20* (MGG_11916) (Tab. 15).

By comparing predicted fungal mRNA targets of Bd ck-sRNAs in infected leaf and root tissue, we found a considerable overlap in significantly downregulated Mo targets between leaf and root samples (42 Mo mRNAs) and between the two leaf setups (140 Mo mRNAs), representing the biotrophic and necrotrophic phase of fungal colonization (Fig. 23).

Next, we searched the PHI-base database for available information on the loss of virulence for the respective potential Mo target genes. A list of down-regulated shared predicted Mo mRNA targets and the PHI-base phenotypes is shown in (Tab. 16). Several

of the identified Mo targets are known to be involved in Mo virulence and pathogenicity, namely *CON7* transcription factor (MGG_05287) targeted in the root setup, the effector molecule *AvrPiz-t* (MGG_09055) targeted in the 4 DPI leaf setup and the vacuolar glucoamylase *SGA1* (MGG_01096) targeted in the 2 DPI leaf setup.

Additionally, targets shared between more than one setup included *N-acetylglucosamine-6-phosphate deacetylase* (MGG_00620), SNARE protein *Sso1* (MGG_04090) and mitochondrial DNA replication protein *YHM2* (MGG_07201), potentially targeted in the 2 DPI leaf and the root setups, and autophagy-related protein *MoATG17* (MGG_07667) targeted in both biotrophic and necrotrophic leaves setups, whose respective mutants are also known to be compromised in pathogenicity (Kershaw and Talbot, 2009; Giraldo et al., 2013)(Tab. 16).

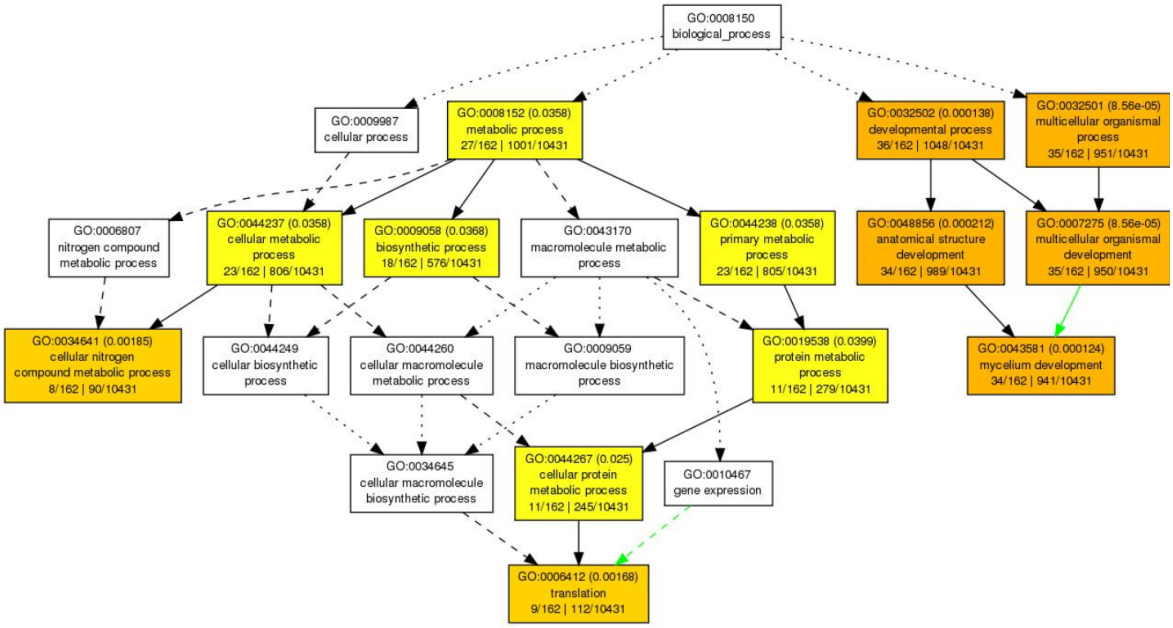

Figure 22. Results of gene ontology enrichment (GOE) analysis for significantly downregulated Mo mRNA targets in the root setup. GOE analysis done with AgriGO v2.

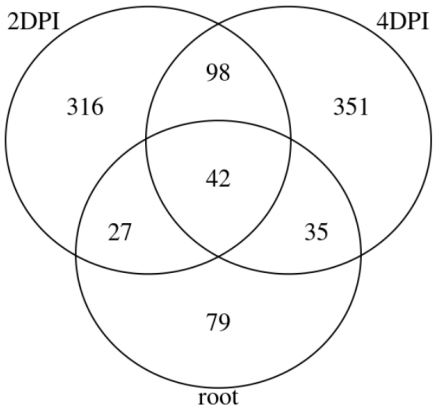

Figure 23. Venn diagram of downregulation Mo targets. Significantly downregulated (FC < 0 padj < 0.05) Mo mRNA targets with complementarity to Bd ck-sRNAs shared between setups: Leaf biotrophic phase (“2 DPI”) Leaf necrotrophic phase (“4 DPI”), and root (“root”). Transcript downregulation was assessed from mRNAseq data with DESeq2.

Table 14. Selection of significantly enriched Mo GO terms from 2DPI, 4DPI and root Bd-ck-sRNAs Mo target dataset. GO terms and GOE analysis was done with AgriGO v2 against the pre-compiled Mo reference. Abbreviations: P= biological process, F = molecular function, C = cellular component, BG = background, FDR = false discovery rate

Setup	GO term	O	Description	Input list	BG/ Ref	p-value	FDR
2DPI	GO:0034641	P	cellular nitrogen compound metabolic process	15	90	1.80E-05	5.50E-03
2DPI	GO:0044271	P	cellular nitrogen compound biosynthetic process	13	86	1.60E-04	2.40E-02
4DPI	GO:0034641	F	substrate-specific transporter activity	13	95	8.90E-04	3.40E-02
4DPI	GO:0044271	F	transporter activity	15	119	7.90E-04	3.40E-02
Root	GO:0007275	P	multicellular organismal development	35	950	1.60E-06	8.60E-05
Root	GO:0032501	P	multicellular organismal process	35	951	1.60E-06	8.60E-05
Root	GO:0043581	P	mycelium development	34	941	3.50E-06	1.20E-04
Root	GO:0032502	P	developmental process	36	1048	5.30E-06	1.40E-04
Root	GO:0048856	P	anatomical structure development	34	989	1.00E-05	2.10E-04
Root	GO:0006412	P	translation	9	112	9.60E-05	1.70E-03
Root	GO:0034641	P	cellular nitrogen compound metabolic process	8	90	1.20E-04	1.90E-03
Root	GO:0044267	P	cellular protein metabolic process	11	245	1.90E-03	2.50E-02
Root	GO:0008152	P	metabolic process	27	1001	3.60E-03	3.60E-02
Root	GO:0009058	P	biosynthetic process	18	576	4.20E-03	3.70E-02
Root	GO:0019538	P	protein metabolic process	11	279	4.90E-03	4.00E-02
Root	GO:0005198	F	structural molecule activity	6	71	1.10E-03	4.70E-03
Root	GO:0003735	F	structural constituent of ribosome	6	65	7.40E-04	4.70E-03

Table 15. Selected *Mo* mRNA targets of Bd ck-sRNA candidates from the three different setups (leaf 2DPI , leaf 4DPI and root). X is assigned if the gene is predicted to be targeted by ck-sRNA candidates in the corresponding setup. Abbreviations; FC = fold change, n.s. = not significant

Predicted target					**LogFC**		
2DPI	4DPI	Root	Target	Description	2DPI	4DPI	Root
X	X	X	MGG_00254	Ornithine decarboxylase antizyme	-1.775	-0.475	-1.633
X	X	X	MGG_02127	Alcohol oxidase	-5.460	-2.534	-3.114
X	X	X	MGG_08692	Alpha-1,2 mannosyltransferase KTR1	-2.298	-1.423	-1.839
X	X	X	MGG_03714	Annexin ANXC4	-1.796	-0.798	-1.365
X	X	X	MGG_06222	CobW domain-containing protein	-7.920	-9.221	-10.137
X	X	X	MGG_02695	Cysteine proteinase 1	-4.725	-1.347	-2.464
X	X	X	MGG_06494	D-arabinitol 2-dehydrogenase	-5.519	-1.161	-3.213
X	X	X	MGG_01245	Endoplasmic reticulum-Golgi intermediate compartment protein 3	-0.895	-0.983	-1.956
X	X	X	MGG_01386	FAD dependent oxidoreductase superfamily protein	-5.186	-2.159	-4.511
X	X	X	MGG_05981	Glutamine amidotransferase subunit pdxT	-4.790	-2.343	-4.252
X	X	X	MGG_14279	Glutamine synthetase	-1.967	-1.167	-2.558
X	X	X	MGG_10400	GPI-anchored cell wall beta-1,3-endoglucanase EglC	-0.987	-2.049	-2.108
X	X	X	MGG_16361	H/K ATPase alpha subunit	-3.974	-3.984	-2.219
X	X	X	MGG_13239	Linoleate diol synthase	-6.991	-2.080	-2.675
X	X	X	MGG_05746	Multidrug resistance protein 1	-4.868	-3.160	-3.867
X	X	X	MGG_08580	Na(+)/H(+) antiporter	-2.506	-0.763	-2.153
X	X	X	MGG_09355	NACHT domain-containing protein	-7.808	-1.417	-5.268
X	X	X	MGG_01906	Nicotianamine synthase 3	-2.799	-4.851	-6.447
X	X	X	MGG_01361	PHO85 cyclin-1	-5.812	-1.270	-2.854
X	X	X	MGG_04787	Tetracenomycin polyketide synthesis O-methyltransferase	-5.378	-3.560	-4.799
X	X	X	MGG_01862	Zinc/iron transporter	-4.110	-1.174	-3.751

	X		MGG_15576	DNA repair protein rhp51	n.s.	-1.050	n.s.
	X		MGG_03587	Essential for mitotic growth	n.s.	-0.602	n.s.
X	X		MGG_04345	Cytochrome P450 17A1	-4.404	-1.056	n.s.
X		X	MGG_03201	Acetyl-coenzyme A synthetase	-1.391	0.865	-1.838
	X		MGG_09950	C2H2 type zinc finger domain-containing protein	n.s.	-1.492	n.s.
	X	X	MGG_16901	ATP-dependent RNA helicase DBP2	n.s.	-1.044	-1.179
X	X	X	MGG_07667	Autophagy-related protein 17	-2.452	-1.334	n.s.
X	X	X	MGG_01391	Ent-kaurene oxidase	-3.895	-2.445	n.s.
X	X	X	MGG_01624	Fungal specific transcription factor domain-containing protein	-3.746	-3.880	n.s.
X	X	X	MGG_11962	G-protein coupled receptor	-5.753	-3.422	n.s.
X	X	X	MGG_04378	Integral membrane protein	-3.992	-1.043	n.s.
X	X	X	MGG_04935	Integral membrane protein	-3.580	-1.398	n.s.
X	X	X	MGG_11754	SMDR1	-6.757	-2.330	n.s.
X	X	X	MGG_03123	MATE efflux family protein subfamily	-4.685	-1.112	n.s.
X	X	X	MGG_14872	Calpain-9	-4.189	-1.174	n.s.
X	X	X	MGG_09460	Cell wall protein	-4.724	-3.916	n.s.
X	X	X	MGG_09460	Cell wall protein	-4.724	-3.916	n.s.
X	X	X	MGG_03186	1,4-alpha-glucan-branching enzyme	-1.522	n.s.	-1.356
X	X	X	MGG_14154	RETRO5, retrotransposons MoTeR1s and MoTeR2	-6.040	-1.146	n.s.
X	X		MGG_08072	Cholesterol oxidase	-4.403	n.s.	n.s.
X		X	MGG_06393	Serine/threonine-protein kinase ATG1	-3.243	n.s.	n.s.
	X	X	MGG_04938	C-3 sterol dehydrogenase/C-4 decarboxylase	n.s.	-1.848	n.s.
X	X	X	MGG_10568	Sterol 24-C-methyltransferase	n.s.	n.s.	-1.241
X		X	MGG_06371	Pyruvate dehydrogenase E1 component subunit alpha	n.s.	n.s.	-1.755

Table 16. Mo ckRNAi predicted targets with known infection-impaired phenotypes in the corresponding KO mutants. Information derived from PHI-Base search.

Transcript ID	Gene ID	Gene function	Phenotype	Host species	Reference Phi-Base
MGG_00063T0	AGL1	glycogen debranching enzyme	reduced_virulence	Os_Hv	PHI:3814
MGG_00365T0	MAGB	G alpha protein subunit	reduced_virulence	Os	PHI:83
MGG_00620T0	Dac	GlcNAc-6-phosphate deacetylase	reduced_virulence	Os	PHI:5471
MGG_01096T0	SGA1	vacuolar glucoamylase	loss_of_pathogenicity	Os_Hv	PHI:2138
MGG_01180T0	SCAD3	Short-chain specific acyl-CoA dehydrogenase	reduced_virulence	Os_Hv	PHI:8929
MGG_01285T0	Tpc1	Transcription factor for Polarity Control 1	reduced_virulence	Os_Hv	PHI:7317
MGG_01819T0	Gph1	Phosphorylase	loss_of_pathogenicity / reduced_virulence	Os_Hv	PHI:2062 /3815
MGG_02444T0	PLC1	modulator of calcium flux	loss_of_pathogenicity	Os	PHI:2057
MGG_02457T0	RHO2	Rho GTPase	reduced_virulence	Os	PHI:8752
MGG_02884T0	FLP1	fasciclin-like protein	reduced_virulence	Os_Hv	PHI:4231
MGG_03148T0	TDG4	Trigalactosyldiacylglycerol-4	reduced_virulence	Os_Hv	PHI:3811
MGG_03198T0	TIG1	Histone Deacetylation	loss_of_pathogenicity	Os_Hv	PHI:2002
MGG_03451T0		uncharacterized	reduced_virulence	Os	PHI:795
MGG_03670T0	SPM1	Subtilisin-like proteinase Spm1	reduced_virulence	Os_Hv	PHI:2117
MGG_03860T0	TPS1	Trehalose-6-phosphate synthase	loss_of_pathogenicity / reduced_virulence	Os_Hv	PHI:322/ 1064
MGG_04895T0	ICL1	Isocitrate lyase	reduced_virulence	Os	PHI:305
MGG_05344T0	SM1	effector	increased_virulence	At	PHI:2118 /5540
MGG_05631T0	Ngt1	GlcNAc transporter	reduced_virulence	Os	PHI:5470
MGG_05871T0	PTH11	CFEM domain-containing protein	reduced_virulence	Os_Hv	PHI:2165 /404
MGG_05905T0	PLC1	Phospholipase C	reduced_virulence	Os_Hv	PHI:2107
MGG_06263T0	YPEL1	Yippee domain-containing protein	loss_of_pathogenicity	Os	PHI:8522

MGG_06393T0	ATG1	Autophagy-related protein 1	loss_of_pathogenicity	Os_Hv	PHI:2035 /2069/86 12
MGG_06971T0	SFl1	Flocculation suppression protein	reduced_virulence	Os	PHI:2178
MGG_07312T0	SLN1	Osmosensing histidine protein kinase SLN1	loss_of_pathogenicity / reduced_virulence	Os_Hv	PHI:2200 /3163
MGG_07667T0	atg17	Autophagy-related protein 17	loss_of_pathogenicity	Os_Hv	PHI:2083
MGG_08054T0	Chi1	Chitinase 1	reduced_virulence	Os_Hv	PHI:8753 /8806
MGG_08370T0	gel3	1,3-beta-glucanosyltransferase	loss_of_pathogenicity	Os	PHI:6713
MGG_08556T0	VEA	Developmental and secondary metabolism regulator veA	reduced_virulence	Os	PHI:4113
MGG_09471T0	NTH1	Neutral trehalase	reduced_virulence	Os_Hv	PHI:123/ 775/794
MGG_10859T0	LDS1	heme peroxidase	reduced_virulence	Os	PHI:5189
MGG_11862T0	ABC4	ABC Transporter	reduced_virulence / loss_of_pathogenicity	Hv	PHI:1017 /2067
MGG_12122T0	GSK1	Glycogen synthase kinase 1	loss_of_pathogenicity	Os_Hv	PHI:7117
MGG_12814T0	MoAP1	BZIP domain-containing protein	loss_of_pathogenicity	Os_Hv	PHI:2142
MGG_17909T0	ATG3	Autophagy-related protein 3	loss_of_pathogenicity	Os	PHI:2071
MGG_05287T0	CON7	transcription factor CON7	loss_of_pathogenicity	Os_Hv	PHI:2039
MGG_09055T0	AvrPiz-t	Avrpiz-tgene, effector protein	increased_virulence	Os	PHI:7896

4. Discussion

4.1 MoAGOs and MoDCLs

In parallel with the work done to elucidate the function and 3D structure of *Brachypodium distachyon* AGO and DCL proteins published in Šečić et al., (2019), I set out to investigate these RNAi machinery components in *Magnaporthe oryzae*. Contrary to the purple false brome, Mo has being extensively studied as a model for RNAi in fungi, and it is known to encode 3 AGOs, 2 DCLs and 3 RdRP (Kadotani et al., 2003; Murphy et al., 2008). Additionally, KO mutants of these genes have been characterized both for their sRNA accumulation patterns and their virulence (Raman et al., 2013;2017), confirming the key roles played by MoAGO3, MoDCL2, MoRdRP1 and MoRdRP2 in these processes. Interestingly, while the phylogeny with other fungal RNAi machineries (e.g *Neurospora crassa*, *Mucor circinelloides*, *Cryphonectria parasitica* and *Schizosaccharomyces pombe*) and the domain conservation have been reported, I found no information regarding the proteins' predicted interactome, subcellular localization or 3D structures. Hence, I first reproduced the preliminary identification steps, including phylogenetic analysis with known fungal RNAi AGOs and DCLs (Fig. 4), domain conservation assessment (Fig. 5) and QF-V motif and catalytic tetrad (DEDD) presence (Fig. 6). All 3 AGOs have the characteristic PAZ (Piwi Argonaut and Zwille) and Piwi (P-element Induced WImpy testis) domains: the first is involved in the recognition of the 3' end of the guide sRNA molecule (Cenik and Zamore, 2011), while the second is an RNase H domain that confers AGOs the ability to cleave single stranded RNAs complementary to the guide sRNA sequence (Song et al., 2004). A closer look at the Piwi domains via MSA (Multiple sequence alignment) confirmed the conservation of both the QF-V motif, involved in the sorting of sRNAs based on their sequence and secondary structure (Zhang et al., 2014) and the DEDD catalytic tetrad, critical for the protein 'slicer' activity (Song et al., 2004). Similar to NcDCLs, both MoDCLs lacked predicted PAZ domain but differed from the *N. crassa* ortholog showing predicted dicer dimer domains and lacking predicted dsRNA-specific ribonuclease and ds-RNA binding (DSRM) domains (Raman et al., 2017). At this point of the analysis, no major differences were recorded among either Mo protein families, which would help elucidate the clear differences in both sRNA production and virulence reported in the RNAi KO

components by Raman et al., (2017). Interestingly, protein subcellular localization helped shed additional light on MoAGO3 and MoDCL2 non-redundant roles, with MoAGO3 predicted to localize exclusively in the nucleus, compared to MoAGO1, predicted in both the nucleus and the cytosol, and MoAGO2, predicted to localize in the cytosol and plastid (Tab. 2). MoDCL2 was predicted to exclusively localize in the cytosol, while MoDCL1 in the nucleus, confirming the possibility of distinct roles for these proteins in contrast with their redundant function of NcDCLs (Katodani et al., 2008). Interestingly, predicted interactomes of MoAGOs showed significant differences between MoAGO1 and MoAGO2 and 3, which would point to a unique role of this protein, not yet investigated. Specifically, the predicted interaction with a ATP-dependent RNA helicase DED1 (MGG_02762) and a Pumilio-family RNA binding repeat protein (MGG_03158) would suggest a unique role for MoAGO1 in translation regulation (Chuang et al., 1997; Spassov et al., 2003).

4.2 Mo virulence gene expression and DEG GO enrichment

GOE analysis of differentially expressed Mo genes highlighted an enrichment of terms mainly related to fungal growth and development throughout the setups, with the addition in the root setup of terms related to interactions with other organisms, in particular via protein secretion. By checking the gene expression of specific effectors, we confirmed the upregulation of know AVR genes, including AVR Pita1 (encoding for a metalloprotease) and PWL2 (a glycine-rich protein recognized by weeping lovegrass and finger millet R proteins), highly upregulated in the foliar biotrophic phase and Avr-Pik/km/kp, upregulated at both leaf infection time-points (Zhang & Xu, 2014).

Genes involved in appressoria and penetration peg functionality were found upregulated in all three setups, such as the WISH (Water wettability, Infection, Surface sensing and Hyper-conidiation) G-protein coupled receptor protein, whose KO renders the mutant unable to develop appressoria and establish the infection on intact rice leaves (Sabnam & Barman, 2017) and superoxide-generating NADPH oxidases NOX1 (MGG_00750) and NoxD (MGG_09956). NOX1 is involved in cell wall biogenesis, affecting both chitin and melanin biosynthesis and deposition, and KO of this gene resulted in a complete loss of appressorium-mediated cuticle penetration and failed *in planta* proliferation even when inoculated onto wounded rice seedlings (Egan et al., 2007). Similar defects were

detected in rice leaves and roots inoculated with *ΔnoxD* (Galhano et al., 2017), confirming the key role played by NOX proteins not only in its growth and sexual reproduction but also in fungal virulence. PLC3, significantly upregulated at both foliar time-points in our analysis, is also required for normal conidiation and appressorium function, but contrary to NOXs, normal infection was observed when *moplc3* was inoculated by infiltration into wounded rice leaves, excluding a function of PLC3 in fungal growth once inside host cells (Choi et al., 2011). As expected, we detected in the later time-point the upregulation of genes known to be required for the infection maintenance and expansion, including S-(Hydroxymethyl)glutathione dehydrogenase (MGG_06011), exclusively found upregulated in the 4 DPI foliar dataset and proven to be involved in the infection rate and growth of infectious hyphae on barley leaves (Zhang et al., 2015).

Overall, this analysis shows an extensive reprogramming that the fungus undergoes during the establishment and maintenance of the infection and highlights the commonalities and differences in expression patterns depending on the inoculated tissue and the progression of the colonization. Consistent with the detection of necrotrophic lesions on Bd roots, we confirmed that the Mo gene expression reprogramming during the root infection is closer to the one reported in the foliar necrotrophic phase (with 701 DEG shared between the setups) compared to the biotrophic phase (only 392 DEG shared between the setups).

4.3 Bd genes upregulated during Mo infection

mRNA sequencing of both infected and non-infected Brachypodium leaves (at two time-points) and root samples allowed for a systemic analysis and comparison of expression pattern alterations of Bd genes in response to rice blast. As expected, the highest amount of DE genes was observed at 4 DPI in the leaves setup, when the infection is spreading outside of the inoculation point and the fungus has switched to a more aggressive necrotrophic lifestyle. The relatively low amount of differentially expressed genes in the other two setups is consistent with the early infection stages and the limited presence of fungal mass both in the root and the 2 DPI leaf samples. Additionally, in all three setups the percentage of genes upregulated out of all DEG was higher than the downregulated, with 96% DEG being upregulated at 2 DPI, 60.7% at 4 DPI and 69.5% in the root setup,

indicating a widespread induction of gene expression. To determine the function of these DE genes subsets, gene descriptions and GOE analysis were investigated. Consistent with the highest numbers of DEG detected at 4 DPI, most GO terms reported in Table 17 belong to this dataset, with terms related to metabolic and biosynthetic processes being the most prevalent. Interestingly, all datasets had enriched terms related to oxidoreductase activities (GO:001649) confirmed also by the upregulation of BdiBd21-3.4G0171000, coding for a multicopper oxidase, in all setups, and BdiBd21-3.1G0233800 and BdiBd21-3.1G0233900, coding for a peroxidase, in the 4 DPI leaves datasets. Peroxidases are commonly associated with plant responses to stress and specifically fungal infection, as they are involved in a variety of processes including the synthesis of compounds toxic for pathogens (phenols such as tanins and melanins), ROS removal, lignin biosynthesis and induction of defense responses by stimulating intracellular Ca^{2+} signaling (Kawano, 2003). Another gene upregulated in all three setups is a secologanin synthase-like (BdiBd21-3.2G0563800), an enzyme involved in the biosynthesis of monoterpenoid indole alkaloids (MIAs), also reported upregulated in Brachypodium following *F. pseudograminearum* infection (Powell et al., 2017). Other known defense-related genes expression levels were found upregulated in one or more of our datasets, including: known pathogenesis-related proteins (BdiBd21-3.2G0114800, BdiBd21-3.1G0165000, BdiBd21-3.4G0068000, BdiBd21-3.4G0043000, BdiBd21-3.1G0772600, BdiBd21-3.1G0772700, BdiBd21-3.3G0422200, BdiBd21-3.3G0639500), receptor kinases (BdiBd21-3.4G0554000, BdiBd21-3.1G0774200, BdiBd21-3.2G0545400, BdiBd21-3.3G0144800, BdiBd21-3.1G0773700, BdiBd21-3.2G0632400, BdiBd21-3.2G0663500), transcription factors (BdiBd21-3.2G0688100, BdiBd21-3.2G0615100, BdiBd21-3.3G0652700, BdiBd21-3.3G0652800, BdiBd21-3.3G0669400, BdiBd21-3.1G0054700, BdiBd21-3.1G0780100) and ABC transporters (BdiBd21-3.3G0465100, BdiBd21-3.3G0464900, BdiBd21-3.2G0605400, BdiBd21-3.2G0605600, BdiBd21-3.2G0550500). Once again, 2 DPI and root samples were found overlapping in only a few of these genes. Examples of genes consistently found upregulated in all three setups are BdiBd21-3.3G0144800, encoding a protein kinase xa21 which confers resistance to *Xanthomonas oryzae* pv. *oryzae* race 6 (Song et al., 1995), an ABC transporter A family member 2-like (BdiBd21-3.3G0465100) and the pleiotropic drug resistance protein 3-like (BdiBd21-3.2G0550500).

Interestingly, all PR proteins mentioned in Table 5 were detected upregulated at 4 DPI in the foliar infection, while 2 DPI and root PR protein expression patterns did not overlap, with only two (BdiBd21-3.2G0114800 and BdiBd21-3.1G0165000) upregulated at 2 DPI, and three (BdiBd21-3.4G0068000, BdiBd21-3.1G0772600, BdiBd21-3.1G0772700) in the root datasets. Similarly, the strongest and most widespread upregulation in the other pathogen sensing / defense-related genes was observed at 4 DPI, with an upregulation of transcription factors belonging to MYB, WRKY and NAC families consistent with the upregulation observed in Bd after *F. pseudograminearum* infection (Powell et al., 2017) and the knowledge that these families regulate a variety of plant responses, including to biotic stresses (Ambawat et al., 2013; Bakshi et al., 2014; Murozuka et al., 2018). In line with the considerable overlap in Mo gene expression patterns between 4 DPI leaf and root setups, majority of genes found upregulated in Bd roots (80.9%) are also detected upregulated in the foliar necrotrophic datasets, compared to 18% shared with the 2 DPI samples. Altogether, these results highlight differences in the upregulation of specific protein family members depending on the infected tissue and fungal lifestyle, while confirming the relevance of these families upregulation in response to Mo infections.

4.4 Bd endo-sRNA (miRNA) induced by Mo infection

Candidate Bd miRNA-generating loci were identified with Shortstack from both control and infected filtered sRNA datasets. Given that the program-assigned cluster IDs are specific to the dataset analyzed and are not comparable between different files, we compared clusters based on their genomic coordinates, and further analyzed loci from the infected sample that had higher RPM (reads per million) than in control, or that were found exclusively in the presence of Mo. This resulted in the identification of 12 miRNA stem loop precursor sequences and 17 mature miRNAs across setups. Additional to their known roles as abiotic stress regulators, we predicted with psRNATarget several candidate transcript targets, and assessed their downregulation from our DGE data.

Specifically, we identified five mature miRNAs belonging to the MIR156 family, shown to be induced by *F. oxysporum* in *Persicaria minor* (Samad et al., 2016) and known to be induced by environmental stresses, resulting in the cleavage of a SPL transcription factor and overall modulation of anthocyanin biosynthesis (Cui et al., 2014, Jeong et al., 2013).

Bd-MIR529, also predicted to target this gene, was found upregulated at 4 DPI in our datasets. Another miRNA involved in the plant response to abiotic stresses is miR159b, found upregulated during Mo leaf infection at both time-points (2 and 4 DPI), and known to be targeting two MYB transcription factors in cucumber (*CsGAMYB1* and *CsMYB29*-like), involved in ABA signalling (Li et al., 2016). Finally, four additional miRNA families were detected as induced by Mo infection (MIR9484, miR9481b, MIR531 and miR7723a). While cleavage sites were detected by Jeong et al., (2013) for miR9481b, MIR9484, Bdi-miR168, Bdi-miR529, Bdi-miR159b, Bdi-miR156b-i, we only detected successful downregulation of some predicted targets, which could be due to an antagonistic upregulation of these genes via other mechanisms under our conditions.

4.5 Clues for the involvement of ck-sRNAs in the communication between Mo and Bd

To establish the origin of the sRNA reads detected in the different root and leaf setups of the Mo-Bd interaction, sRNAseq datasets from infected samples were aligned to both the Bd *21-3* and the Mo 70-15 genome. Only reads aligning without mismatches to Mo and with at least two mismatches to Bd were assigned to the fungus and vice-versa, only reads aligning without mismatches to Bd and with at least two mismatches to Mo were assigned to the plant. As expected from the low amount of Mo in infected samples from leaves at 2 DPI, most of the reads were assigned to Bd, whereas higher levels of Mo reads were detected at 4 DPI (leaf) consistent with proliferating infection. All assigned reads were then filtered based on their read counts to select only reads either induced or upregulated in the datasets of infected tissues compared to uninfected tissues and axenic mycelia. We noted that most of the reads (>50%) found in infected samples are specific and are not detected in healthy tissues and axenic culture (Fig. 17), showing that sRNA production both in the plant and the fungus is strongly responsive to infection. It follows that sRNA datasets from healthy plants and axenic fungal culture do not represent the full diversity of infection-related sRNA communities. As an additional step, we selected for sRNAs that were not aligning to the coding sequences of the organism of origin. The reasoning behind this filtering step is that we avoided accidental mRNA degradation to be kept as candidate ck-sRNAs, and more important, we removed the sRNA sequences more likely to play an endogenous role. Given that the size distribution of

upregulated/induced sRNA reads did not show variation in peaks compared to the total sRNA reads (Fig. 16), we decided to select 20-22nt sRNAs (canonical length range for PTGS) for further analysis. Target prediction was carried out with psRNATarget, a web-based prediction software specifically designed for plant sRNA investigations. It allowed for the identification of complementary mRNA sequences in the interacting organism. In PTGS, sRNAs are loaded onto AGO proteins, which guide them towards a complementary mRNA sequence that will then be degraded or sequestered, resulting in reduced levels of the encoded protein. Knowing the expression levels of the predicted targets from the same biological samples used for the sRNA sequencing, we proceeded with further selection of candidate sRNAs based on the significant downregulation of their mRNA targets. Most of the predicted Mo ck-sRNAs in the 2 DPI leaf (biotrophic phase) and root samples did not pass this filtering step, as their predicted targets were either upregulated or had the comparable expression levels in the corresponding control datasets. There are a few possible explanations as to why the potential targets would not be significantly downregulated in our mRNAseq datasets, including: i. the sRNA has not yet been transported throughout the tissue, so the downregulation is occurring only at the penetration site, where the fungus is physically interacting with the plant cells, and that is masked by the upregulation in distal parts of the tissue, ii. the target mRNA is not cleaved, but its translation is inhibited by the RISC complex acting as a physical barrier, in which case the measurable effect would not be at the mRNA level but only at the protein level, and iii. the target is indeed cleaved, but concurrently with the downregulating effect of the sRNA, there is a stronger endogenous upregulation of the gene, leading to either similar levels of mRNA as the control, or even higher.

4.6 Prediction of Bd ck-sRNAs

We anticipated the plant to fight the spread of the infection by targeting fungal metabolism/ virulence genes of *Mo*. To test this hypothesis, all confirmed downregulated Mo targets from leaves and roots were analyzed for gene ontology enrichment (GOE). While only two terms were found to be enriched in the 2 DPI and 4 DPI leaf samples, related to cellular nitrogen compound metabolic and biosynthetic processes (biotrophic phase) and transporters activity (necrotrophic phase), several metabolism and mycelia

development related terms were enriched in the root downregulated target list, consistent with the aforementioned hypothesis.

Comparison of Mo mRNA target lists between the different setups highlighted substantial target conservation between the leaf biotrophic and necrotrophic phases, with 140 shared Mo targets between the two, and 42 Mo targets conserved among all three setups. Subjecting the shortlisted Mo target genes to a PHI-base database survey for mutations in Mo with lethal or detrimental outcome, we found clear indication for a reduction or loss of virulence in respective KO mutants (Tab. 16). Specific predicted targets confirmed downregulated during the interaction included MoATG17 (MGG_07667) an autophagy-related protein, whose KO was previously shown to impair appressorium formation and function, resulting in a complete lack of disease symptoms on rice leaves (Kershaw and Talbot, 2009). Similarly, MoATG1 (MGG_06393) was also predicted to be targeted by Bd ck-sRNAs and downregulated at 2 DPI, with *Mgatg1* mutant reported to be unable to infect rice and barley leaves by Liu et al., (2007). Additionally, we predicted sRNAs targeting the mRNA encoding the avirulence effector molecule AvrPiz-t (MGG_09055). AvrPiz-t suppresses rice PTI signaling pathway by targeting the E3 ubiquitin ligase APIP6 and suppressing its ligase activity, resulting in reduced flg22-induced ROS generation and overall enhanced susceptibility *in vivo* (Park et al., 2012).

Interestingly, we detected Calpain-9 to be targeted in all three datasets and significantly downregulated in the foliar ones, both at 2 and 4 DPI. While downregulation in the root setup did not reach a significant padj value, targeting of this transcript would match the finding in the cotton-*V. dahliae* pathosystem, where the host was found to be expressing and exporting miRNAs to the infecting fungus to inhibit its virulence via the targeting of *Clp-1* (Zhang et al., 2016).

Additional predicted targets included integral membrane proteins (MGG_04378T0, MGG_04935T0), ergosterol biosynthesis enzymes (ERG6, MGG_10568T0; ERG26, MGG_04938T0) and fungal cell wall related genes such as GPI-anchored cell wall beta-1,3-endoglucanase EglC (MGG_10400T0, targeted and significantly dowregulated in all three datasets), cell wall protein MGG_09460T0 (targeted and significantly downregulated in both foliar samples), chitin deacetylase (MGG_08774T0), and chitinase 1 (MGG_08054T0). Targeting fungal membrane components and ergosterol homeostasis has already being proven to be a successful strategy in crop protection

against fungal pathogens, both via the application of DMI fungicides (sterol demethylation inhibitors) and with the RNAi-based HIGS (Host-Induced Gene Silencing) and SIGS (Spray Induced Gene Silencing) approaches, where artificial sRNAs are introduced in the plant either via transformation or external application are then transferred to the fungal cells during infection (Koch et al., 2013; 2016; 2019). It is interesting to observe how the plant appears to have naturally evolved to produce sRNAs potentially able to target fungal essential and pathogenicity related genes. However, Mo is still able to progress its infection both in Bd leaves and roots, and the most likely factors behind this fungal success are the countermeasures it employs in this crosstalk, from the extensive reprogramming of gene expression to the release of effectors and sRNAs.

4.7 Prediction of fungal sRNA effectors

In order to substantiate the hypothesis that fungal ck-sRNAs function as effectors to aid the establishment and maintenance of infection, we investigated the role of putative downregulated Bd targets. Due to the low numbers of confirmed downregulated Bd targets in the 2 DPI leaf and root samples, we performed Gene Ontology Enrichment (GOE) only on the downregulated targets of the 4 DPI sample to assess whether specific functions or pathways were targeted in Bd by Mo sRNAs.

Interestingly, enriched GO terms spanned from gene expression (GO:0010467), to translation and RNA processing (GO:0006412; GO:0006396) and peptide and organic substance biosynthetic process (GO:0043043;GO:1901576), indicating a clear “intent” to modulate on all levels the metabolic and biosynthetic reprogramming that host plants utilize in response to infections. Additionally, GO terms associated with ribosomes (GO:0005840; GO:0019843) and the photosystems (GO:0042651; GO:0009654) were enriched in the target list compared to background, consistent with the hypothesis that Mo targets energy and metabolism of the plant to hinder its response to infection. Targeting conserved sequences such as ribosome- and photosynthesis-related ones, and hampering gene expression and biosynthetic processes would prove to be a more effective strategy than specific defense / immunity genes, which are more prone to mutate in the arms race between plants and pathogens.

We confirmed the targeting of a variety of RNA helicases genes, including BdDCL3b (BdiBd21-3.2G0305700), identified in our recent work (Šečić et al., 2019) and predicted to be involved in the preprocessing of sRNA precursor molecules involved in chromatin modification (Margis et al., 2006). Specific plant targets included extracellular vesicle and exosome components (BdiBd21-3.4G0276900.1) that have been recently discussed as the most likely mean of transport vehicle for ck-sRNAs and usually cargo plant defense molecules to the infecting fungus (Rutter and Innes, 2017; Baldrich et al., 2019; Cai et al., 2018b).

Another subset of downregulated target transcripts included gene families known to be involved in the plant response to both biotic and abiotic stresses, including hormones responsive proteins (BdiBd21-3.5G0286800.1, BdiBd21-3.4G0347500.1), transcription factors such as members of the GATA bHLH families (BdiBd21-3.1G0507400.1, BdiBd21-3.1G0170300.1), peroxidases (BdiBd21-3.3G0739100.1, BdiBd21-3.1G0796400.1, BdiBd21-3.3G0559700.1, BdiBd21-3.2G0492900.1), disease resistance proteins (BdiBd21-3.2G0771500.1, BdiBd21-3.3G0396200.1) and ABC transporters (BdiBd21-3.5G0309700.1, BdiBd21-3.4G0207200.1, BdiBd21-3.2G0019400.1) (Ambawat et al., 2013; Feller et al., 2011; Kang et al., 2011; Powell et al., 2017). Interestingly, *Brachypodium* aquaporins (BdiBd21-3.5G0237900.1) were also found downregulated and potential targets of Mo sRNAs during the infection, consistent with the knowledge that aquaporins play a role in the interaction between plants and microbial pathogens, most likely by modulating both H_2O availability and transport of reactive oxygen species (ROS; Afzal et al., 2016).

Altogether, the detection of several potential Mo ck-sRNAs with corresponding Bd targets involved in the plant response to biotic and abiotic stress is a first indication of their possible function as effector-like molecules in this pathosystem and paves the way for further validation of selected ck-sRNA/mRNA interactions, including: *i.* proof of target cleavage via RACE or degradome sequencing; *ii.* verification of sRNA-target interaction in transient expression systems such as leaves of *Nicotiana benthamiana*; *iii.* mutational knockdown (KO) strategies of target genes and/or precursor loci of candidate ck-sRNAs; and *iv.* detection of direct association of ck-RNAs or their target mRNA with the respective microbial or plant AGO1-like protein by immunopurification techniques (Riley et al., 2012; Carbonell, 2017).

5. Conclusions

In the present work we analyzed and characterized the interaction between *Brachypodium distachyon* and *Magnaporthe oryzae* at different fungal lifestyles and infection sites, both from a transcriptomic and sRNA expression profiles point of view. The pathosystem has been studied as a model for the effect of blast disease on staple crops leaves (e.g. rice, wheat and barley), owing to Bd's short maturation phase, its smaller genome and space-saving production (Routledge et al., 2004; Parker et al., 2008; Vogel et al., 2006). Beside foliar infections, we also established and characterized the interaction and responses to Bd root colonization by *Mo*. Additional to the confirmation of the extensive reprogramming in both organisms throughout the interaction, our results support the possibility that major staple crops co-evolved mechanisms of RNA-based communication with their microbial pathogens. This notion is consistent with earlier observations that cereal plants are vastly amenable to biotechnological applications of dsRNA to control their pests and diseases (Koch et al., 2013; 2016; 2019; Cheng et al., 2015; Chen et al., 2016). Based on concomitant deep sequencing of mRNA and sRNA fractions, our work provides first indication of both plant and fungal sRNAs involvement in the communication between *Magnaporthe oryzae* with the model grass *Brachypodium distachyon*, further supporting the theory of ckRNAi participation in plant - pathogen interactions. Interestingly, sRNAs induced during infection setups show only partial overlap both among the different tissues (leaves, roots) and the different infection phases (leaf: biotrophic, necrotrophic), raising the possibility that ckRNAi in a given host - pathogen interaction exhibits tissue- and lifestyle-specificity.

6. Abstract

Magnaporthe oryzae (Mo) is the causal agent of one of the most economically relevant diseases of rice, rice blast, and has been extensively studied as a model Ascomycetes. In addition to colonizing rice aerial parts, Mo is also capable of infecting root tissues and has a wide range of Poaceae hosts, including *Brachypodium distachyon* (Bd). Recently, it has been suggested that beside protein effectors, fungi produce small (s)RNAs that can be secreted and exchanged with the infected organism in order to silence genes directly associated with the outcome of the infection, a process termed cross-kingdom RNAi (ck-RNA). At the same time, the infection is known to induce sRNA expression in the host, with a subset of them potentially transported to the pathogen to target pathogenicity/virulence genes, resulting in a bidirectional RNAi-based cross-talk between the interacting organisms.

In the present work I examined tissue specific mRNA and sRNA expression profiles in Mo-Bd interaction in order to characterize the pathosystem and shed further light on the crucial role that sRNAs play in the establishment and maintenance of fungal infection. By comparative deep sequencing of sRNAs and mRNAs from axenic fungal cultures and infected leaves and roots, I found a wide range of fungal sRNAs that accumulated exclusively in infected tissues. Among those, 20-22 nt candidate sRNAs were predicted *in silico* by selecting Mo reads that had predicted targets in the Bd transcriptome for a possible cross-kingdom function. Vice versa, we found that during the infection Bd produces sRNAs not only to fulfill an endogenous function, but also to target a variety of fungal transcripts, encoding fungal cell wall components, virulence genes and transcription factors. Consistent with a potential function as effectors, the Bd sRNAs' predicted fungal targets were significantly down-regulated in the infected tissues compared to axenic cultures, and deletion mutants for some of these target genes are known to result in heavily impaired virulence phenotypes. Overall, this work provides a comprehensive picture of the interaction between rice blast and Bd, both in the transcriptomic reprogramming and the sRNA species produced and potentially exchanged between the pathogenic fungus and its host plant, paving the way for further characterization studies, and contributing to the emerging research on naturally occurring cross-kingdom communication and its implications for agriculture.

7. Zusammenfassung

Magnaporthe oryzae (Mo) ist der Erreger einer der wirtschaftlich relevantesten Reiskrankheiten, dem “Reisbrand”, und wurde als Modell für Ascomyceten eingehend untersucht. Neben der Besiedlung von oberirdischen Organen ist Mo auch in der Lage, Wurzelgewebe zu infizieren, und hat ein breites Spektrum von Poaceae-Wirten, darunter *Brachypodium distachyon* (Bd). Kürzlich wurde vorgeschlagen, dass Pilze neben den bekannten Proteineffektoren kleine (s)RNAs produzieren, die sekretiert und mit dem infizierten Organismus ausgetauscht werden können, um Gene zu inaktivieren (gene silencing), die direkt mit der Infektion in Verbindung stehen, ein Prozess, der als Cross-Kingdom-RNAi (ck-RNA) bezeichnet wird. Gleichzeitig ist bekannt, dass die Infektion die Expression von sRNA im Wirt induziert, wobei eine Untergruppe dieser sRNAs möglicherweise zum Pathogen transportiert wird, um Pathogenitäts-/Virulenzgene zu inaktivieren, was zu einem bidirektionalen RNAi-basierten Cross-Talk zwischen den interagierenden Organismen führt. In der vorliegenden Arbeit untersuchte ich gewebespezifische mRNA- und sRNA-Expressionsprofile in der Mo-Bd-Interaktion, um das Pathosystem zu charakterisieren und die entscheidende Rolle, die sRNAs bei der Etablierung und Aufrechterhaltung einer Pilzinfektion spielen, weiter zu beleuchten. Durch vergleichende Tiefensequenzierung von sRNAs und mRNAs aus axenischen Pilzkulturen und infizierten Blättern und Wurzeln fand ich ein breites Spektrum von Pilz-sRNAs, die ausschließlich in infizierten Geweben akkumulierten. Unter diesen wurden 20-22 nt Kandidaten-sRNAs *in silico* vorhergesagt, indem Mo-Reads ausgewählt wurden, die Ziele im Bd-Transkriptom für eine mögliche Cross-Kingdom-Funktion vorhergesagt hatten. Umgekehrt stellten wir fest, dass auch Bd während der Infektion sRNAs produziert, die nicht nur eine endogene Funktion erfüllen, sondern auch gegen eine Vielzahl von Pilztranskripten gerichtet sind, die für pilzliche Zellwandkomponenten, Virulenzgene und Transkriptionsfaktoren kodieren. In Übereinstimmung mit einer potenziellen Funktion als Effektoren wurden die vorhergesagten Pilztargets der Bd sRNAs im infizierten Gewebe im Vergleich zu axenischen Kulturen signifikant herunterreguliert, und es ist bekannt, dass Deletionsmutanten für einige dieser Zielgene zu stark beeinträchtigten Virulenzphänotypen führen. Insgesamt liefert diese Arbeit ein umfassendes Bild der Wechselwirkung zwischen Mo und Bd, sowohl bei der transkriptomischen Reprogrammierung, als auch bei den sRNA-Spezies, die

möglicherweise zwischen dem pathogenen Pilz und seiner Wirtspflanze ausgetauscht werden. Die Arbeit ebnet damit den Weg für weitere Charakterisierungsstudien und leistet einen Beitrag zur Forschung über die Kommunikation zwischen Krankheitserregern und Wirtspflanzen mittels sRNA und deren Auswirkungen auf die landwirtschaftliche Produktion.

8. References

Afzal, Z., Howton, T. C., Sun, Y., & Mukhtar, M. S. (2016). The roles of aquaporins in plant stress responses. *Journal of developmental biology*, *4*(1), 9.

Altschul, S. F., Gish, W., Miller, W., Myers, E. W., & Lipman, D. J. (1990). Basic local alignment search tool. *Journal of molecular biology*, *215*(3), 403-410.

Ambawat, S., Sharma, P., Yadav, N. R., & Yadav, R. C. (2013). MYB transcription factor genes as regulators for plant responses: an overview. *Physiology and Molecular Biology of Plants*, *19*(3), 307-321.

An, J., Lai, J., Sajjanhar, A., Lehman, M. L., & Nelson, C. C. (2014). miRPlant: an integrated tool for identification of plant miRNA from RNA sequencing data. *BMC bioinformatics*, *15*(1), 275.

An, Q., Ehlers, K., Kogel, K. H., Van Bel, A. J., & Hückelhoven, R. (2006a). Multivesicular compartments proliferate in susceptible and resistant MLA12-barley leaves in response to infection by the biotrophic powdery mildew fungus. *New Phytologist*, *172*(3), 563-576.

An, Q., Hückelhoven, R., Kogel, K. H., & Van Bel, A. J. (2006b). Multivesicular bodies participate in a cell wall-associated defence response in barley leaves attacked by the pathogenic powdery mildew fungus. *Cellular microbiology*, *8*(6), 1009-1019.

Anders, S., & Huber, W. (2010). Differential expression analysis for sequence count data. *Nature Precedings*, 1-1.

Anders, S., Pyl, P. T., & Huber, W. (2015). HTSeq—a Python framework to work with high-throughput sequencing data. *Bioinformatics*, *31*(2), 166-169.

Andrews, S. (2010). FastQC: a quality control tool for high throughput sequence data. Available online at: http://www.bioinformatics.babraham.ac.uk/projects/fastqc

Asibi, A. E., Chai, Q., & Coulter, J. A. (2019). Rice Blast: A Disease with Implications for Global Food Security. *Agronomy*, *9*(8), 451.

Bakshi, M., & Oelmüller, R. (2014). WRKY transcription factors: Jack of many trades in plants. *Plant signaling & behavior*, *9*(2), e27700.

Baldrich, P., Rutter, B. D., Karimi, H. Z., Podicheti, R., Meyers, B. C., & Innes, R. W. (2019). Plant extracellular vesicles contain diverse small RNA species and are enriched in 10-to 17-nucleotide “tiny” RNAs. *The Plant Cell*, *31*(2), 315-324.

Baldwin, T. K., Winnenburg, R., Urban, M., Rawlings, C., Koehler, J., & Hammond-Kosack, K. E. (2006). The pathogen-host interactions database (PHI-base) provides insights into generic and novel themes of pathogenicity. *Molecular plant-microbe interactions*, *19*(12), 1451-1462.

Baulcombe, D. (2004). RNA silencing in plants. *Nature*, *431*(7006), 356-363.

Benkert, P., Biasini, M., & Schwede, T. (2011). Toward the estimation of the absolute quality of individual protein structure models. *Bioinformatics*, *27*(3), 343-350.

Bertolini, E., Verelst, W., Horner, D. S., Gianfranceschi, L., Piccolo, V., Inzé, D., ... & Mica, E. (2013). Addressing the role of microRNAs in reprogramming leaf growth during drought stress in Brachypodium distachyon. *Molecular plant*, *6*(2), 423-443.

Bonnet, E., He, Y., Billiau, K., & Van de Peer, Y. (2010). TAPIR, a web server for the prediction of plant microRNA targets, including target mimics. *Bioinformatics*, *26*(12), 1566-1568.

Borges, F., & Martienssen, R. A. (2015). The expanding world of small RNAs in plants. *Nature reviews Molecular cell biology*, *16*(12), 727-741.

Brown, N. P., Leroy, C., & Sander, C. (1998). MView: a web-compatible database search or multiple alignment viewer. *Bioinformatics (Oxford, England)*, *14*(4), 380-381.

Brutnell, T. P., Bennetzen, J. L., & Vogel, J. P. (2015). Brachypodium distachyon and Setaria viridis: model genetic systems for the grasses. *Annual review of plant biology*, *66*, 465-485.

Buck, A. H., Coakley, G., Simbari, F., McSorley, H. J., Quintana, J. F., Le Bihan, T., ... & Ceroni, A. (2014). Exosomes secreted by nematode parasites transfer small RNAs to mammalian cells and modulate innate immunity. *Nature communications*, *5*, 5488.

Cai, Q., He, B., Kogel, K. H., & Jin, H. (2018a). Cross-kingdom RNA trafficking and environmental RNAi—nature's blueprint for modern crop protection strategies. *Current opinion in microbiology*, *46*, 58-64.

Cai, Q., Qiao, L., Wang, M., He, B., Lin, F. M., Palmquist, J., ... & Jin, H. (2018b). Plants send small RNAs in extracellular vesicles to fungal pathogen to silence virulence genes. *Science*, *360*(6393), 1126-1129.

Carbonell, A. (2017). Plant ARGONAUTEs: features, functions, and unknowns. In *Plant Argonaute Proteins* (pp. 1-21). Humana Press, New York, NY.

Castel, S. E., & Martienssen, R. A. (2013). RNA interference in the nucleus: roles for small RNAs in transcription, epigenetics and beyond. *Nature Reviews Genetics*, *14*(2), 100.

Cenik, E. S., & Zamore, P. D. (2011). Argonaute proteins. *Current Biology*, *21*(12), R446-R449.

Chen, H., & Boutros, P. C. (2011). VennDiagram: a package for the generation of highly-customizable Venn and Euler diagrams in R. *BMC bioinformatics*, *12*(1), 35.

Chen, T. W., Gan, R. C., Fang, Y. K., Chien, K. Y., Liao, W. C., Chen, C. C., ... & Yeh, Y. M. (2017). FunctionAnnotator, a versatile and efficient web tool for non-model organism annotation. *Scientific reports*, *7*(1), 1-9.

Chen, W., Kastner, C., Nowara, D., Oliveira-Garcia, E., Rutten, T., Zhao, Y., ... & Schweizer, P. (2016). Host-induced silencing of Fusarium culmorum genes protects wheat from infection. *Journal of experimental botany*, *67*(17), 4979-4991.

Cheng, W., Song, X. S., Li, H. P., Cao, L. H., Sun, K., Qiu, X. L., ... & Qu, B. (2015). Host-induced gene silencing of an essential chitin synthase gene confers durable resistance to F usarium head blight and seedling blight in wheat. *Plant biotechnology journal*, *13*(9), 1335-1345.

Choi, J., Kim, K. S., Rho, H. S., & Lee, Y. H. (2011). Differential roles of the phospholipase C genes in fungal development and pathogenicity of Magnaporthe oryzae. *Fungal genetics and biology*, *48*(4), 445-455.

Chuang, R. Y., Weaver, P. L., Liu, Z., & Chang, T. H. (1997). Requirement of the DEAD-Box protein ded1p for messenger RNA translation. *Science*, *275*(5305), 1468-1471.

Conesa, A., Madrigal, P., Tarazona, S., Gomez-Cabrero, D., Cervera, A., McPherson, A., ... & Mortazavi, A. (2016). A survey of best practices for RNA-seq data analysis. *Genome biology*, *17*(1), 13.

Cui, L. G., Shan, J. X., Shi, M., Gao, J. P., & Lin, H. X. (2014). The miR156-SPL 9-DFR pathway coordinates the relationship between development and abiotic stress tolerance in plants. *The Plant Journal*, *80*(6), 1108-1117.

Dai, M., Thompson, R. C., Maher, C., Contreras-Galindo, R., Kaplan, M. H., Markovitz, D. M., ... & Meng, F. (2010, December). NGSQC: cross-platform quality analysis pipeline for deep sequencing data. In *BMC genomics* (Vol. 11, No. S4, p. S7). BioMed Central.

Dai, X., & Zhao, P. X. (2011). psRNATarget: a plant small RNA target analysis server. *Nucleic acids research*, *39*(suppl_2), W155-W159.

Dean, R. A., Talbot, N. J., Ebbole, D. J., Farman, M. L., Mitchell, T. K., Orbach, M. J., ... & Read, N. D. (2005). The genome sequence of the rice blast fungus Magnaporthe grisea. *Nature*, *434*(7036), 980-986.

Dean, R., Van Kan, J. A., Pretorius, Z. A., Hammond-Kosack, K. E., Di Pietro, A., Spanu, P. D., ... & Foster, G. D. (2012). The Top 10 fungal pathogens in molecular plant pathology. *Molecular plant pathology*, *13*(4), 414-430.

Dereeper, A., Audic, S., Claverie, J. M., & Blanc, G. (2010). BLAST-EXPLORER helps you building datasets for phylogenetic analysis. *BMC evolutionary biology*, *10*(1), 8.

Dereeper, A., Guignon, V., Blanc, G., Audic, S., Buffet, S., Chevenet, F., ... & Claverie, J. M. (2008). Phylogeny. fr: robust phylogenetic analysis for the non-specialist. *Nucleic acids research*, *36*(suppl_2), W465-W469.

Dobin, A., Davis, C. A., Schlesinger, F., Drenkow, J., Zaleski, C., Jha, S., ... & Gingeras, T. R. (2013). STAR: ultrafast universal RNA-seq aligner. *Bioinformatics*, *29*(1), 15-21.

Donofrio, N. M., Hu, J., Mitchell, T. K., & Wilson, R. A. (2014). Facilitating the fungus: Insights from the genome of the rice blast fungus, Magnaporthe Oryzae. In *Genomics of plant-associated fungi: monocot pathogens* (pp. 141-160). Springer, Berlin, Heidelberg.

Draper, J., Mur, L. A., Jenkins, G., Ghosh-Biswas, G. C., Bablak, P., Hasterok, R., & Routledge, A. P. (2001). Brachypodium distachyon. A new model system for functional genomics in grasses. *Plant physiology*, *127*(4), 1539-1555.

Du, Z., Zhou, X., Ling, Y., Zhang, Z., & Su, Z. (2010). agriGO: a GO analysis toolkit for the agricultural community. *Nucleic acids research*, *38*(suppl_2), W64-W70.

Egan, M. J., Wang, Z. Y., Jones, M. A., Smirnoff, N., & Talbot, N. J. (2007). Generation of reactive oxygen species by fungal NADPH oxidases is required for rice blast disease. *Proceedings of the National Academy of Sciences*, *104*(28), 11772-11777.

Feller, A., Machemer, K., Braun, E. L., & Grotewold, E. (2011). Evolutionary and comparative analysis of MYB and bHLH plant transcription factors. *The Plant Journal*, *66*(1), 94-116.

Fire, A., Xu, S., Montgomery, M. K., Kostas, S. A., Driver, S. E., & Mello, C. C. (1998). Potent and specific genetic interference by double-stranded RNA in Caenorhabditis elegans. *Nature*, *391*(6669), 806-811.

Fisher, M. C., Henk, D. A., Briggs, C. J., Brownstein, J. S., Madoff, L. C., McCraw, S. L., & Gurr, S. J. (2012). Emerging fungal threats to animal, plant and ecosystem health. *Nature*, *484*(7393), 186-194.

Fitzgerald, T. L., Powell, J. J., Schneebeli, K., Hsia, M. M., Gardiner, D. M., Bragg, J. N., ... & Vogel, J. P. (2015). Brachypodium as an emerging model for cereal–pathogen interactions. *Annals of Botany*, *115*(5), 717-731.

Franke, K. R., Schmidt, S. A., Park, S., Jeong, D. H., Accerbi, M., & Green, P. J. (2018). Analysis of Brachypodium miRNA targets: evidence for diverse control during stress and conservation in bioenergy crops. *BMC genomics*, *19*(1), 547.

Gaffar, F. Y., & Koch, A. (2019). Catch me if you can! RNA silencing-based improvement of antiviral plant immunity. *Viruses*, *11*(7), 673.

Galhano, R., Illana, A., Ryder, L. S., Rodriguez-Romero, J., Demuez, M., Badaruddin, M., ... & Sesma, A. (2017). Tpc1 is an important Zn (II) 2Cys6 transcriptional regulator required for polarized growth and virulence in the rice blast fungus. *PLoS pathogens*, *13*(7), e1006516.

García-Alcalde, F., Okonechnikov, K., Carbonell, J., Cruz, L. M., Götz, S., Tarazona, S., ... & Conesa, A. (2012). Qualimap: evaluating next-generation sequencing alignment data. *Bioinformatics*, *28*(20), 2678-2679.

Garcia-Silva, M. R., das Neves, R. F. C., Cabrera-Cabrera, F., Sanguinetti, J., Medeiros, L. C., Robello, C., ... & Cayota, A. (2014). Extracellular vesicles shed by Trypanosoma cruzi are linked to small RNA pathways, life cycle regulation, and susceptibility to infection of mammalian cells. *Parasitology research*, *113*(1), 285-304.

Giraldo, M. C., Dagdas, Y. F., Gupta, Y. K., Mentlak, T. A., Yi, M., Martinez-Rocha, A. L., ... & Valent, B. (2013). Two distinct secretion systems facilitate tissue invasion by the rice blast fungus Magnaporthe oryzae. *Nature communications*, *4*(1), 1-12.

Goff, L., Trapnell, C., & Kelley, D. (2012). cummeRbund: Analysis, exploration, manipulation, and visualization of Cufflinks high-throughput sequencing data.

Goujon, M., McWilliam, H., Li, W., Valentin, F., Squizzato, S., Paern, J., & Lopez, R. (2010). A new bioinformatics analysis tools framework at EMBL–EBI. *Nucleic acids research*, *38*(suppl_2), W695-W699.

Grabherr, M. G., Haas, B. J., Yassour, M., Levin, J. Z., Thompson, D. A., Amit, I., ... & Chen, Z. (2011). Full-length transcriptome assembly from RNA-Seq data without a reference genome. *Nature biotechnology*, *29*(7), 644.

Griffiths-Jones, S., Grocock, R. J., Van Dongen, S., Bateman, A., & Enright, A. J. (2006). miRBase: microRNA sequences, targets and gene nomenclature. *Nucleic acids research*, *34*(suppl_1), D140-D144.

Hamilton, A. J., & Baulcombe, D. C. (1999). A species of small antisense RNA in posttranscriptional gene silencing in plants. *Science*, *286*(5441), 950-952.

Hilker, R., Stadermann, K. B., Doppmeier, D., Kalinowski, J., Stoye, J., Straube, J., ... & Goesmann, A. (2014). ReadXplorer—visualization and analysis of mapped sequences. *Bioinformatics*, *30*(16), 2247-2254.

Hooft, R. W., Vriend, G., Sander, C., & Abola, E. E. (1996). Errors in protein structures. *Nature*, *381*(6580), 272-272.

Howard, R. J., Ferrari, M. A., Roach, D. H., & Money, N. P. (1991). Penetration of hard substrates by a fungus employing enormous turgor pressures. *Proceedings of the National Academy of Sciences*, *88*(24), 11281-11284.

Jagtap, U. B., Gurav, R. G., & Bapat, V. A. (2011). Role of RNA interference in plant improvement. *Naturwissenschaften*, *98*(6), 473-492.

Jeong, D. H., Schmidt, S. A., Rymarquis, L. A., Park, S., Ganssmann, M., German, M. A., ... & Garvin, D. F. (2013). Parallel analysis of RNA ends enhances global investigation of microRNAs and target RNAs of Brachypodium distachyon. *Genome biology*, *14*(12), R145.

Johnson, N. R., Yeoh, J. M., Coruh, C., & Axtell, M. J. (2016). Improved placement of multi-mapping small RNAs. *G3: Genes, Genomes, Genetics*, *6*(7), 2103-2111.

Kadotani, N., Nakayashiki, H., Tosa, Y., & Mayama, S. (2003). RNA silencing in the phytopathogenic fungus Magnaporthe oryzae. *Molecular plant-microbe interactions*, *16*(9), 769-776.

Kadotani, N., Nakayashiki, H., Tosa, Y., & Mayama, S. (2004). One of the two Dicer-like proteins in the filamentous fungi Magnaporthe oryzae genome is responsible for

hairpin RNA-triggered RNA silencing and related small interfering RNA accumulation. *Journal of Biological Chemistry*, *279*(43), 44467-44474.

Kadotani, N., Murata, T., Quoc, N. B., Adachi, Y., & Nakayashiki, H. (2008). Transcriptional control and protein specialization have roles in the functional diversification of two dicer-like proteins in Magnaporthe oryzae. *Genetics*, *180*(2), 1245-1249.

Kang, J., Park, J., Choi, H., Burla, B., Kretzschmar, T., Lee, Y., & Martinoia, E. (2011). Plant ABC transporters. *The Arabidopsis book/American Society of Plant Biologists*, *9*.

Kawano, T. (2003). Roles of the reactive oxygen species-generating peroxidase reactions in plant defense and growth induction. *Plant cell reports*, *21*(9), 829-837.

Kehr, J., & Kragler, F. (2018). Long distance RNA movement. *New Phytologist*, *218*(1), 29-40.

Kershaw, M. J., & Talbot, N. J. (2009). Genome-wide functional analysis reveals that infection-associated fungal autophagy is necessary for rice blast disease. *Proceedings of the National Academy of Sciences*, *106*(37), 15967-15972.

Kettles, G. J., Bayon, C., Sparks, C. A., Canning, G., Kanyuka, K., & Rudd, J. J. (2018). Characterization of an antimicrobial and phytotoxic ribonuclease secreted by the fungal wheat pathogen Zymoseptoria tritici. *New Phytologist*, *217*(1), 320-331.

Kim, D., Pertea, G., Trapnell, C., Pimentel, H., Kelley, R., & Salzberg, S.L. (2013). TopHat2: accurate alignment of transcriptomes in the presence of insertions, deletions and gene fusions. *Genome Biology* 14(4):R36.

Kim, D., Langmead, B., & Salzberg, S.L. (2015). HISAT: a fast spliced aligner with low memory requirements. *Nature Methods* 12, 357–360.

Koch, A., Kumar, N., Weber, L., Keller, H., Imani, J., & Kogel, K. H. (2013). Host-induced gene silencing of cytochrome P450 lanosterol C14α-demethylase–encoding genes confers strong resistance to Fusarium species. *Proceedings of the National Academy of Sciences*, *110*(48), 19324-19329.

Koch, A., & Kogel, K. H. (2014). New wind in the sails: improving the agronomic value of crop plants through RNA i-mediated gene silencing. *Plant Biotechnology Journal*, *12*(7), 821-831.

Koch, A., Biedenkopf, D., Furch, A., Weber, L., Rossbach, O., Abdellatef, E., ... & Cardoza, V. (2016). An RNAi-based control of Fusarium graminearum infections

through spraying of long dsRNAs involves a plant passage and is controlled by the fungal silencing machinery. *PLoS pathogens*, *12*(10), e1005901.

Koch, A., Höfle, L., Werner, B. T., Imani, J., Schmidt, A., Jelonek, L., & Kogel, K. H. (2019). SIGS vs HIGS: a study on the efficacy of two dsRNA delivery strategies to silence Fusarium FgCYP51 genes in infected host and non-host plants. *Molecular plant pathology*, *20*(12), 1636-1644.

Kolde, R., & Kolde, M. R. (2015). Package 'pheatmap'. *R Package*, *1*(7).

Krzywinski, M., Schein, J., Birol, I., Connors, J., Gascoyne, R., Horsman, D., ... & Marra, M. A. (2009). Circos: an information aesthetic for comparative genomics. *Genome research*, *19*(9), 1639-1645.

LaMonte, G., Philip, N., Reardon, J., Lacsina, J. R., Majoros, W., Chapman, L., ... & Haystead, T. (2012). Translocation of sickle cell erythrocyte microRNAs into Plasmodium falciparum inhibits parasite translation and contributes to malaria resistance. *Cell host & microbe*, *12*(2), 187-199.

Langmead, B., Trapnell, C., Pop, M., & Salzberg, S. L. (2009). Ultrafast and memory-efficient alignment of short DNA sequences to the human genome. *Genome biology*, *10*(3), R25.

Langmead, B. (2010). Aligning short sequencing reads with Bowtie. *Current protocols in bioinformatics*, *32*(1), 11-7.

Laskowski, R. A., MacArthur, M. W., Moss, D. S., & Thornton, J. M. (1993). PROCHECK: a program to check the stereochemical quality of protein structures. *Journal of applied crystallography*, *26*(2), 283-291.

Law, C. W., Chen, Y., Shi, W., & Smyth, G. K. (2014). voom: Precision weights unlock linear model analysis tools for RNA-seq read counts. *Genome biology*, *15*(2), R29.

Letunic, I., & Bork, P. (2018). 20 years of the SMART protein domain annotation resource. *Nucleic acids research*, *46*(D1), D493-D496.

Li, H., Ruan, J., & Durbin, R. (2008). Mapping short DNA sequencing reads and calling variants using mapping quality scores. *Genome research*, *18*(11), 1851-1858.

Li, H., Wang, Y., Wang, Z., Guo, X., Wang, F., Xia, X. J., ... & Zhou, Y. H. (2016). Microarray and genetic analysis reveals that csa-miR159b plays a critical role in abscisic acid-mediated heat tolerance in grafted cucumber plants. *Plant, cell & environment*, *39*(8), 1790-1804.

Liu, L., Zhang, Z., Mei, Q., & Chen, M. (2013). PSI: a comprehensive and integrative approach for accurate plant subcellular localization prediction. *PLoS One*, *8*(10).

Liu, W., Xie, Y., Ma, J., Luo, X., Nie, P., Zuo, Z., ... & Xue, Y. (2015). IBS: an illustrator for the presentation and visualization of biological sequences. Bioinformatics. 31(20), 3359-3361.

Liu, X. H., Lu, J. P., Zhang, L., Dong, B., Min, H., & Lin, F. C. (2007). Involvement of a Magnaporthe grisea serine/threonine kinase gene, MgATG1, in appressorium turgor and pathogenesis. *Eukaryotic cell*, *6*(6), 997-1005.

Love, M. I., Huber, W., & Anders, S. (2014). Moderated estimation of fold change and dispersion for RNA-seq data with DESeq2. *Genome biology*, *15*(12), 550.

Margis, R., Fusaro, A. F., Smith, N. A., Curtin, S. J., Watson, J. M., Finnegan, E. J., & Waterhouse, P. M. (2006). The evolution and diversification of Dicers in plants. *FEBS letters*, *580*(10), 2442-2450.

Martin, M. (2011). Cutadapt removes adapter sequences from high-throughput sequencing reads. *EMBnet. journal*, *17*(1), 10-12.

Molnar, A., Melnyk, C. W., Bassett, A., Hardcastle, T. J., Dunn, R., & Baulcombe, D. C. (2010). Small silencing RNAs in plants are mobile and direct epigenetic modification in recipient cells. *science*, *328*(5980), 872-875.

Morris, A. L., MacArthur, M. W., Hutchinson, E. G., & Thornton, J. M. (1992). Stereochemical quality of protein structure coordinates. *Proteins: Structure, Function, and Bioinformatics*, *12*(4), 345-364.

Murashige, T., & Skoog, F. (1962). A revised medium for rapid growth and bio assays with tobacco tissue cultures. *Physiologia plantarum*, *15*(3), 473-497.

Murozuka, E., Massange-Sánchez, J. A., Nielsen, K., Gregersen, P. L., & Braumann, I. (2018). Genome wide characterization of barley NAC transcription factors enables the identification of grain-specific transcription factors exclusive for the Poaceae family of monocotyledonous plants. *PloS one*, *13*(12).

Murphy, D., Dancis, B., & Brown, J. R. (2008). The evolution of core proteins involved in microRNA biogenesis. *BMC evolutionary biology*, *8*(1), 92.

Nalley, L., Tsiboe, F., Durand-Morat, A., Shew, A., & Thoma, G. (2016). Economic and environmental impact of rice blast pathogen (Magnaporthe oryzae) alleviation in the United States. *PloS one*, *11*(12).

Nowara, D., Gay, A., Lacomme, C., Shaw, J., Ridout, C., Douchkov, D., ... & Schweizer, P. (2010). HIGS: host-induced gene silencing in the obligate biotrophic fungal pathogen Blumeria graminis. *The Plant Cell*, *22*(9), 3130-3141.

Nunes, C. C., Gowda, M., Sailsbery, J., Xue, M., Chen, F., Brown, D. E., ... & Dean, R. A. (2011). Diverse and tissue-enriched small RNAs in the plant pathogenic fungus, Magnaporthe oryzae. *BMC genomics*, *12*(1), 288.

Osés-Ruiz, M., & Talbot, N. J. (2017). Cell cycle-dependent regulation of plant infection by the rice blast fungus Magnaporthe oryzae. *Communicative & integrative biology*, *10*(5-6), e1372067.

Park, C. H., Chen, S., Shirsekar, G., Zhou, B., Khang, C. H., Songkumarn, P., ... & Valent, B. (2012). The Magnaporthe oryzae effector AvrPiz-t targets the RING E3 ubiquitin ligase APIP6 to suppress pathogen-associated molecular pattern–triggered immunity in rice. *The plant cell*, *24*(11), 4748-4762.

Parker, D., Beckmann, M., Enot, D. P., Overy, D. P., Rios, Z. C., Gilbert, M., ... & Draper, J. (2008). Rice blast infection of Brachypodium distachyon as a model system to study dynamic host/pathogen interactions. *Nature Protocols*, *3*(3), 435.

Peraldi, A., Beccari, G., Steed, A., & Nicholson, P. (2011). Brachypodium distachyon: a new pathosystem to study Fusarium head blight and other Fusarium diseases of wheat. *BMC plant biology*, *11*(1), 100.

Powell, J. J., Carere, J., Sablok, G., Fitzgerald, T. L., Stiller, J., Colgrave, M. L., ... & Kazan, K. (2017). Transcriptome analysis of Brachypodium during fungal pathogen infection reveals both shared and distinct defense responses with wheat. *Scientific reports*, *7*(1), 1-14.

Ramachandran, G. N. (1963). Stereochemistry of polypeptide chain configurations. *J. Mol. Biol.*, *7*, 95-99.

Raman, V., Simon, S. A., Romag, A., Demirci, F., Mathioni, S. M., Zhai, J., ... & Donofrio, N. M. (2013). Physiological stressors and invasive plant infections alter the small RNA transcriptome of the rice blast fungus, Magnaporthe oryzae. *BMC genomics*, *14*(1), 326.

Raman, V., Simon, S. A., Demirci, F., Nakano, M., Meyers, B. C., & Donofrio, N. M. (2017). Small RNA functions are required for growth and development of Magnaporthe oryzae. *Molecular plant-microbe interactions*, *30*(7), 517-530.

Riley, K. J., Yario, T. A., & Steitz, J. A. (2012). Association of Argonaute proteins and microRNAs can occur after cell lysis. *Rna*, *18*(9), 1581-1585.

Robertson, G., Schein, J., Chiu, R., Corbett, R., Field, M., Jackman, S. D., ... & Griffith, M. (2010). De novo assembly and analysis of RNA-seq data. *Nature methods*, *7*(11), 909-912.

Robinson, M. D., McCarthy, D. J., & Smyth, G. K. (2010). edgeR: a Bioconductor package for differential expression analysis of digital gene expression data. *Bioinformatics*, *26*(1), 139-140.

Routledge, A. P., Shelley, G., Smith, J. V., Talbot, N. J., Draper, J., & Mur, L. A. (2004). Magnaporthe grisea interactions with the model grass Brachypodium distachyon closely resemble those with rice (Oryza sativa). *Molecular Plant Pathology*, *5*(4), 253-265.

Rutter, B. D., & Innes, R. W. (2017). Extracellular vesicles isolated from the leaf apoplast carry stress-response proteins. *Plant physiology*, *173*(1), 728-741.

Sabnam, N., & Barman, S. R. (2017). WISH, a novel CFEM GPCR is indispensable for surface sensing, asexual and pathogenic differentiation in rice blast fungus. *Fungal Genetics and Biology*, *105*, 37-51.

Samad, A. F. A., Ali, N. M., Ismail, I., & Murad, A. M. A. (2016, November). Analysis of miRNAs targeting transcription factors in Persicaria minor induced by Fusarium oxysporum. In *AIP Conference Proceedings* (Vol. 1784, No. 1, p. 020009). AIP Publishing LLC.

Schrödinger, LLC. (2010). The {PyMOL} Molecular Graphics System, Version~1.3.

Schultz, J., Milpetz, F., Bork, P., & Ponting, C. P. (1998). SMART, a simple modular architecture research tool: Identification of signaling domains. Proceedings of the National Academy of Sciences. 95(11), 5857 LP-5864.

Schulz, M. H., Zerbino, D. R., Vingron, M., & Birney, E. (2012). Oases: robust de novo RNA-seq assembly across the dynamic range of expression levels. *Bioinformatics*, *28*(8), 1086-1092.

Schurch, N. J., Schofield, P., Gierliński, M., Cole, C., Sherstnev, A., Singh, V., ... & Blaxter, M. (2016). How many biological replicates are needed in an RNA-seq experiment and which differential expression tool should you use?. *Rna*, *22*(6), 839-851.

Sesma, A., & Osbourn, A. E. (2004). The rice leaf blast pathogen undergoes

developmental processes typical of root-infecting fungi. *Nature*, *431*(7008), 582-586.

Šečić, E., Zanini, S., & Kogel, K. H. (2019). Further elucidation of the ARGONAUTE and DICER protein families in the model grass species Brachypodium distachyon. *Frontiers in plant science*, *10*, 1332.

Sievers, F., Wilm, A., Dineen, D., Gibson, T. J., Karplus, K., Li, W., ... & Thompson, J. D. (2011). Fast, scalable generation of high-quality protein multiple sequence alignments using Clustal Omega. *Molecular systems biology*, *7*(1).

Simão, F. A., Waterhouse, R. M., Ioannidis, P., Kriventseva, E. V., & Zdobnov, E. M. (2015). BUSCO: assessing genome assembly and annotation completeness with single-copy orthologs. *Bioinformatics*, *31*(19), 3210-3212.

Song, J. J., Smith, S. K., Hannon, G. J., & Joshua-Tor, L. (2004). Crystal structure of Argonaute and its implications for RISC slicer activity. *Science*, *305*(5689), 1434-1437.

Song, W. Y., Wang, G. L., Chen, L. L., Kim, H. S., Pi, L. Y., Holsten, T., ... & Fauquet, C. (1995). A receptor kinase-like protein encoded by the rice disease resistance gene, Xa21. *science*, *270*(5243), 1804-1806.

Spassov, D., & Jurecic, R. (2003). The PUF family of RNA-binding proteins: does evolutionarily conserved structure equal conserved function?. *IUBMB life*, *55*(7), 359-366.

Szklarczyk, D., Gable, A. L., Lyon, D., Junge, A., Wyder, S., Huerta-Cepas, J., ... & Jensen, L. J. (2019). STRING v11: protein–protein association networks with increased coverage, supporting functional discovery in genome-wide experimental datasets. *Nucleic acids research*, *47*(D1), D607-D613.

Talbot, N. J. (1995). Having a blast: exploring the pathogenicity of Magnaporthe grisea. *Trends in microbiology*, *3*(1), 9-16.

Thorvaldsdóttir, H., Robinson, J. T., & Mesirov, J. P. (2013). Integrative Genomics Viewer (IGV): high-performance genomics data visualization and exploration. *Briefings in bioinformatics*, *14*(2), 178-192.

Trapnell, C., Pachter, L., & Salzberg, S. L. (2009). TopHat: discovering splice junctions with RNA-Seq. *Bioinformatics*, *25*(9), 1105-1111.

Trapnell, C., Williams, B. A., Pertea, G., Mortazavi, A., Kwan, G., Van Baren, M. J., ... & Pachter, L. (2010). Transcript assembly and quantification by RNA-Seq reveals unannotated transcripts and isoform switching during cell differentiation. *Nature*

biotechnology, *28*(5), 511.

Vaucheret, H., & Fagard, M. (2001). Transcriptional gene silencing in plants: targets, inducers and regulators. *TRENDS in Genetics*, *17*(1), 29-35.

Vaucheret, H., Vazquez, F., Crété, P., & Bartel, D. P. (2004). The action of ARGONAUTE1 in the miRNA pathway and its regulation by the miRNA pathway are crucial for plant development. *Genes & development*, *18*(10), 1187-1197.

Vogel, J. P., Garvin, D. F., Leong, O. M., & Hayden, D. M. (2006). Agrobacterium-mediated transformation and inbred line development in the model grass Brachypodium distachyon. *Plant Cell, Tissue and Organ Culture*, *84*(2), 199-211.

Vogel, J., & Hill, T. (2008). High-efficiency Agrobacterium-mediated transformation of Brachypodium distachyon inbred line Bd21-3. *Plant cell reports*, *27*(3), 471-478.

Wang, B., Sun, Y., Song, N., Zhao, M., Liu, R., Feng, H., ... & Kang, Z. (2017). Puccinia striiformis f. sp. tritici mi croRNA-like RNA 1 (Pst-milR1), an important pathogenicity factor of Pst, impairs wheat resistance to Pst by suppressing the wheat pathogenesis-related 2 gene. *New Phytologist*, *215*(1), 338-350.

Wang, H. L. V., Dinwiddie, B. L., Lee, H., & Chekanova, J. A. (2015). Stress-induced endogenous siRNAs targeting regulatory intron sequences in Brachypodium. *RNA*, *21*(2), 145-163.

Wang, L., Wang, S., & Li, W. (2012). RSeQC: quality control of RNA-seq experiments. *Bioinformatics*, *28*(16), 2184-2185.

Wang, M., Weiberg, A., Dellota Jr, E., Yamane, D., & Jin, H. (2017). Botrytis small RNA Bc-siR37 suppresses plant defense genes by cross-kingdom RNAi. *RNA biology*, *14*(4), 421-428.

Waterhouse, A., Bertoni, M., Bienert, S., Studer, G., Tauriello, G., Gumienny, R., ... & Lepore, R. (2018). SWISS-MODEL: homology modelling of protein structures and complexes. *Nucleic acids research*, *46*(W1), W296-W303.

Weiberg, A., Wang, M., Lin, F. M., Zhao, H., Zhang, Z., Kaloshian, I., ... & Jin, H. (2013). Fungal small RNAs suppress plant immunity by hijacking host RNA interference pathways. *Science*, *342*(6154), 118-123.

Wei, B., Cai, T., Zhang, R., Li, A., Huo, N., Li, S., ... & Mao, L. (2009). Novel microRNAs uncovered by deep sequencing of small RNA transcriptomes in bread wheat (Triticum aestivum L.) and Brachypodium distachyon (L.) Beauv. *Functional & integrative genomics*, *9*(4), 499.

Wilson, R. A., & Talbot, N. J. (2009). Under pressure: investigating the biology of plant infection by Magnaporthe oryzae. *Nature Reviews Microbiology*, *7*(3), 185-195.

Xie, Y., Wu, G., Tang, J., Luo, R., Patterson, J., Liu, S., ... & Zhou, X. (2014). SOAPdenovo-Trans: de novo transcriptome assembly with short RNA-Seq reads. *Bioinformatics*, *30*(12), 1660-1666.

Yates, A. D., Achuthan, P., Akanni, W., Allen, J., Allen, J., Alvarez-Jarreta, J., ... & Bhai, J. (2020). Ensembl 2020. *Nucleic acids research*, *48*(D1), D682-D688.

Zanini, S., Šečić, E., Jelonek, L., & Kogel, K. H. (2018). A Bioinformatics Pipeline for the Analysis and Target Prediction of RNA Effectors in Bidirectional Communication During Plant–Microbe Interactions. *Frontiers in plant science*, *9*, 1212.

Zanini, S., Šečić, E., Busche, T., Kalinowski, J., & Kogel, K. H. (2019). Discovery of interaction-related sRNAs and their targets in the Brachypodium distachyon and Magnaporthe oryzae pathosystem. *BioRxiv*, 631945.

Zerbino, D. R., Achuthan, P., Akanni, W., Amode, M. R., Barrell, D., Bhai, J., ... & Gil, L. (2018). Ensembl 2018. *Nucleic acids research*, *46*(D1), D754-D761.

Zhang, J., Xu, Y., Huan, Q., & Chong, K. (2009). Deep sequencing of Brachypodium small RNAs at the global genome level identifies microRNAs involved in cold stress response. *BMC genomics*, *10*(1), 449.

Zhang, X., Niu, D., Carbonell, A., Wang, A., Lee, A., Tun, V., ... & Jin, H. (2014). ARGONAUTE PIWI domain and microRNA duplex structure regulate small RNA sorting in Arabidopsis. *Nature communications*, *5*(1), 1-11.

Zhang, S., & Xu, J. R. (2014). Effectors and effector delivery in Magnaporthe oryzae. *PLoS pathogens*, *10*(1).

Zhang, T., Zhao, Y. L., Zhao, J. H., Wang, S., Jin, Y., Chen, Z. Q., ... & Guo, H. S. (2016). Cotton plants export microRNAs to inhibit virulence gene expression in a fungal pathogen. *Nature plants*, *2*(10), 1-6.

Zhang, Z., Wang, J., Chai, R., Qiu, H., Jiang, H., Mao, X., ... & Sun, G. (2015). An S-(hydroxymethyl) glutathione dehydrogenase is involved in conidiation and full virulence in the rice blast fungus Magnaporthe oryzae. *PLoS One*, *10*(3).

9. List of attachments

Attachment 1: Table of Mo ck-sRNA candidates with corresponding downregulated Bd targets in the three setups (2DPI, 4DPI, Root)

Attachment 2: Table of Bd ck-sRNA candidates with corresponding downregulated Mo targets in the three setups (2DPI, 4DPI, Root)

Mo ck-sRNA candidates with corresponding downregulated Bd targets in the three setups (2DPI, 4DPI, Root)

Setup	ck-sRNA	nt	Log(RPM)	Target	LogFC
2DPI	TCCATTCGGGCGGCTAGCTT	20	1.634	BdiBd21-3.4G0610700.1	-1.250
2DPI	TCATCTTTCAACTGAGGCTC	20	4.314	BdiBd21-3.1G0750300.1	-1.112
2DPI	TTTTCAGTGTATCGAAAGCG	20	6.774	BdiBd21-3.1G0045900.1	-0.487
2DPI	CTGGCATCGATGAAGAACGCA	21	6.774	BdiBd21-3.4G0610700.1	-1.250
2DPI	TAGGCTGAGAAGCTGGGGGT	20	7.774	BdiBd21-3.3G0559800.1	-0.812
2DPI	TTTCGACGCTGCCCTGACTT	20	#N/A	BdiBd21-3.4G0610700.1	-1.250
2DPI	GGTTATCATCGTCCCAGCCC	20	#N/A	BdiBd21-3.4G0347500.1	-0.698
2DPI	TTTCGACGCTGCCCTGACTT	20	#N/A	BdiBd21-3.1G0045900.1	-0.487
4DPI	TCCTTCCGTCGAATACTTCG	20	1.001	BdiBd21-3.2G0692200.1	-1.386
4DPI	TCCTTCCGTCGAATACTTCG	20	1.001	BdiBd21-3.1G0263200.1	-0.981
4DPI	TCCTTCCGTCGAATACTTCG	20	1.001	BdiBd21-3.3G0419700.1	-0.937
4DPI	TCCTTCCGTCGAATACTTCG	20	1.001	BdiBd21-3.1G0356400.1	-0.828
4DPI	TAAGGGACAGGCCTAACCGC	20	1.016	BdiBd21-3.2G0686100.1	-2.543
4DPI	TGATAAATAATTGGTTGGGG	20	1.016	BdiBd21-3.3G0734900.1	-0.974
4DPI	TTGGAAGAACTTGGGACCCT	20	1.040	BdiBd21-3.1G0151100.1	-1.305
4DPI	TTGGAAGAACTTGGGACCCT	20	1.040	BdiBd21-3.1G0797500.1	-1.167
4DPI	TTGGAAGAACTTGGGACCCT	20	1.040	BdiBd21-3.1G0290900.1	-0.877
4DPI	TTGGAAGAACTTGGGACCCT	20	1.040	BdiBd21-3.1G0320800.1	-0.804
4DPI	CGAATCTTTGAACGCACATT	20	1.088	BdiBd21-3.3G0419700.1	-0.937
4DPI	TTCAGCAGTCGGAAGGCGGT	20	1.104	BdiBd21-3.5G0017400.1	-1.246
4DPI	TTCAGCAGTCGGAAGGCGGT	20	1.104	BdiBd21-3.1G0041600.1	-1.048
4DPI	TGACTGAACCCCAGATTGGA	20	1.144	BdiBd21-3.2G0803500.1	-1.242
4DPI	TCGAAGAGATCCTCGACTCC	20	1.158	BdiBd21-3.1G0251800.1	-1.062
4DPI	TACTGTTTCCGTTCGGGGAG	20	1.223	BdiBd21-3.3G0005900.1	-2.047
4DPI	TACTGTTTCCGTTCGGGGAG	20	1.223	BdiBd21-3.1G0915800.1	-1.099
4DPI	TACTGTTTCCGTTCGGGGAG	20	1.223	BdiBd21-3.4G0111900.1	-0.872
4DPI	TACTGTTTCCGTTCGGGGAG	20	1.223	BdiBd21-3.5G0361100.1	-0.835
4DPI	TAAAGCGCCGGTAAAAGTTG	20	1.244	BdiBd21-3.3G0193400.1	-1.237
4DPI	TAAAGCGCCGGTAAAAGTTG	20	1.244	BdiBd21-3.3G0787100.1	-1.132
4DPI	AATCCAGGTTGAAATTCGGA	20	1.286	BdiBd21-3.2G0613800.1	-1.146
4DPI	AATCCAGGTTGAAATTCGGA	20	1.286	BdiBd21-3.4G0103100.1	-0.909
4DPI	CAAACTGGCTGTTTCTGATT	20	1.286	BdiBd21-3.4G0466500.1	-0.899
4DPI	AATCCAGGTTGAAATTCGGA	20	1.286	BdiBd21-3.1G0415900.1	-0.860
4DPI	TGACACAGCCAGCGAGTCCT	20	1.329	BdiBd21-3.2G0386500.1	-0.917
4DPI	TGAGCAGTGGATAGCAGGCT	20	1.342	BdiBd21-3.1G0983900.1	-1.476
4DPI	TGAGCAGTGGATAGCAGGCT	20	1.342	BdiBd21-3.1G0449300.1	-0.859
4DPI	TCGTACTGGAAGCCCTGAGG	20	1.367	BdiBd21-3.1G0784600.1	-1.278
4DPI	TCGTACTGGAAGCCCTGAGG	20	1.367	BdiBd21-3.2G0596400.1	-1.071
4DPI	TCCAAAACCACGTCGAAGCCG	21	1.373	BdiBd21-3.2G0283400.1	-1.397
4DPI	TATATATCCCCTCGTTTGGA	20	1.419	BdiBd21-3.2G0774100.1	-1.341
4DPI	TATATATCCCCTCGTTTGGA	20	1.419	BdiBd21-3.5G0057900.1	-1.340
4DPI	TATTGCAGTGTCGGCGGCAA	20	1.432	BdiBd21-3.1G0212700.1	-0.953
4DPI	TGCTTCACGCAGGGCTTCCG	20	1.441	BdiBd21-3.2G0686100.1	-2.543
4DPI	TGCTTCACGCAGGGCTTCCG	20	1.441	BdiBd21-3.2G0686100.1	-2.543
4DPI	TGCTTCACGCAGGGCTTCCG	20	1.441	BdiBd21-3.5G0362300.1	-1.203

4DPI	TGCTTCACGCAGGGCTTCCG	20	1.441	BdiBd21-3.4G0506800.1	-0.840
4DPI	TGCTTCACGCAGGGCTTCCG	20	1.441	BdiBd21-3.3G0608400.1	-0.802
4DPI	TCGGCGCCTGTCCTCAACGC	20	1.448	BdiBd21-3.1G0583500.1	-0.955
4DPI	TAGGTTTTTGCTTTGCCGGGG	21	1.466	BdiBd21-3.1G0278900.1	-0.889
4DPI	TAGGTTTTTGCTTTGCCGGGG	21	1.466	BdiBd21-3.3G0019700.1	-0.883
4DPI	TCTCAAAGATCGTAGCCCCT	20	1.491	BdiBd21-3.2G0073500.1	-1.324
4DPI	TACTCTCATAGACGACGGCAG	21	1.507	BdiBd21-3.2G0692200.1	-1.386
4DPI	TACTCTCATAGACGACGGCAG	21	1.507	BdiBd21-3.4G0461700.1	-1.184
4DPI	AGGCTGTCGATTTTCAAACGG	21	1.528	BdiBd21-3.1G0110700.1	-0.861
4DPI	TGGCAGCGGCGCAGGATCTCG	21	1.537	BdiBd21-3.1G0285600.1	-2.117
4DPI	TGGCAGCGGCGCAGGATCTCG	21	1.537	BdiBd21-3.5G0309700.1	-1.387
4DPI	TTTCGAGATTGGAAACGGCT	20	1.540	BdiBd21-3.2G0348300.1	-0.977
4DPI	TGGATTGGAAGAACTTGGGA	20	1.549	BdiBd21-3.5G0215700.2	-4.140
4DPI	TGGATTGGAAGAACTTGGGA	20	1.549	BdiBd21-3.5G0316300.1	-1.803
4DPI	TGGATTGGAAGAACTTGGGA	20	1.549	BdiBd21-3.4G0529400.1	-1.762
4DPI	TGGATTGGAAGAACTTGGGA	20	1.549	BdiBd21-3.2G0705000.1	-1.606
4DPI	TGGATTGGAAGAACTTGGGA	20	1.549	BdiBd21-3.1G0549600.1	-1.327
4DPI	TGGATTGGAAGAACTTGGGA	20	1.549	BdiBd21-3.1G0797500.1	-1.167
4DPI	TGAAGATCAATGGCCCCTGG	20	1.566	BdiBd21-3.4G0529400.1	-1.762
4DPI	GCCGACTAGGGATCGGACGGTG	22	1.566	BdiBd21-3.2G0546200.1	-0.995
4DPI	TGTGGGGGCAGCTTCTCGGC	20	1.592	BdiBd21-3.1G0271200.1	-2.996
4DPI	TGTGGGGGCAGCTTCTCGGC	20	1.592	BdiBd21-3.2G0593000.1	-1.683
4DPI	TGTGGGGGCAGCTTCTCGGC	20	1.592	BdiBd21-3.2G0079800.1	-1.587
4DPI	TGTGGGGGCAGCTTCTCGGC	20	1.592	BdiBd21-3.1G0561500.1	-1.148
4DPI	TTCCGGGCCAGTAATATTCT	20	1.592	BdiBd21-3.1G0026500.1	-1.134
4DPI	TGTGGGGGCAGCTTCTCGGC	20	1.592	BdiBd21-3.3G0157400.1	-1.056
4DPI	TTCCGGGCCAGTAATATTCT	20	1.592	BdiBd21-3.1G0110700.1	-0.861
4DPI	TGTGGGGGCAGCTTCTCGGC	20	1.592	BdiBd21-3.2G0789700.1	-0.835
4DPI	TCGGTGTCCAGCTTGTGCTG	20	1.599	BdiBd21-3.2G0023200.1	-1.623
4DPI	TCGGTGTCCAGCTTGTGCTG	20	1.599	BdiBd21-3.2G0023200.1	-1.623
4DPI	TCGGTGTCCAGCTTGTGCTG	20	1.599	BdiBd21-3.4G0417800.1	-1.437
4DPI	TCGGTGTCCAGCTTGTGCTG	20	1.599	BdiBd21-3.2G0323300.1	-1.203
4DPI	TCGGTGTCCAGCTTGTGCTG	20	1.599	BdiBd21-3.4G0429100.1	-1.093
4DPI	TCGGTGTCCAGCTTGTGCTG	20	1.599	BdiBd21-3.3G0771200.1	-0.939
4DPI	TCGGTGTCCAGCTTGTGCTG	20	1.599	BdiBd21-3.4G0110800.1	-0.913
4DPI	TCGGTGTCCAGCTTGTGCTG	20	1.599	BdiBd21-3.2G0525500.1	-0.851
4DPI	TCCATTCGGGCGGCTAGCTT	20	1.612	BdiBd21-3.4G0539400.1	-1.072
4DPI	TCCATTCGGGCGGCTAGCTT	20	1.612	BdiBd21-3.3G0525200.1	-0.979
4DPI	TCCATTCGGGCGGCTAGCTT	20	1.612	BdiBd21-3.2G0580200.1	-0.893
4DPI	TTCGGCGCGGGCTTGTTCCA	20	1.618	BdiBd21-3.3G0671500.1	-1.106
4DPI	TTCGGCGCGGGCTTGTTCCA	20	1.618	BdiBd21-3.5G0283700.1	-1.018
4DPI	TTCGGCGCGGGCTTGTTCCA	20	1.618	BdiBd21-3.2G0093700.1	-1.012
4DPI	TTCGGCGCGGGCTTGTTCCA	20	1.618	BdiBd21-3.3G0416100.1	-0.984
4DPI	TGAACCAGCCTTTGCCCGCC	20	1.631	BdiBd21-3.2G0145300.1	-1.300
4DPI	TGAACCAGCCTTTGCCCGCC	20	1.631	BdiBd21-3.5G0125100.1	-0.864
4DPI	TGATCCTGGAGACCGACGCT	20	1.642	BdiBd21-3.3G0525200.1	-0.979
4DPI	TGATCCTGGAGACCGACGCT	20	1.642	BdiBd21-3.1G0404800.1	-0.875
4DPI	TGATCCTGGAGACCGACGCT	20	1.642	BdiBd21-3.2G0480500.1	-0.841
4DPI	TACAAACAGGACAGGCGCTG	20	1.651	BdiBd21-3.2G0695900.1	-1.751
4DPI	TACAAACAGGACAGGCGCTG	20	1.651	BdiBd21-3.5G0309700.1	-1.387

4DPI	TCAAAGGGGCTACGATCTTT	20	1.673	BdiBd21-3.4G0605700.1	-2.243
4DPI	TCTTGACAGGAATTCGGCCC	20	1.673	BdiBd21-3.3G0344100.1	-1.524
4DPI	TCTTGACAGGAATTCGGCCC	20	1.673	BdiBd21-3.2G0132900.1	-1.522
4DPI	TCGGACTTGTGGGAGTTGGC	20	1.673	BdiBd21-3.2G0692200.1	-1.386
4DPI	TCGGACTTGTGGGAGTTGGC	20	1.673	BdiBd21-3.1G0591400.1	-1.368
4DPI	TCGGACTTGTGGGAGTTGGC	20	1.673	BdiBd21-3.1G0011700.1	-1.077
4DPI	TCTTGACAGGAATTCGGCCC	20	1.673	BdiBd21-3.1G1013900.1	-1.047
4DPI	TCGGACTTGTGGGAGTTGGC	20	1.673	BdiBd21-3.1G0775600.1	-1.013
4DPI	TCGGACTTGTGGGAGTTGGC	20	1.673	BdiBd21-3.3G0485400.1	-0.899
4DPI	TCGGACTTGTGGGAGTTGGC	20	1.673	BdiBd21-3.1G0677400.1	-0.885
4DPI	TAGACTGTACAGGCCAGGGA	20	1.691	BdiBd21-3.5G0361100.1	-0.835
4DPI	TTAAAACGCTCGGTCTGTCC	20	1.694	BdiBd21-3.1G0197800.1	-0.976
4DPI	TTAAAACGCTCGGTCTGTCC	20	1.694	BdiBd21-3.4G0506800.1	-0.840
4DPI	TTAAAACGCTCGGTCTGTCC	20	1.694	BdiBd21-3.1G0711600.1	-0.820
4DPI	TGGCGTCGTGGCCGTTGCTT	20	1.729	BdiBd21-3.5G0321100.1	-2.236
4DPI	TGGCGTCGTGGCCGTTGCTT	20	1.729	BdiBd21-3.1G0671500.1	-1.344
4DPI	TAGGGGTTTGTTTTGGCGGA	20	1.729	BdiBd21-3.1G0419300.1	-1.286
4DPI	TAGGGGTTTGTTTTGGCGGA	20	1.729	BdiBd21-3.3G0545700.1	-1.116
4DPI	TGGCGCGGGGACCTGGACCT	20	1.729	BdiBd21-3.2G0084000.1	-1.038
4DPI	TGGCGCGGGGACCTGGACCT	20	1.729	BdiBd21-3.2G0357000.1	-0.961
4DPI	TAGGGGTTTGTTTTGGCGGA	20	1.729	BdiBd21-3.2G0453500.1	-0.940
4DPI	TAGGGGTTTGTTTTGGCGGA	20	1.729	BdiBd21-3.4G0110800.1	-0.913
4DPI	TGGCGTCGTGGCCGTTGCTT	20	1.729	BdiBd21-3.1G0677400.1	-0.885
4DPI	TGGCGTCGTGGCCGTTGCTT	20	1.729	BdiBd21-3.3G0420100.1	-0.874
4DPI	TCGGAGTAGGAAGCGCCGTC	20	1.729	BdiBd21-3.3G0446100.1	-0.821
4DPI	TGGCGTCGTGGCCGTTGCTT	20	1.729	BdiBd21-3.2G0321800.1	-0.812
4DPI	TGGCGTCGTGGCCGTTGCTT	20	1.729	BdiBd21-3.2G0321800.1	-0.812
4DPI	TTCCAGGTAATCGGCAGGTT	20	1.765	BdiBd21-3.4G0539400.1	-1.072
4DPI	TTCCAGGTAATCGGCAGGTT	20	1.765	BdiBd21-3.3G0774600.1	-0.887
4DPI	TGAACCAGCCTTTGCCCGCCC	21	1.771	BdiBd21-3.1G0933800.1	-1.352
4DPI	TTTCAACTCTGCGGTCAGCC	20	1.788	BdiBd21-3.1G0212700.1	-0.953
4DPI	TTCGACGCAAATCTGACAGGC	21	1.808	BdiBd21-3.5G0309700.1	-1.387
4DPI	TTCGACGCAAATCTGACAGGC	21	1.808	BdiBd21-3.1G0028200.1	-1.001
4DPI	TGGCGGATTATGGGTTGTAA	20	1.819	BdiBd21-3.1G0122000.1	-0.949
4DPI	AGCAAACTGGCTGTTTCTGATT	22	1.881	BdiBd21-3.1G0840500.1	-0.993
4DPI	TACACTACAATACAGGGGGC	20	1.881	BdiBd21-3.4G0562600.1	-0.892
4DPI	TACACTACAATACAGGGGGC	20	1.881	BdiBd21-3.4G0095000.1	-0.845
4DPI	TTGTGTCCAAGCGTTCTGAAA	21	1.896	BdiBd21-3.3G0416400.1	-1.300
4DPI	TTGTGTCCAAGCGTTCTGAAA	21	1.896	BdiBd21-3.2G0285000.1	-1.059
4DPI	TTGTGTCCAAGCGTTCTGAAA	21	1.896	BdiBd21-3.2G0019400.1	-0.885
4DPI	TTGTGTCCAAGCGTTCTGAAA	21	1.896	BdiBd21-3.1G0146700.1	-0.860
4DPI	TTTCAGCCGGCGGCCTCCTC	20	1.904	BdiBd21-3.1G0493600.1	-1.477
4DPI	TTTCAGCCGGCGGCCTCCTC	20	1.904	BdiBd21-3.2G0253300.1	-1.004
4DPI	TTTCAGCCGGCGGCCTCCTC	20	1.904	BdiBd21-3.3G0419700.1	-0.937
4DPI	TTTCAGCCGGCGGCCTCCTC	20	1.904	BdiBd21-3.3G0450300.1	-0.902
4DPI	TCTCAAAGATCGTAGCCCCTT	21	1.914	BdiBd21-3.2G0073500.1	-1.324
4DPI	TCACTGGGCTATTAGCGGGC	20	1.914	BdiBd21-3.1G0415900.1	-0.860
4DPI	TGTAGGTACAGGTTGGCGGT	20	1.927	BdiBd21-3.5G0099300.1	-1.006
4DPI	TGTAGGTACAGGTTGGCGGT	20	1.927	BdiBd21-3.1G0865400.1	-0.966
4DPI	TCGGGCGGCTAGCTTTTCGGC	21	1.929	BdiBd21-3.1G0358400.1	-1.142

4DPI	TCGGGCGGCTAGCTTTTCGGC	21	1.929	BdiBd21-3.1G0999000.1	-0.984
4DPI	TGTGGGAGTTGGCTGTGAAT	20	1.936	BdiBd21-3.1G0701500.1	-1.829
4DPI	TCAGCCGGCGGCCTCCTCGG	20	1.936	BdiBd21-3.1G0493600.1	-1.477
4DPI	TGTGGGAGTTGGCTGTGAAT	20	1.936	BdiBd21-3.2G0604500.1	-1.467
4DPI	TGTGGGAGTTGGCTGTGAAT	20	1.936	BdiBd21-3.1G0385500.1	-1.394
4DPI	TGTGGGAGTTGGCTGTGAAT	20	1.936	BdiBd21-3.5G0057900.1	-1.340
4DPI	TGTGGGAGTTGGCTGTGAAT	20	1.936	BdiBd21-3.2G0213600.1	-1.328
4DPI	TCAGCCGGCGGCCTCCTCGG	20	1.936	BdiBd21-3.3G0267900.1	-1.122
4DPI	TCAGCCGGCGGCCTCCTCGG	20	1.936	BdiBd21-3.1G0212700.1	-0.953
4DPI	TGTGGGAGTTGGCTGTGAAT	20	1.936	BdiBd21-3.5G0325900.1	-0.928
4DPI	TGTGGGAGTTGGCTGTGAAT	20	1.936	BdiBd21-3.2G0430900.1	-0.828
4DPI	TGAGGGCATAGGTTGGGAGG	20	1.981	BdiBd21-3.1G0561500.1	-1.148
4DPI	TAAAGAAATGCCAGACCTGC	20	1.981	BdiBd21-3.1G0064400.1	-1.081
4DPI	TGAGGGCATAGGTTGGGAGG	20	1.981	BdiBd21-3.3G0734900.1	-0.974
4DPI	TGAGGGCATAGGTTGGGAGG	20	1.981	BdiBd21-3.2G0509400.1	-0.864
4DPI	TGGGGGGCGAACAGTAGACT	20	2.007	BdiBd21-3.4G0506800.1	-0.840
4DPI	TCGACGCAAATCTGACAGGC	20	2.012	BdiBd21-3.5G0309700.1	-1.387
4DPI	TCGACGCAAATCTGACAGGC	20	2.012	BdiBd21-3.1G0028200.1	-1.001
4DPI	CTTCGACGCAAATCTGACAGGC	22	2.014	BdiBd21-3.5G0309700.1	-1.387
4DPI	CTTCGACGCAAATCTGACAGGC	22	2.014	BdiBd21-3.1G0028200.1	-1.001
4DPI	TATCCCAGGCGGGCTCCGTT	20	2.016	BdiBd21-3.1G0493600.1	-1.477
4DPI	TATCCCAGGCGGGCTCCGTT	20	2.016	BdiBd21-3.1G0677400.1	-0.885
4DPI	TATCCCAGGCGGGCTCCGTT	20	2.016	BdiBd21-3.4G0600500.1	-0.817
4DPI	TGGCGGTGCAGGTTGTTGGC	20	2.026	BdiBd21-3.3G0728900.1	-1.025
4DPI	TGGCGGTGCAGGTTGTTGGC	20	2.026	BdiBd21-3.2G0086100.1	-0.882
4DPI	TGGCGGTGCAGGTTGTTGGC	20	2.026	BdiBd21-3.1G0235400.1	-0.816
4DPI	TATTTCAGCCGGCGGCCTCC	20	2.034	BdiBd21-3.3G0450300.1	-0.902
4DPI	TTCCGTCGTCGCCGTATTGT	20	2.034	BdiBd21-3.3G0782600.1	-1.234
4DPI	TTCCGTCGTCGCCGTATTGT	20	2.034	BdiBd21-3.1G0032200.1	-0.838
4DPI	TCTCATCTTAGTCAGGCGGT	20	2.051	BdiBd21-3.1G0531500.1	-1.705
4DPI	TAATCGGGACGCTAGAACTT	20	2.051	BdiBd21-3.3G0267900.1	-1.122
4DPI	TGGCTGTGAATTCGGCGAGGG	21	2.051	BdiBd21-3.5G0099300.1	-1.006
4DPI	TGAGCAGCGTTTTCCAGGTA	20	2.051	BdiBd21-3.1G0642800.1	-0.914
4DPI	TGGCTGTGAATTCGGCGAGGG	21	2.051	BdiBd21-3.1G0032200.1	-0.838
4DPI	TAACGACCCTATGGACCTGA	20	2.051	BdiBd21-3.4G0603600.1	-0.831
4DPI	TAACGACCCTATGGACCTGA	20	2.051	BdiBd21-3.5G0074200.1	-0.803
4DPI	TCAGTTCGGCAGGCAGGATC	20	2.104	BdiBd21-3.1G0782600.1	-0.984
4DPI	TCAGTTCGGCAGGCAGGATC	20	2.104	BdiBd21-3.3G0606400.1	-0.953
4DPI	ATACCGTCGTAGTCTTAACCA	21	2.113	BdiBd21-3.1G0296100.1	-0.853
4DPI	ATACCGTCGTAGTCTTAACCA	21	2.113	BdiBd21-3.4G0106400.1	-0.809
4DPI	TCGGACTTGTGGGAGTTGGCT	21	2.116	BdiBd21-3.2G0233500.1	-2.069
4DPI	TCGGACTTGTGGGAGTTGGCT	21	2.116	BdiBd21-3.2G0692200.1	-1.386
4DPI	TCGGACTTGTGGGAGTTGGCT	21	2.116	BdiBd21-3.1G0591400.1	-1.368
4DPI	TCGGACTTGTGGGAGTTGGCT	21	2.116	BdiBd21-3.1G0677400.1	-0.885
4DPI	TAAGGCGTCGGTTTCGGCTT	20	2.125	BdiBd21-3.5G0013300.1	-1.674
4DPI	TAAGGCGTCGGTTTCGGCTT	20	2.125	BdiBd21-3.2G0141900.1	-1.278
4DPI	TAAGTCGCGTAAAACGGGGA	20	2.125	BdiBd21-3.3G0782600.1	-1.234
4DPI	TAAGGCGTCGGTTTCGGCTT	20	2.125	BdiBd21-3.1G0258400.1	-1.224
4DPI	CGCACATTGCGCCCGCCGGTAT	22	2.125	BdiBd21-3.2G0707700.1	-1.005
4DPI	TAAGTCGCGTAAAACGGGGA	20	2.125	BdiBd21-3.5G0222200.1	-0.940

4DPI	TCGCTTTGGCGGCGCGCCGGC	21	2.132	BdiBd21-3.1G0133400.1	-1.695
4DPI	TCGCTTTGGCGGCGCGCCGGC	21	2.132	BdiBd21-3.1G0937800.1	-1.149
4DPI	TCGCTTTGGCGGCGCGCCGGC	21	2.132	BdiBd21-3.3G0040500.1	-1.069
4DPI	TGACGGAGCTCGGCCTGGAA	20	2.139	BdiBd21-3.3G0697400.1	-1.331
4DPI	TGACGGAGCTCGGCCTGGAA	20	2.139	BdiBd21-3.2G0675000.1	-1.083
4DPI	TGACGGAGCTCGGCCTGGAA	20	2.139	BdiBd21-3.1G0122000.1	-0.949
4DPI	TGACGGAGCTCGGCCTGGAA	20	2.139	BdiBd21-3.5G0304000.1	-0.904
4DPI	TTCGGCATCCCGCTGGGCGG	20	2.177	BdiBd21-3.1G0436600.1	-2.139
4DPI	TTCGGCATCCCGCTGGGCGG	20	2.177	BdiBd21-3.4G0104000.1	-2.025
4DPI	CACCTGGCCTACACTCTGAA	20	2.177	BdiBd21-3.2G0719000.1	-1.497
4DPI	CACCTGGCCTACACTCTGAA	20	2.177	BdiBd21-3.2G0062600.1	-1.152
4DPI	TTCGGCATCCCGCTGGGCGG	20	2.177	BdiBd21-3.2G0601700.1	-0.842
4DPI	TAATGTAGCATTCCGGGCCA	20	2.187	BdiBd21-3.5G0013300.1	-1.674
4DPI	TGCCCACTCCTGAACGCTCA	20	2.189	BdiBd21-3.4G0079700.1	-0.855
4DPI	TGAATTGGAAGCGTTAGGGG	20	2.198	BdiBd21-3.1G0841300.1	-0.897
4DPI	TAGGTACAGGTTGGCGGTGT	20	2.203	BdiBd21-3.1G0454500.1	-1.304
4DPI	TATCGTACAGGACCGGGTAG	20	2.203	BdiBd21-3.1G0258400.1	-1.224
4DPI	TATCGTACAGGACCGGGTAG	20	2.203	BdiBd21-3.4G0228800.1	-1.174
4DPI	TATCGTACAGGACCGGGTAG	20	2.203	BdiBd21-3.1G0882100.1	-1.137
4DPI	TGACCGCCGCCCAAGCCCGT	20	2.203	BdiBd21-3.2G0674800.1	-1.065
4DPI	TAGGTACAGGTTGGCGGTGT	20	2.203	BdiBd21-3.4G0092400.1	-1.011
4DPI	TAGGTACAGGTTGGCGGTGT	20	2.203	BdiBd21-3.5G0099300.1	-1.006
4DPI	TGACCGCCGCCCAAGCCCGT	20	2.203	BdiBd21-3.3G0699800.1	-0.950
4DPI	TGACCGCCGCCCAAGCCCGT	20	2.203	BdiBd21-3.4G0103100.1	-0.909
4DPI	TATCGTACAGGACCGGGTAG	20	2.203	BdiBd21-3.1G0277900.1	-0.836
4DPI	TTCGACTGTTGAGCCGGGGG	20	2.218	BdiBd21-3.5G0250000.1	-1.193
4DPI	TTCGACTGTTGAGCCGGGGG	20	2.218	BdiBd21-3.2G0618500.1	-1.071
4DPI	TCGACCTGTAAAAACCCCCT	20	2.244	BdiBd21-3.4G0529400.1	-1.762
4DPI	TTTGGACCTGCCGTCGTCTA	20	2.244	BdiBd21-3.1G0784600.1	-1.278
4DPI	TGATTCGGCGGCAGGTCTGGC	21	2.244	BdiBd21-3.1G0170300.1	-1.169
4DPI	TTTGGACCTGCCGTCGTCTA	20	2.244	BdiBd21-3.3G0545700.1	-1.116
4DPI	TGATTCGGCGGCAGGTCTGGC	21	2.244	BdiBd21-3.5G0246500.1	-1.102
4DPI	TGATTCGGCGGCAGGTCTGGC	21	2.244	BdiBd21-3.5G0025600.1	-1.019
4DPI	TTCTGAAGATCAATGGCCCC	20	2.244	BdiBd21-3.4G0101300.1	-0.935
4DPI	TGATTCGGCGGCAGGTCTGGC	21	2.244	BdiBd21-3.1G0857400.1	-0.875
4DPI	TTACACGAAAGTACAAGTTTC	21	2.267	BdiBd21-3.1G0035700.1	-1.150
4DPI	TTACACGAAAGTACAAGTTTC	21	2.267	BdiBd21-3.1G0411600.1	-0.950
4DPI	TACGCCCGCCGCCGATCCTG	20	2.271	BdiBd21-3.1G0692900.1	-1.352
4DPI	TATATTTTGTTAAAACGGGCT	21	2.286	BdiBd21-3.1G0490900.1	-1.104
4DPI	TATATTTTGTTAAAACGGGCT	21	2.286	BdiBd21-3.1G0583500.1	-0.955
4DPI	TCGGGACAGCAGGTCGTAGG	20	2.296	BdiBd21-3.1G0151100.1	-1.305
4DPI	TCGGGACAGCAGGTCGTAGG	20	2.296	BdiBd21-3.1G0937800.1	-1.149
4DPI	TCGGGACAGCAGGTCGTAGG	20	2.296	BdiBd21-3.2G0093700.1	-1.012
4DPI	TCGGGACAGCAGGTCGTAGG	20	2.296	BdiBd21-3.3G0450300.1	-0.902
4DPI	TAGCGCCTGCGAAACCGCCT	20	2.338	BdiBd21-3.3G0797000.1	-1.474
4DPI	TAGCGCCTGCGAAACCGCCT	20	2.338	BdiBd21-3.5G0006400.1	-1.054
4DPI	TCGTTCAGAAAGGCGGGCGGA	21	2.341	BdiBd21-3.3G0420100.1	-0.874
4DPI	TGAGCAGGGTAGGTTTGGGT	20	2.351	BdiBd21-3.2G0233500.1	-2.069
4DPI	TAAAAATCGCTAGGTCGCCC	20	2.351	BdiBd21-3.5G0187400.1	-1.251
4DPI	TGAGCAGGGTAGGTTTGGGT	20	2.351	BdiBd21-3.2G0681400.1	-1.226

4DPI	TGAGCAGGGTAGGTTTGGGT	20	2.351	BdiBd21-3.4G0095000.1	-0.845
4DPI	TGAGCAGGGTAGGTTTGGGT	20	2.351	BdiBd21-3.1G0812400.1	-0.836
4DPI	TAGACCGCCTGACTAAGATG	20	2.363	BdiBd21-3.2G0051100.1	-0.899
4DPI	TAGACCGCCTGACTAAGATG	20	2.363	BdiBd21-3.1G0404800.1	-0.875
4DPI	AGATGAACTTTCACCTGACC	20	2.372	BdiBd21-3.4G0101300.1	-0.935
4DPI	TACGACATGATAAGACGCCT	20	2.373	BdiBd21-3.1G0677400.1	-0.885
4DPI	TAACGGGCTTGGGCGGCGGT	20	2.388	BdiBd21-3.3G0524900.1	-1.007
4DPI	TAACGGGCTTGGGCGGCGGT	20	2.388	BdiBd21-3.2G0208300.1	-0.813
4DPI	TAATGTAGCATTCCGGGCCAG	21	2.391	BdiBd21-3.5G0013300.1	-1.674
4DPI	TCGCACTTCGCGGCGTTGGCG	21	2.399	BdiBd21-3.1G0757300.1	-1.810
4DPI	TCGCACTTCGCGGCGTTGGCG	21	2.399	BdiBd21-3.2G0079800.1	-1.587
4DPI	TCGCACTTCGCGGCGTTGGCG	21	2.399	BdiBd21-3.3G0682100.1	-1.517
4DPI	TCGCACTTCGCGGCGTTGGCG	21	2.399	BdiBd21-3.3G0497100.1	-1.109
4DPI	TCGCACTTCGCGGCGTTGGCG	21	2.399	BdiBd21-3.1G0296400.1	-1.053
4DPI	TCGCACTTCGCGGCGTTGGCG	21	2.399	BdiBd21-3.1G0996900.1	-1.047
4DPI	TCGCACTTCGCGGCGTTGGCG	21	2.399	BdiBd21-3.1G0411600.1	-0.950
4DPI	TGAACAACCTGGCCGGCATGA	21	2.437	BdiBd21-3.2G0723200.1	-1.386
4DPI	TGGGCGGCGGTCATTTCGGC	20	2.466	BdiBd21-3.3G0739100.1	-1.864
4DPI	TCGGTTTCGGCTTCTGGGGT	20	2.466	BdiBd21-3.5G0316400.1	-1.672
4DPI	TGGGCGGCGGTCATTTCGGC	20	2.466	BdiBd21-3.2G0290700.1	-1.587
4DPI	TGGGCGGCGGTCATTTCGGC	20	2.466	BdiBd21-3.4G0237000.1	-1.411
4DPI	CGCCGGGCGGATCATCCAGCG	21	2.466	BdiBd21-3.2G0213600.1	-1.328
4DPI	TCGGTTTCGGCTTCTGGGGT	20	2.466	BdiBd21-3.2G0141900.1	-1.278
4DPI	TCGGTTTCGGCTTCTGGGGT	20	2.466	BdiBd21-3.2G0063400.1	-1.192
4DPI	TAGAGATTAGTCTACGGCCT	20	2.466	BdiBd21-3.3G0671500.1	-1.106
4DPI	TTTCAGGCACTGCAGCGCTCG	21	2.466	BdiBd21-3.3G0020900.1	-1.040
4DPI	TGAGCGTTCAGGAGTGGGCA	20	2.466	BdiBd21-3.3G0452400.1	-1.006
4DPI	TGGGCGGCGGTCATTTCGGC	20	2.466	BdiBd21-3.2G0010300.1	-0.907
4DPI	TGAGCGTTCAGGAGTGGGCA	20	2.466	BdiBd21-3.4G0622000.1	-0.868
4DPI	TCGTAGACCGCCTGACTAAG	20	2.466	BdiBd21-3.3G0034900.1	-0.860
4DPI	TGGGCGGCGGTCATTTCGGC	20	2.466	BdiBd21-3.2G0601700.1	-0.842
4DPI	TACCAAAAACAACCTCTGAAT	21	2.466	BdiBd21-3.4G0504700.1	-0.816
4DPI	TACCAAAAACAACCTCTGAAT	21	2.466	BdiBd21-3.3G0041500.1	-0.814
4DPI	TAAATAATTGGTTGGGGGAG	20	2.525	BdiBd21-3.5G0321100.1	-2.236
4DPI	TAAATAATTGGTTGGGGGAG	20	2.525	BdiBd21-3.2G0618500.1	-1.071
4DPI	TAAATAATTGGTTGGGGGAG	20	2.525	BdiBd21-3.3G0714200.1	-0.962
4DPI	ACGATCTTTGAGAAATCTCGGA	22	2.528	BdiBd21-3.1G0258400.1	-1.224
4DPI	TGCACCAAATCGATTGCGGGC	21	2.532	BdiBd21-3.5G0236400.1	-0.804
4DPI	GGGCCGGTTCGGGGTGTAGGC	21	2.537	BdiBd21-3.1G0722200.1	-1.633
4DPI	TAGGCAGGAGTTCAGGCGGA	20	2.537	BdiBd21-3.5G0099300.1	-1.006
4DPI	TAGGCAGGAGTTCAGGCGGA	20	2.537	BdiBd21-3.5G0304000.1	-0.904
4DPI	GGGCCGGTTCGGGGTGTAGGC	21	2.537	BdiBd21-3.1G0553500.1	-0.870
4DPI	GGGCCGGTTCGGGGTGTAGGC	21	2.537	BdiBd21-3.4G0048900.1	-0.846
4DPI	TCTGAAACAGGGCCCAAGAG	20	2.556	BdiBd21-3.1G0892700.1	-1.047
4DPI	TAACGGGCTTGGGCGGCGGTC	21	2.566	BdiBd21-3.3G0524900.1	-1.007
4DPI	TTTTGGGAAACCCGCGGCCG	20	2.570	BdiBd21-3.3G0524900.1	-1.007
4DPI	ACGGCGTTCTTTGGAGTGTA	20	2.577	BdiBd21-3.2G0204500.1	-2.494
4DPI	ACGGCGTTCTTTGGAGTGTA	20	2.577	BdiBd21-3.5G0036800.1	-1.081
4DPI	ACGGCGTTCTTTGGAGTGTA	20	2.577	BdiBd21-3.1G0978900.1	-0.818
4DPI	ACGGCGTTCTTTGGAGTGTA	20	2.577	BdiBd21-3.2G0321800.1	-0.812

4DPI	TGGCTGTGAATTCGGCGAGGGG	22	2.586	BdiBd21-3.1G0032200.1	-0.838
4DPI	TCGGTCAGCCTGGTACTGGG	20	2.592	BdiBd21-3.1G1013900.1	-1.047
4DPI	TCGGTCAGCCTGGTACTGGG	20	2.592	BdiBd21-3.1G0999000.1	-0.984
4DPI	TCGGTCAGCCTGGTACTGGG	20	2.592	BdiBd21-3.4G0103100.1	-0.909
4DPI	TCGGTCAGCCTGGTACTGGG	20	2.592	BdiBd21-3.1G0449300.1	-0.859
4DPI	TCGGTCAGCCTGGTACTGGG	20	2.592	BdiBd21-3.2G0560600.1	-0.834
4DPI	TGCAATGCCGAGGACACCGC	20	2.601	BdiBd21-3.1G0086100.1	-1.346
4DPI	TGCAATGCCGAGGACACCGC	20	2.601	BdiBd21-3.1G0122000.1	-0.949
4DPI	TAAAGGGACCTGCAATGCCG	20	2.636	BdiBd21-3.3G0743700.1	-1.041
4DPI	TAAAGGGACCTGCAATGCCG	20	2.636	BdiBd21-3.2G0084900.1	-1.026
4DPI	TAGGTACAAACAGGACAGGC	20	2.659	BdiBd21-3.5G0309700.1	-1.387
4DPI	TGTATCGAAAGCGACGCGGC	20	2.673	BdiBd21-3.1G0930600.1	-1.610
4DPI	TGTATCGAAAGCGACGCGGC	20	2.673	BdiBd21-3.1G0296400.1	-1.053
4DPI	TCCGTCGTCGCCGTATTGTA	20	2.703	BdiBd21-3.3G0623700.1	-1.051
4DPI	TCCGTCGTCGCCGTATTGTA	20	2.703	BdiBd21-3.1G0032200.1	-0.838
4DPI	TACCTGCCCGCCCCACCCGG	20	2.729	BdiBd21-3.1G0062100.1	-1.825
4DPI	TCCACCAGGGAGCCGAGCTGT	21	2.729	BdiBd21-3.1G0133400.1	-1.695
4DPI	TTCTGCGGGCGGGCGGTCTG	20	2.729	BdiBd21-3.4G0237000.1	-1.411
4DPI	TCGACTGTTGAGCCGGGGGTA	21	2.729	BdiBd21-3.2G0618500.1	-1.071
4DPI	TCCACCAGGGAGCCGAGCTGT	21	2.729	BdiBd21-3.3G0459600.1	-0.998
4DPI	TCCACCAGGGAGCCGAGCTGT	21	2.729	BdiBd21-3.4G0218500.1	-0.945
4DPI	TTCTGCGGGCGGGCGGTCTG	20	2.729	BdiBd21-3.1G0347500.1	-0.839
4DPI	TCGACTGTTGAGCCGGGGGT	20	2.734	BdiBd21-3.1G0578200.1	-1.156
4DPI	TCGACTGTTGAGCCGGGGGT	20	2.734	BdiBd21-3.2G0618500.1	-1.071
4DPI	TCTGTGACAGTATTCCCCCC	20	2.734	BdiBd21-3.5G0031700.1	-0.840
4DPI	TCTGTGACAGTATTCCCCCC	20	2.734	BdiBd21-3.1G0167300.1	-0.811
4DPI	TGATCCTGGAGACCGACGCTT	21	2.746	BdiBd21-3.1G0404800.1	-0.875
4DPI	TGATCCTGGAGACCGACGCTT	21	2.746	BdiBd21-3.2G0480500.1	-0.841
4DPI	TTCTTCTGCGGGCGGGCGGT	20	2.762	BdiBd21-3.5G0017400.1	-1.246
4DPI	TAGTAGGGCTGCAAGATCTA	20	2.762	BdiBd21-3.1G0271300.1	-1.221
4DPI	TGGGAATCCTCGGTGTTGTATG	22	2.762	BdiBd21-3.3G0434700.1	-1.203
4DPI	TCGGCATGAAATACGCGGCT	20	2.762	BdiBd21-3.1G0322600.1	-1.138
4DPI	TGGGAATCCTCGGTGTTGTATG	22	2.762	BdiBd21-3.4G0272600.1	-0.984
4DPI	TAGTAGGGCTGCAAGATCTA	20	2.762	BdiBd21-3.5G0116500.1	-0.909
4DPI	TTCTTCTGCGGGCGGGCGGT	20	2.762	BdiBd21-3.1G0073200.1	-0.877
4DPI	TTCTTCTGCGGGCGGGCGGT	20	2.762	BdiBd21-3.1G0327300.1	-0.843
4DPI	TTCTTCTGCGGGCGGGCGGT	20	2.762	BdiBd21-3.1G0347500.1	-0.839
4DPI	TAAACGCGGTAAGGACCCTCG	21	2.771	BdiBd21-3.1G0843800.1	-0.900
4DPI	CGCCGGGCGGATCATCCAGC	20	2.784	BdiBd21-3.2G0733800.1	-2.299
4DPI	CGCCGGGCGGATCATCCAGC	20	2.784	BdiBd21-3.2G0213600.1	-1.328
4DPI	CGCCGGGCGGATCATCCAGC	20	2.784	BdiBd21-3.1G0073200.1	-0.877
4DPI	CGCCGGGCGGATCATCCAGC	20	2.784	BdiBd21-3.2G0560600.1	-0.834
4DPI	TATATTTCAGCCGGCGGCCT	20	2.785	BdiBd21-3.3G0020900.1	-1.040
4DPI	TGAGGGCGCAACCTTTGGTCG	21	2.788	BdiBd21-3.5G0013300.1	-1.674
4DPI	TGATTCGGCGGCAGGTCTGG	20	2.788	BdiBd21-3.1G0170300.1	-1.169
4DPI	AGAGGGGGATTCTAATTCTGAA	22	2.788	BdiBd21-3.4G0445800.1	-1.137
4DPI	TGATTCGGCGGCAGGTCTGG	20	2.788	BdiBd21-3.5G0246500.1	-1.102
4DPI	TGATTCGGCGGCAGGTCTGG	20	2.788	BdiBd21-3.5G0025600.1	-1.019
4DPI	TGATTCGGCGGCAGGTCTGG	20	2.788	BdiBd21-3.1G0857400.1	-0.875
4DPI	AGAGGGGGATTCTAATTCTGAA	22	2.788	BdiBd21-3.4G0162100.1	-0.857

4DPI	TGCCCGCAATCGATTTGGTG	20	2.788	BdiBd21-3.2G0608000.1	-0.826
4DPI	TACCGACCCGGGAAACAAGG	20	2.829	BdiBd21-3.5G0232700.1	-1.197
4DPI	TCGGCGCGGGCTTGTTCCAG	20	2.829	BdiBd21-3.2G0063400.1	-1.192
4DPI	TACCGACCCGGGAAACAAGG	20	2.829	BdiBd21-3.2G0233800.1	-1.122
4DPI	TCGGCGCGGGCTTGTTCCAG	20	2.829	BdiBd21-3.2G0093700.1	-1.012
4DPI	CCGGCATGAAATTCTTCTCGAA	22	2.829	BdiBd21-3.1G0093800.1	-0.994
4DPI	TCGGCGCGGGCTTGTTCCAG	20	2.829	BdiBd21-3.3G0416100.1	-0.984
4DPI	TCGAACTTCGGCTGCTGGAG	20	2.881	BdiBd21-3.4G0575200.1	-0.938
4DPI	TCGAACTTCGGCTGCTGGAG	20	2.881	BdiBd21-3.2G0086100.1	-0.882
4DPI	TACGACGATTGCCGGTGAGT	20	2.904	BdiBd21-3.1G0385500.1	-1.394
4DPI	TACGACGATTGCCGGTGAGT	20	2.904	BdiBd21-3.3G0215700.1	-1.115
4DPI	TACGACGATTGCCGGTGAGT	20	2.904	BdiBd21-3.1G0278900.1	-0.889
4DPI	TAAGTCGTTCATCCCCCTCC	20	2.904	BdiBd21-3.1G0312200.1	-0.811
4DPI	TAGAAAATAGGCTGCAGGGC	20	2.910	BdiBd21-3.1G0110700.1	-0.861
4DPI	TAGAAAATAGGCTGCAGGGC	20	2.910	BdiBd21-3.1G0110700.1	-0.861
4DPI	TAGCCATGTAGCGTTCTGCT	20	2.914	BdiBd21-3.5G0227400.1	-1.284
4DPI	TAGCCATGTAGCGTTCTGCT	20	2.914	BdiBd21-3.1G0298500.1	-1.209
4DPI	TAGCCATGTAGCGTTCTGCT	20	2.914	BdiBd21-3.1G0490900.1	-1.104
4DPI	TAGCCATGTAGCGTTCTGCT	20	2.914	BdiBd21-3.1G0028200.1	-1.001
4DPI	TCGGAACTTTGGCTGATCGA	20	2.932	BdiBd21-3.2G0285000.1	-1.059
4DPI	TCGGAACTTTGGCTGATCGA	20	2.932	BdiBd21-3.2G0748600.1	-1.024
4DPI	TACCGTCGTAGTCTTAACCA	20	2.952	BdiBd21-3.1G0041600.1	-1.048
4DPI	TCGCTTAGTCATGACCCCTG	20	2.952	BdiBd21-3.3G0694000.1	-0.933
4DPI	TACCGTCGTAGTCTTAACCA	20	2.952	BdiBd21-3.1G0296100.1	-0.853
4DPI	TACCGTCGTAGTCTTAACCA	20	2.952	BdiBd21-3.4G0106400.1	-0.809
4DPI	TGGCCAGCTCGTCAGCCCGG	20	2.956	BdiBd21-3.5G0321100.1	-2.236
4DPI	TGGCCAGCTCGTCAGCCCGG	20	2.956	BdiBd21-3.3G0682100.1	-1.517
4DPI	TGGCCAGCTCGTCAGCCCGG	20	2.956	BdiBd21-3.1G0020300.1	-1.143
4DPI	TTTTCGGCATCCCGCTGGGC	20	2.964	BdiBd21-3.1G0436600.1	-2.139
4DPI	CGCCGGGCGGATCATCCAGCGT	22	2.964	BdiBd21-3.2G0213600.1	-1.328
4DPI	TTTTCGGCATCCCGCTGGGC	20	2.964	BdiBd21-3.3G0250700.1	-1.097
4DPI	TTTTCGGCATCCCGCTGGGC	20	2.964	BdiBd21-3.2G0601700.1	-0.842
4DPI	TGACGTTGAGCCCCTGCCGG	20	2.997	BdiBd21-3.3G0171900.1	-1.436
4DPI	TGACGTTGAGCCCCTGCCGG	20	2.997	BdiBd21-3.2G0245400.1	-1.330
4DPI	TGACGTTGAGCCCCTGCCGG	20	2.997	BdiBd21-3.2G0100000.1	-1.134
4DPI	TGACGTTGAGCCCCTGCCGG	20	2.997	BdiBd21-3.4G0081500.1	-0.915
4DPI	TGACGTTGAGCCCCTGCCGG	20	2.997	BdiBd21-3.4G0416900.1	-0.831
4DPI	CAATCGTTGTCTGGCATTGA	20	3.030	BdiBd21-3.2G0771500.1	-1.331
4DPI	TCGGCGAACGCGACGGGGAA	20	3.051	BdiBd21-3.1G0531500.1	-1.705
4DPI	TCATCCTCCGGGCTTTTCCA	20	3.051	BdiBd21-3.2G0593000.1	-1.683
4DPI	TCGGCGAACGCGACGGGGAA	20	3.051	BdiBd21-3.2G0687400.1	-1.674
4DPI	AGCGTTTTCCAGGTAATCGGC	21	3.051	BdiBd21-3.5G0013300.1	-1.674
4DPI	TTCCACCGTCGATACCCCCA	20	3.051	BdiBd21-3.5G0057900.1	-1.340
4DPI	TACGGTCAAGGCCCGAGCTG	20	3.051	BdiBd21-3.1G0549600.1	-1.327
4DPI	TCATCCTCCGGGCTTTTCCA	20	3.051	BdiBd21-3.4G0518100.1	-1.218
4DPI	TCATCCTCCGGGCTTTTCCA	20	3.051	BdiBd21-3.1G0298500.1	-1.209
4DPI	TTCCACCGTCGATACCCCCA	20	3.051	BdiBd21-3.1G0341200.1	-1.167
4DPI	TCGGCGAACGCGACGGGGAA	20	3.051	BdiBd21-3.1G0578200.1	-1.156
4DPI	TCGACAGGACGGAAAATAGC	20	3.051	BdiBd21-3.3G0215700.1	-1.115
4DPI	TGTATTTACCTCGTGCCCCC	20	3.051	BdiBd21-3.2G0044700.1	-1.047

4DPI	TCATCCTCCGGGCTTTTCCA	20	3.051	BdiBd21-3.3G0690400.1	-1.035
4DPI	TGTATTTACCTCGTGCCCCC	20	3.051	BdiBd21-3.1G0128900.1	-0.993
4DPI	AGCGTTTTCCAGGTAATCGGC	21	3.051	BdiBd21-3.1G0263200.1	-0.981
4DPI	TAATTTCGACGCTGCCCTGA	20	3.051	BdiBd21-3.4G0432900.1	-0.961
4DPI	TCGGCGAACGCGACGGGGAA	20	3.051	BdiBd21-3.4G0276900.1	-0.933
4DPI	TCATCCTCCGGGCTTTTCCA	20	3.051	BdiBd21-3.1G0073200.1	-0.877
4DPI	GCGGGTGCTGAGAAAGCGTTTC	22	3.051	BdiBd21-3.4G0048900.1	-0.846
4DPI	GTTTAGTCTTTCGCAACATAC	21	3.051	BdiBd21-3.2G0430900.1	-0.828
4DPI	TTGTAAGGCCGTCAGCGGGC	20	3.111	BdiBd21-3.1G0635100.1	-1.050
4DPI	TGAGCTTCGCGGATGAGAGC	20	3.115	BdiBd21-3.4G0529400.1	-1.762
4DPI	TGAGCTTCGCGGATGAGAGC	20	3.115	BdiBd21-3.2G0606700.1	-0.844
4DPI	TGAGCTTCGCGGATGAGAGC	20	3.115	BdiBd21-3.1G0277900.1	-0.836
4DPI	TTGGACGAACCCCCGAATTG	20	3.125	BdiBd21-3.2G0604300.1	-0.915
4DPI	TTGGACGAACCCCCGAATTG	20	3.125	BdiBd21-3.3G0446100.1	-0.821
4DPI	TAACCCGCTGGAATTCGGAC	20	3.144	BdiBd21-3.1G0404800.1	-0.875
4DPI	TGACCCGCAAGGCAGAGGAT	20	3.177	BdiBd21-3.3G0130600.1	-1.882
4DPI	TTTCATCTTTCAACTGAGGCTC	22	3.177	BdiBd21-3.3G0697400.1	-1.331
4DPI	TCAATTTCGTCAAAGGGGCCA	21	3.177	BdiBd21-3.5G0227400.1	-1.284
4DPI	TGACTGAACCCCAGATTGGACG	22	3.177	BdiBd21-3.2G0803500.1	-1.242
4DPI	TCAATTTCGTCAAAGGGGCCA	21	3.177	BdiBd21-3.2G0550200.1	-1.176
4DPI	TTTCGACTGTTGAGCCGGGGG	21	3.177	BdiBd21-3.2G0618500.1	-1.071
4DPI	TCTTGACAGGAATTCGGCCCA	21	3.177	BdiBd21-3.1G1013900.1	-1.047
4DPI	ACACCTGATAGAGCTACTAA	20	3.203	BdiBd21-3.3G0699800.1	-0.950
4DPI	TCGAAAAACGGAGCCCGCCT	20	3.203	BdiBd21-3.4G0303000.1	-0.821
4DPI	TAATTCCGTCTCCTTCAGCTG	21	3.263	BdiBd21-3.5G0298100.1	-0.953
4DPI	TAATTCCGTCTCCTTCAGCTG	21	3.263	BdiBd21-3.1G0122000.1	-0.949
4DPI	TATTCCCCCCTTCCAGGCCG	20	3.274	BdiBd21-3.3G0130600.1	-1.882
4DPI	TATTCCCCCCTTCCAGGCCG	20	3.274	BdiBd21-3.1G0747800.1	-1.294
4DPI	TATTCCCCCCTTCCAGGCCG	20	3.274	BdiBd21-3.1G0128600.1	-1.133
4DPI	TATTCCCCCCTTCCAGGCCG	20	3.274	BdiBd21-3.5G0036800.1	-1.081
4DPI	TGTACATCCTCTGCCTTGCGG	21	3.314	BdiBd21-3.2G0094400.1	-1.628
4DPI	TAACCGGGTGGGGCGGGCAG	20	3.314	BdiBd21-3.3G0695300.1	-1.465
4DPI	TGGGACGAACATTGCCGCGT	20	3.314	BdiBd21-3.3G0059500.1	-1.242
4DPI	TGTACATCCTCTGCCTTGCGG	21	3.314	BdiBd21-3.1G0692300.1	-1.206
4DPI	TAACCGGGTGGGGCGGGCAG	20	3.314	BdiBd21-3.4G0461700.1	-1.184
4DPI	TCATTTCGGCGCGGGCTTGT	20	3.314	BdiBd21-3.5G0283700.1	-1.018
4DPI	TGGGACGAACATTGCCGCGT	20	3.314	BdiBd21-3.1G0132300.1	-1.017
4DPI	TCATTTCGGCGCGGGCTTGT	20	3.314	BdiBd21-3.2G0093700.1	-1.012
4DPI	CACTGCCTGGAGGCGACGCGAA	22	3.314	BdiBd21-3.1G0028200.1	-1.001
4DPI	TCATTTCGGCGCGGGCTTGT	20	3.314	BdiBd21-3.4G0311300.1	-0.968
4DPI	TAGTGCAAAAACCCCTGAAA	20	3.314	BdiBd21-3.3G0730700.1	-0.968
4DPI	TGGGACGAACATTGCCGCGT	20	3.314	BdiBd21-3.4G0110600.1	-0.899
4DPI	TGTACATCCTCTGCCTTGCGG	21	3.314	BdiBd21-3.3G0007100.1	-0.890
4DPI	TACCCCTCGGGCCGCAGCGC	20	3.314	BdiBd21-3.1G0277900.1	-0.836
4DPI	TGGGACGAACATTGCCGCGT	20	3.314	BdiBd21-3.4G0603600.1	-0.831
4DPI	TGTACATCCTCTGCCTTGCGG	21	3.314	BdiBd21-3.2G0627900.1	-0.821
4DPI	TGACAGCGATTTTGCCGGGGC	21	3.353	BdiBd21-3.1G0747800.1	-1.294
4DPI	TGACAGCGATTTTGCCGGGGC	21	3.353	BdiBd21-3.2G0604300.1	-0.915
4DPI	TATTTTAGCACACCCGGCTG	20	3.373	BdiBd21-3.1G0944500.1	-2.292
4DPI	TTTCGGCATCCCGCTGGGCG	20	3.414	BdiBd21-3.1G0436600.1	-2.139

4DPI	TTTCGGCATCCCGCTGGGCG	20	3.414	BdiBd21-3.4G0104000.1	-2.025
4DPI	TTTCGGCATCCCGCTGGGCG	20	3.414	BdiBd21-3.3G0250700.1	-1.097
4DPI	TTTCGGCATCCCGCTGGGCG	20	3.414	BdiBd21-3.2G0601700.1	-0.842
4DPI	TGACCGGCGACGGGGGAGTCGT	22	3.466	BdiBd21-3.2G0699400.1	-2.218
4DPI	TGACCGGCGACGGGGGAGTCGT	22	3.466	BdiBd21-3.2G0699400.1	-2.218
4DPI	ATGAAACCGACTTTCTCTGAAG	22	3.466	BdiBd21-3.3G0340300.1	-1.750
4DPI	TGACCGGCGACGGGGGAGTCGT	22	3.466	BdiBd21-3.1G0488800.1	-1.049
4DPI	GCACATTGCGCCCGCCGGTAT	21	3.466	BdiBd21-3.2G0707700.1	-1.005
4DPI	TGACCGGCGACGGGGGAGTCGT	22	3.466	BdiBd21-3.2G0663700.1	-0.837
4DPI	TGACCGGCGACGGGGGAGTCGT	22	3.466	BdiBd21-3.1G0659000.1	-0.815
4DPI	TATGTCGGGTTGGGTTCGGG	20	3.521	BdiBd21-3.3G0496800.1	-1.284
4DPI	TATGTCGGGTTGGGTTCGGG	20	3.521	BdiBd21-3.3G0532600.1	-1.121
4DPI	TATGTCGGGTTGGGTTCGGG	20	3.521	BdiBd21-3.2G0614200.1	-1.065
4DPI	TAGATCGGTTGGTGTCGGGC	20	3.548	BdiBd21-3.2G0145300.1	-1.300
4DPI	TAGATCGGTTGGTGTCGGGC	20	3.548	BdiBd21-3.1G0782600.1	-0.984
4DPI	TAGATCGGTTGGTGTCGGGC	20	3.548	BdiBd21-3.2G0430900.1	-0.828
4DPI	TCTTGGTCATCCTCCGGGCT	20	3.566	BdiBd21-3.5G0057900.1	-1.340
4DPI	TCTTGGTCATCCTCCGGGCT	20	3.566	BdiBd21-3.3G0180800.1	-1.251
4DPI	TCGTTTCCGACAGAGGCCCG	20	3.566	BdiBd21-3.1G0674700.1	-1.158
4DPI	TCGTTTCCGACAGAGGCCCG	20	3.566	BdiBd21-3.3G0002900.1	-1.093
4DPI	TCTTGGTCATCCTCCGGGCT	20	3.566	BdiBd21-3.3G0690400.1	-1.035
4DPI	TCGTTTCCGACAGAGGCCCG	20	3.566	BdiBd21-3.2G0577900.1	-0.941
4DPI	TCTTGGTCATCCTCCGGGCT	20	3.566	BdiBd21-3.2G0764000.1	-0.893
4DPI	TCTTGGTCATCCTCCGGGCT	20	3.566	BdiBd21-3.2G0215800.1	-0.836
4DPI	TGGCCGGATTGTTCACAAGC	20	3.566	BdiBd21-3.1G0277900.1	-0.836
4DPI	TCTTGGTCATCCTCCGGGCT	20	3.566	BdiBd21-3.1G0235400.1	-0.816
4DPI	TGCGTTCGGCGCTGGCTGAA	20	3.592	BdiBd21-3.1G0499400.1	-1.366
4DPI	TGCGTTCGGCGCTGGCTGAA	20	3.592	BdiBd21-3.2G0062600.1	-1.152
4DPI	TGCGTTCGGCGCTGGCTGAA	20	3.592	BdiBd21-3.4G0343200.1	-1.031
4DPI	TGCGTTCGGCGCTGGCTGAA	20	3.592	BdiBd21-3.3G0419700.1	-0.937
4DPI	TCGGATGCCATTCTTGGGTG	20	3.611	BdiBd21-3.2G0079800.1	-1.587
4DPI	TAAACGGTCCGGCGTTGTCGG	21	3.636	BdiBd21-3.3G0250700.1	-1.097
4DPI	GGCCGGTTCGGGGTGTAGGC	20	3.636	BdiBd21-3.1G0722200.1	-1.633
4DPI	GGCCGGTTCGGGGTGTAGGC	20	3.636	BdiBd21-3.2G0161200.1	-1.463
4DPI	TAGGAACTCGGATATAAACG	20	3.636	BdiBd21-3.2G0062600.1	-1.152
4DPI	TCGGACTAGCGGCAGCGGGT	20	3.636	BdiBd21-3.1G0561500.1	-1.148
4DPI	TGCCCGGCCGTCGAAAGCTT	20	3.636	BdiBd21-3.3G0497100.1	-1.109
4DPI	TCGGACTAGCGGCAGCGGGT	20	3.636	BdiBd21-3.1G0915800.1	-1.099
4DPI	TCGGACTAGCGGCAGCGGGT	20	3.636	BdiBd21-3.3G0003800.1	-1.090
4DPI	GGCCGGTTCGGGGTGTAGGC	20	3.636	BdiBd21-3.1G0553500.1	-0.870
4DPI	GGCCGGTTCGGGGTGTAGGC	20	3.636	BdiBd21-3.4G0048900.1	-0.846
4DPI	TGGCAGAACGTCCGAACGAA	20	3.636	BdiBd21-3.1G0277900.1	-0.836
4DPI	TCGGAAAAGAATGCGATCGG	20	3.689	BdiBd21-3.5G0227400.1	-1.284
4DPI	TGCGAAGAACGATCCGGCTA	20	3.729	BdiBd21-3.2G0290700.1	-1.587
4DPI	TAGGAAGGATCGTACTGCGG	20	3.729	BdiBd21-3.2G0614200.1	-1.065
4DPI	TAGGAAGGATCGTACTGCGG	20	3.729	BdiBd21-3.3G0264400.1	-0.991
4DPI	TAGGAAGGATCGTACTGCGG	20	3.729	BdiBd21-3.4G0308100.1	-0.916
4DPI	CCAATCGTTGTCTGGCATTGA	21	3.753	BdiBd21-3.2G0771500.1	-1.331
4DPI	TTGTCGATCCGGCACGGGTA	20	3.762	BdiBd21-3.1G0118300.1	-1.947
4DPI	TTGTCGATCCGGCACGGGTA	20	3.762	BdiBd21-3.2G0271500.1	-0.888

4DPI	TTTCAACTCTGCGGTCAGCCA	21	3.788	BdiBd21-3.2G0348300.1	-0.977
4DPI	TTTCAACTCTGCGGTCAGCCA	21	3.788	BdiBd21-3.1G0212700.1	-0.953
4DPI	TCGGCAGATGAAGACCCAGA	20	3.788	BdiBd21-3.2G0375600.1	-0.818
4DPI	TACTCCCGCTTCGCGGCCCG	20	3.810	BdiBd21-3.2G0687400.1	-1.674
4DPI	TACTCCCGCTTCGCGGCCCG	20	3.810	BdiBd21-3.3G0432500.1	-1.293
4DPI	TACTCCCGCTTCGCGGCCCG	20	3.810	BdiBd21-3.1G0996900.1	-1.047
4DPI	TACTCCCGCTTCGCGGCCCG	20	3.810	BdiBd21-3.3G0369400.1	-1.007
4DPI	TACTCCCGCTTCGCGGCCCG	20	3.810	BdiBd21-3.3G0369400.1	-1.007
4DPI	TAGATCGGTTGGTGTCGGGCT	21	3.812	BdiBd21-3.2G0145300.1	-1.300
4DPI	TAGATCGGTTGGTGTCGGGCT	21	3.812	BdiBd21-3.1G0782600.1	-0.984
4DPI	TAGATCGGTTGGTGTCGGGCT	21	3.812	BdiBd21-3.2G0430900.1	-0.828
4DPI	TACCGTTGGGGCAATTCCTG	20	3.829	BdiBd21-3.2G0198200.1	-1.675
4DPI	TTGAAAGGTGCCTTGTCGGG	20	3.829	BdiBd21-3.3G0371400.1	-1.603
4DPI	TGCTTCGATCGGTGCCATGC	20	3.829	BdiBd21-3.2G0245400.1	-1.330
4DPI	TACCGTTGGGGCAATTCCTG	20	3.829	BdiBd21-3.1G0612700.1	-1.297
4DPI	TGTGTGACGAAGAACAGCGC	20	3.829	BdiBd21-3.2G0323300.1	-1.203
4DPI	TGTGTGACGAAGAACAGCGC	20	3.829	BdiBd21-3.3G0267900.1	-1.122
4DPI	TGTGTGACGAAGAACAGCGC	20	3.829	BdiBd21-3.4G0429100.1	-1.093
4DPI	TGTGTGACGAAGAACAGCGC	20	3.829	BdiBd21-3.3G0690400.1	-1.035
4DPI	TTGAAAGGTGCCTTGTCGGG	20	3.829	BdiBd21-3.5G0283700.1	-1.018
4DPI	TGCAGTAGAGGGCTGAATCCT	21	3.859	BdiBd21-3.1G0251800.1	-1.062
4DPI	TCCGCGAAGCTCATGAGCCC	20	3.899	BdiBd21-3.3G0346600.1	-1.665
4DPI	TCCGCGAAGCTCATGAGCCC	20	3.899	BdiBd21-3.3G0419700.1	-0.937
4DPI	TCCGCGAAGCTCATGAGCCC	20	3.899	BdiBd21-3.2G0727900.1	-0.932
4DPI	TCCGCGAAGCTCATGAGCCC	20	3.899	BdiBd21-3.1G0675600.1	-0.888
4DPI	TATCGGGGTCTGGAAGTCGT	20	3.914	BdiBd21-3.2G0692200.1	-1.386
4DPI	TATCGGGGTCTGGAAGTCGT	20	3.914	BdiBd21-3.4G0499200.1	-0.935
4DPI	TGATCTGAGCCTGGTTTCCG	20	3.936	BdiBd21-3.1G0146700.1	-0.860
4DPI	TGATCTGAGCCTGGTTTCCG	20	3.936	BdiBd21-3.4G0303000.1	-0.821
4DPI	TGAATGCTCGTTGGCCCTGA	20	4.005	BdiBd21-3.1G0086100.1	-1.346
4DPI	TGAATGCTCGTTGGCCCTGA	20	4.005	BdiBd21-3.1G0268500.1	-1.138
4DPI	TGAATGCTCGTTGGCCCTGA	20	4.005	BdiBd21-3.4G0081700.1	-1.011
4DPI	TAATGGATCCGTTGCTGCTT	20	4.051	BdiBd21-3.1G0163700.1	-2.053
4DPI	TTCGGCGGAGGATGACCTGC	20	4.051	BdiBd21-3.2G0687400.1	-1.674
4DPI	TGACGTTGAGCCCCTGCCGGG	21	4.051	BdiBd21-3.3G0171900.1	-1.436
4DPI	TTCCTGGGCCTGCTGGTCGG	20	4.051	BdiBd21-3.2G0774100.1	-1.341
4DPI	TTCGGCGGAGGATGACCTGC	20	4.051	BdiBd21-3.1G0024400.1	-1.281
4DPI	TTACGGACCACCGCAACCTG	20	4.051	BdiBd21-3.4G0228800.1	-1.174
4DPI	TGACGTTGAGCCCCTGCCGGG	21	4.051	BdiBd21-3.2G0100000.1	-1.134
4DPI	AAGGGGCTACGATCTTTGAGAA	22	4.051	BdiBd21-3.3G0787100.1	-1.132
4DPI	TTCGGCGGAGGATGACCTGC	20	4.051	BdiBd21-3.4G0031600.1	-1.100
4DPI	AGATTGGACGAACCCCCGAA	20	4.051	BdiBd21-3.1G0915800.1	-1.099
4DPI	TACTGTCACAGACCTGAAGGA	21	4.051	BdiBd21-3.1G0899500.1	-1.067
4DPI	TCATAATCTCTGCTTGCCCTG	21	4.051	BdiBd21-3.5G0132000.1	-1.041
4DPI	TCTCCGTTAATCTCGACCGG	20	4.051	BdiBd21-3.2G0670300.1	-1.032
4DPI	TTCCTGGGCCTGCTGGTCGG	20	4.051	BdiBd21-3.3G0728900.1	-1.025
4DPI	TTCGGCGGAGGATGACCTGC	20	4.051	BdiBd21-3.4G0218500.1	-0.945
4DPI	TAATGGATCCGTTGCTGCTT	20	4.051	BdiBd21-3.4G0575200.1	-0.938
4DPI	TGCGGTCTAGCACAGCTCGGG	21	4.051	BdiBd21-3.2G0404400.1	-0.917
4DPI	TGACGTTGAGCCCCTGCCGGG	21	4.051	BdiBd21-3.4G0081500.1	-0.915

4DPI	TTACGGACCACCGCAACCTG	20	4.051	BdiBd21-3.1G0642800.1	-0.914
4DPI	TTCGGCGGAGGATGACCTGC	20	4.051	BdiBd21-3.4G0110600.1	-0.899
4DPI	TTCGGCGGAGGATGACCTGC	20	4.051	BdiBd21-3.4G0214900.1	-0.863
4DPI	TAATCGGGTCAGAGGTTCTGC	21	4.051	BdiBd21-3.1G0415900.1	-0.860
4DPI	TAATGGATCCGTTGCTGCTT	20	4.051	BdiBd21-3.2G0606700.1	-0.844
4DPI	TTGAGGACAGGCGCCGACCG	20	4.051	BdiBd21-3.5G0124000.1	-0.839
4DPI	TGACGTTGAGCCCCTGCCGGG	21	4.051	BdiBd21-3.4G0416900.1	-0.831
4DPI	TCTCCGTTAATCTCGACCGG	20	4.051	BdiBd21-3.1G0659000.1	-0.815
4DPI	TGCTCCGGGTCTTCGCCTGC	20	4.221	BdiBd21-3.3G0767200.1	-1.593
4DPI	TAAATCAAGGCCTGGTGATC	20	4.221	BdiBd21-3.1G0296400.1	-1.053
4DPI	TAAATCAAGGCCTGGTGATC	20	4.221	BdiBd21-3.2G0748600.1	-1.024
4DPI	AGGGGCTACGATCTTTGAGAA	21	4.258	BdiBd21-3.3G0787100.1	-1.132
4DPI	AGGGGCTACGATCTTTGAGAA	21	4.258	BdiBd21-3.1G0028200.1	-1.001
4DPI	TCGAAATGCATATGGGCCGG	20	4.274	BdiBd21-3.1G0857400.1	-0.875
4DPI	TCGAAATGCATATGGGCCGG	20	4.274	BdiBd21-3.1G0277900.1	-0.836
4DPI	TCGCTAGGTCGCCCAAAACG	20	4.314	BdiBd21-3.1G0493600.1	-1.477
4DPI	TATCGTCGCGCAGTTGGTCG	20	4.314	BdiBd21-3.1G0501700.1	-1.317
4DPI	TATCGTCGCGCAGTTGGTCG	20	4.314	BdiBd21-3.4G0103100.1	-0.909
4DPI	TATCGTCGCGCAGTTGGTCG	20	4.314	BdiBd21-3.4G0111900.1	-0.872
4DPI	TCGCTAGGTCGCCCAAAACG	20	4.314	BdiBd21-3.2G0637600.1	-0.866
4DPI	TGACAGCGATTTTGCCGGGGCT	22	4.341	BdiBd21-3.3G0002900.1	-1.093
4DPI	TGACAGCGATTTTGCCGGGGCT	22	4.341	BdiBd21-3.2G0604300.1	-0.915
4DPI	ACTTGTGGGAGTTGGCTGTA	20	4.373	BdiBd21-3.1G0385500.1	-1.394
4DPI	ACTTGTGGGAGTTGGCTGTA	20	4.373	BdiBd21-3.5G0057900.1	-1.340
4DPI	TACGTCTGGGTCTTCATCTG	20	4.373	BdiBd21-3.5G0227500.1	-1.334
4DPI	TCACGAATCACTTTGGCGGGC	21	4.373	BdiBd21-3.1G0501700.1	-1.317
4DPI	TACGTCTGGGTCTTCATCTG	20	4.373	BdiBd21-3.5G0006200.1	-1.293
4DPI	TACGTCTGGGTCTTCATCTG	20	4.373	BdiBd21-3.3G0365000.1	-1.076
4DPI	TACGTCTGGGTCTTCATCTG	20	4.373	BdiBd21-3.3G0365000.1	-1.076
4DPI	TACGTCTGGGTCTTCATCTG	20	4.373	BdiBd21-3.3G0459600.1	-0.998
4DPI	TGATTAAGGAGAAGCGGGGG	20	4.373	BdiBd21-3.5G0286800.1	-0.951
4DPI	TACGTCTGGGTCTTCATCTG	20	4.373	BdiBd21-3.4G0276900.1	-0.933
4DPI	ACTTGTGGGAGTTGGCTGTA	20	4.373	BdiBd21-3.1G0110700.1	-0.861
4DPI	TACGTCTGGGTCTTCATCTG	20	4.373	BdiBd21-3.5G0236400.1	-0.804
4DPI	TGACGTCGTCCCATTGCCAG	20	4.399	BdiBd21-3.5G0362300.1	-1.203
4DPI	TGACGTCGTCCCATTGCCAG	20	4.399	BdiBd21-3.1G0550000.1	-1.030
4DPI	TGAATTCGGCGAGGGGAAGC	20	4.414	BdiBd21-3.2G0707700.1	-1.005
4DPI	TCCGCCTGAACTCCTGCCTA	20	4.430	BdiBd21-3.1G0954600.1	-0.817
4DPI	TGCGACGTCGCCGGTGAAGA	20	4.466	BdiBd21-3.2G0023200.1	-1.623
4DPI	TGCGACGTCGCCGGTGAAGA	20	4.466	BdiBd21-3.5G0057900.1	-1.340
4DPI	TGCGACGTCGCCGGTGAAGA	20	4.466	BdiBd21-3.2G0535200.1	-1.104
4DPI	TCAATCGGCAGATGAAGACC	20	4.466	BdiBd21-3.5G0036800.1	-1.081
4DPI	TGCGACGTCGCCGGTGAAGA	20	4.466	BdiBd21-3.2G0707700.1	-1.005
4DPI	TGCGACGTCGCCGGTGAAGA	20	4.466	BdiBd21-3.1G0122100.1	-0.957
4DPI	TCAATCGGCAGATGAAGACC	20	4.466	BdiBd21-3.4G0101300.1	-0.935
4DPI	TGAATTGGAAGCGTTAGGGGC	21	4.494	BdiBd21-3.3G0025900.1	-0.820
4DPI	GGGGCTACGATCTTTGAGAA	20	4.511	BdiBd21-3.1G0258400.1	-1.224
4DPI	GGGGCTACGATCTTTGAGAA	20	4.511	BdiBd21-3.3G0787100.1	-1.132
4DPI	GGGGCTACGATCTTTGAGAA	20	4.511	BdiBd21-3.1G0028200.1	-1.001
4DPI	ACTGATCATAAGGCCTTGGAA	21	4.511	BdiBd21-3.1G0774700.1	-0.860

4DPI	ACTGATCATAAGGCCTTGGAA	21	4.511	BdiBd21-3.4G0416900.1	-0.831
4DPI	ACTGATCATAAGGCCTTGGAA	21	4.511	BdiBd21-3.3G0025900.1	-0.820
4DPI	TAAAGAATCGAGCCTTGGAG	20	4.566	BdiBd21-3.3G0546000.1	-1.209
4DPI	TAAAGAATCGAGCCTTGGAG	20	4.566	BdiBd21-3.2G0789700.1	-0.835
4DPI	TCCATTGTTGCGGGCCAGCT	20	4.636	BdiBd21-3.2G0258800.1	-2.095
4DPI	TAAGGAATGGCTGACCGCAA	20	4.636	BdiBd21-3.5G0187400.1	-1.251
4DPI	TCCATTGTTGCGGGCCAGCT	20	4.636	BdiBd21-3.5G0276700.1	-0.974
4DPI	TCCATTGTTGCGGGCCAGCT	20	4.636	BdiBd21-3.2G0705400.1	-0.958
4DPI	TAAGGAATGGCTGACCGCAA	20	4.636	BdiBd21-3.1G0426800.1	-0.930
4DPI	TAAGGAATGGCTGACCGCAA	20	4.636	BdiBd21-3.1G0188400.1	-0.803
4DPI	TATGTCAGCCTGGAGTCCAGC	21	4.636	BdiBd21-3.2G0697700.1	-2.139
4DPI	TCGAATAGCGGGCTGGCCTC	20	4.636	BdiBd21-3.4G0393500.1	-1.622
4DPI	TATGTCAGCCTGGAGTCCAGC	21	4.636	BdiBd21-3.5G0304100.1	-1.185
4DPI	TCGAATAGCGGGCTGGCCTC	20	4.636	BdiBd21-3.1G0073200.1	-0.877
4DPI	TCTTTATACAAAATCTGATT	20	4.729	BdiBd21-3.5G0244900.1	-1.521
4DPI	TCTTTATACAAAATCTGATT	20	4.729	BdiBd21-3.1G0132300.1	-1.017
4DPI	TGAATTGGAAGCGTTAGGGGCT	22	4.758	BdiBd21-3.3G0025900.1	-0.820
4DPI	TCGGTCGGGCCACCAATAGT	20	4.788	BdiBd21-3.3G0346600.1	-1.665
4DPI	TGGCCAAGGTCTCCGCGGTG	20	4.788	BdiBd21-3.1G1048800.1	-1.402
4DPI	TGGCCAAGGTCTCCGCGGTG	20	4.788	BdiBd21-3.1G0317900.1	-1.313
4DPI	TTTCCAGCGCGGCTTCAGTA	20	4.788	BdiBd21-3.3G0583900.1	-1.297
4DPI	TGGCCAAGGTCTCCGCGGTG	20	4.788	BdiBd21-3.4G0228800.1	-1.174
4DPI	TTTCCAGCGCGGCTTCAGTA	20	4.788	BdiBd21-3.2G0766100.1	-1.132
4DPI	TGGCCAAGGTCTCCGCGGTG	20	4.788	BdiBd21-3.2G0614200.1	-1.065
4DPI	TCGGTCGGGCCACCAATAGT	20	4.788	BdiBd21-3.1G0994700.1	-0.999
4DPI	TGGCCAAGGTCTCCGCGGTG	20	4.788	BdiBd21-3.3G0419700.1	-0.937
4DPI	CCGGGGGTTGTTACAATTCTG	21	4.829	BdiBd21-3.3G0734900.1	-0.974
4DPI	CCGGGGGTTGTTACAATTCTG	21	4.829	BdiBd21-3.3G0523400.1	-0.919
4DPI	TAGCCATCGGCCGCGGATCC	20	4.859	BdiBd21-3.1G0933800.1	-1.352
4DPI	AGAAGAATTTCATGCCGGCCAG	22	4.859	BdiBd21-3.3G0292300.1	-1.001
4DPI	TAGCCATCGGCCGCGGATCC	20	4.859	BdiBd21-3.1G0073200.1	-0.877
4DPI	TAGCCATCGGCCGCGGATCC	20	4.859	BdiBd21-3.1G0415900.1	-0.860
4DPI	TAATCGGGTCAGAGGTTCTG	20	4.926	BdiBd21-3.1G0128600.1	-1.133
4DPI	TAGGCACCAAGGGCGTCGCTG	21	4.964	BdiBd21-3.2G0705000.1	-1.606
4DPI	TAGGCACCAAGGGCGTCGCTG	21	4.964	BdiBd21-3.3G0564000.1	-0.908
4DPI	TGCGCGAAAGGGCATCGGCT	20	4.966	BdiBd21-3.2G0546200.1	-0.995
4DPI	TGCGCGAAAGGGCATCGGCT	20	4.966	BdiBd21-3.4G0162100.1	-0.857
4DPI	TCGCACTTCGCGGCGTTGGCGT	22	5.051	BdiBd21-3.2G0079800.1	-1.587
4DPI	TCGCACTTCGCGGCGTTGGCGT	22	5.051	BdiBd21-3.3G0682100.1	-1.517
4DPI	TATCGAAAGCGACGCGGCAA	20	5.051	BdiBd21-3.2G0719000.1	-1.497
4DPI	TCGCACTTCGCGGCGTTGGCGT	22	5.051	BdiBd21-3.1G0188900.1	-1.437
4DPI	CGAGAATATTACTGGCCCGGAA	22	5.051	BdiBd21-3.3G0486700.1	-1.233
4DPI	TATCGAAAGCGACGCGGCAA	20	5.051	BdiBd21-3.1G0937800.1	-1.149
4DPI	TGTCCCTTTTTCCCGCCGGC	20	5.051	BdiBd21-3.1G1011900.1	-1.114
4DPI	TTTCAGGCACTGCAGCGCTCGC	22	5.051	BdiBd21-3.3G0020900.1	-1.040
4DPI	TCTGCGGGCGGGCGGTCTGG	20	5.051	BdiBd21-3.2G0348300.1	-0.977
4DPI	TCGCACTTCGCGGCGTTGGCGT	22	5.051	BdiBd21-3.1G0411600.1	-0.950
4DPI	TCTGCGGGCGGGCGGTCTGG	20	5.051	BdiBd21-3.1G0675600.1	-0.888
4DPI	TCTGCGGGCGGGCGGTCTGG	20	5.051	BdiBd21-3.1G0347500.1	-0.839
4DPI	TATCGAAAGCGACGCGGCAA	20	5.051	BdiBd21-3.2G0608000.1	-0.826

4DPI	TGATCCCGGTCGAAAAGGCG	20	5.134	BdiBd21-3.2G0097700.1	-1.557
4DPI	TGATCCCGGTCGAAAAGGCG	20	5.134	BdiBd21-3.3G0782600.1	-1.234
4DPI	TGATCCCGGTCGAAAAGGCG	20	5.134	BdiBd21-3.1G0561500.1	-1.148
4DPI	TGATCCCGGTCGAAAAGGCG	20	5.134	BdiBd21-3.1G0994700.1	-0.999
4DPI	TATCGAGGTGCAGTAGAGGG	20	5.221	BdiBd21-3.2G0231500.1	-1.504
4DPI	TAGAGGCGTGAACGGACGAA	20	5.221	BdiBd21-3.5G0025500.1	-0.947
4DPI	TATCGAGGTGCAGTAGAGGG	20	5.221	BdiBd21-3.5G0238400.1	-0.872
4DPI	TATTGCCGCCGACACTGCAA	20	5.274	BdiBd21-3.2G0204500.1	-2.494
4DPI	TATTGCCGCCGACACTGCAA	20	5.274	BdiBd21-3.1G0663500.1	-1.361
4DPI	TATTGCCGCCGACACTGCAA	20	5.274	BdiBd21-3.2G0680000.1	-1.244
4DPI	TGACGGGATAGGTAAAGAACTA	22	5.274	BdiBd21-3.1G0133700.1	-1.133
4DPI	TATTGCCGCCGACACTGCAA	20	5.274	BdiBd21-3.4G0361700.1	-0.990
4DPI	AATGCTAAGCTCTCCTGATC	20	5.314	BdiBd21-3.2G0689500.1	-1.110
4DPI	AATGCTAAGCTCTCCTGATC	20	5.314	BdiBd21-3.2G0357000.1	-0.961
4DPI	TGAGCAACCGTTTCGTAGAAA	21	5.373	BdiBd21-3.3G0235200.1	-1.454
4DPI	TAGAGTCGAAGCTGCGGTCT	20	5.414	BdiBd21-3.5G0013300.1	-1.674
4DPI	TAGAGTCGAAGCTGCGGTCT	20	5.414	BdiBd21-3.4G0208200.1	-1.044
4DPI	TAGAGTCGAAGCTGCGGTCT	20	5.414	BdiBd21-3.3G0693600.1	-0.921
4DPI	TGGCCTCGCGACTATTCGGA	20	5.554	BdiBd21-3.2G0596100.1	-1.437
4DPI	TCCATCTTGCGGTCCCGGCG	20	5.636	BdiBd21-3.2G0079800.1	-1.587
4DPI	TCCATCTTGCGGTCCCGGCG	20	5.636	BdiBd21-3.2G0084000.1	-1.038
4DPI	TCCATCTTGCGGTCCCGGCG	20	5.636	BdiBd21-3.2G0280900.1	-0.939
4DPI	TGCGAGAGGAACCTTCGGCC	20	5.788	BdiBd21-3.3G0802200.1	-1.090
4DPI	TGCGAGAGGAACCTTCGGCC	20	5.788	BdiBd21-3.2G0310700.1	-1.038
4DPI	TAGTTGAGTTCCGCCTGCTG	20	5.936	BdiBd21-3.1G0118300.1	-1.947
4DPI	TAGTTGAGTTCCGCCTGCTG	20	5.936	BdiBd21-3.4G0492900.1	-1.477
4DPI	TAGTTGAGTTCCGCCTGCTG	20	5.936	BdiBd21-3.4G0092400.1	-1.011
4DPI	TAGTTGAGTTCCGCCTGCTG	20	5.936	BdiBd21-3.1G0806900.1	-0.923
4DPI	TTGTTAATTGTTGGAGGGGG	20	6.051	BdiBd21-3.4G0393400.1	-1.087
4DPI	TTGTTAATTGTTGGAGGGGG	20	6.051	BdiBd21-3.1G0046900.1	-1.042
4DPI	TCAATGGTCTGTGTGCGGGT	20	6.051	BdiBd21-3.2G0086100.1	-0.882
4DPI	TCAATGGTCTGTGTGCGGGT	20	6.051	BdiBd21-3.1G0961000.1	-0.860
4DPI	TTGTTAATTGTTGGAGGGGG	20	6.051	BdiBd21-3.1G0774800.1	-0.802
4DPI	TAGCCCCGGCAAAATCGCTGT	21	6.314	BdiBd21-3.3G0053000.1	-0.984
4DPI	CGGATTAAAAAGGGGGAAGAA	21	6.373	BdiBd21-3.5G0013300.1	-1.674
4DPI	TGCTGCAGCAACGCTCCGGC	20	6.373	BdiBd21-3.1G0385500.1	-1.394
4DPI	CGGATTAAAAAGGGGGAAGAA	21	6.373	BdiBd21-3.1G0933800.1	-1.352
4DPI	TAGCTCCTGGTCCTGAATCGG	21	6.373	BdiBd21-3.1G0674700.1	-1.158
4DPI	TGGGTGTTTGGGTTCTGCTG	20	6.373	BdiBd21-3.5G0169300.1	-1.108
4DPI	TGGGTGTTTGGGTTCTGCTG	20	6.373	BdiBd21-3.3G0308700.1	-1.053
4DPI	TGGGTGTTTGGGTTCTGCTG	20	6.373	BdiBd21-3.1G0843800.1	-0.900
4DPI	TGCTGCAGCAACGCTCCGGC	20	6.373	BdiBd21-3.1G0841300.1	-0.897
4DPI	TGCTGCAGCAACGCTCCGGC	20	6.373	BdiBd21-3.4G0303000.1	-0.821
4DPI	CGGATTAAAAAGGGGGAAGAA	21	6.373	BdiBd21-3.1G0924800.1	-0.815
4DPI	TTATTCCGTCGATGCCCGGG	20	6.636	BdiBd21-3.2G0692200.1	-1.386
4DPI	TACCGCATGGCCAAGGTCTC	20	6.636	BdiBd21-3.1G0419300.1	-1.286
4DPI	TACCGCATGGCCAAGGTCTC	20	6.636	BdiBd21-3.2G0527900.1	-1.169
4DPI	TGACTTTGAGGGTGGCGGGCG	21	6.636	BdiBd21-3.3G0545700.1	-1.116
4DPI	TGACTTTGAGGGTGGCGGGCG	21	6.636	BdiBd21-3.3G0793500.1	-1.109
4DPI	TACCGCATGGCCAAGGTCTC	20	6.636	BdiBd21-3.2G0528200.1	-1.057

4DPI	TAGATCGGTTGGTGTCGGGCTA	22	6.636	BdiBd21-3.1G0782600.1	-0.984
4DPI	TAGATCGGTTGGTGTCGGGCTA	22	6.636	BdiBd21-3.2G0430900.1	-0.828
4DPI	AGGGCAAGCAGAGATTATGAA	21	6.859	BdiBd21-3.1G0272400.1	-1.218
4DPI	AGGATGAATTTCTGCCGTGGGA	22	6.859	BdiBd21-3.2G0019400.1	-0.885
4DPI	TAGCACAGCTCGGGCCTTGA	20	6.926	BdiBd21-3.1G0032200.1	-0.838
4DPI	TGATAAGACGCCTGGGCTGT	20	6.990	BdiBd21-3.3G0371400.1	-1.603
4DPI	TGATAAGACGCCTGGGCTGT	20	6.990	BdiBd21-3.2G0525500.1	-0.851
4DPI	TAGGCTGAGAAGCTGGGGGT	20	7.221	BdiBd21-3.2G0692200.1	-1.386
4DPI	TAGGCTGAGAAGCTGGGGGT	20	7.221	BdiBd21-3.3G0434700.1	-1.203
4DPI	TAGGCTGAGAAGCTGGGGGT	20	7.221	BdiBd21-3.1G0812400.1	-0.836
4DPI	TAAGACGCCTGGGCTGTTGC	20	7.554	BdiBd21-3.3G0496800.1	-1.284
4DPI	TAAGACGCCTGGGCTGTTGC	20	7.554	BdiBd21-3.2G0525500.1	-0.851
4DPI	AGAAACACGATTCCTGGGCT	20	#N/A	BdiBd21-3.1G0146200.1	-2.685
4DPI	TGTGAGGGTTAGGTTTAAGGG	21	#N/A	BdiBd21-3.3G0010000.1	-1.200
4DPI	TGACTTTGAGGGTGGCGGGCGC	22	#N/A	BdiBd21-3.3G0545700.1	-1.116
4DPI	TGACGGAGGAAGAGTTGGAAGC	22	#N/A	BdiBd21-3.2G0675000.1	-1.083
4DPI	TATGGAACTCCAGAAAGGCC	20	#N/A	BdiBd21-3.2G0596400.1	-1.071
4DPI	TACCCGTGCCGGATCGACAA	20	#N/A	BdiBd21-3.5G0312200.2	-1.015
4DPI	TACCCGTGCCGGATCGACAA	20	#N/A	BdiBd21-3.1G0163900.1	-1.003
4DPI	TGACGGAGGAAGAGTTGGAAGC	22	#N/A	BdiBd21-3.1G0924800.1	-0.815
Root	AGATGAACTTTCACCTGACC	20	2.171	BdiBd21-3.3G0139200.1	-0.912
Root	TGTGGGAGTTGGCTGTGAAT	20	2.451	BdiBd21-3.3G0257700.1	-1.616
Root	TGAAGTATCTTGCGGACCTG	20	2.904	BdiBd21-3.3G0280200.1	-0.553
Root	CGCCGGGCGGATCATCCAGC	20	3.300	BdiBd21-3.5G0271900.1	-0.762
Root	TAGTTGAGTTCCGCCTGCTG	20	3.451	BdiBd21-3.4G0058900.1	-0.707
Root	AGTATTCCGTCGTCGCCGTA	20	3.759	BdiBd21-3.3G0257600.1	-0.783
Root	ACCCCCGATTGACTGAACCC	20	5.567	BdiBd21-3.3G0139200.1	-0.912
Root	CGCGGCTCGGCCTCGAGGACG	21	5.567	BdiBd21-3.5G0271900.1	-0.762
Root	TAGGGTGGCCTGAATTATAGT	21	6.152	BdiBd21-3.2G0378400.1	-0.743
Root	TGAAGGGCGAGAACGGCGGC	20	7.152	BdiBd21-3.3G0009900.1	-0.867
Root	CGGGGCTAGGGAAGATTCAAA	21	7.152	BdiBd21-3.4G0058900.1	-0.707
Root	ATCGTCCTAGACTAGTTGGA	20	#N/A	BdiBd21-3.2G0492900.1	-1.370
Root	GCATATTGCAGTGTCGGCGGCA	22	#N/A	BdiBd21-3.2G0521700.1	-0.798
Root	TGAACCAGCCGTTGAGTAAG	20	#N/A	BdiBd21-3.3G0280200.1	-0.553

Bd ck-sRNA candidates with corresponding downregulated Mo targets in the three setups (2DPI, 4DPI, Root)

Setup	ck-sRNA	nt	Log(RPM)	Target	LogFC
2DPI	GGAGACGCCGGCGGGGGCCTC	21	1.393	MGG_00853T0	-1.042
2DPI	AAAAGGATTGGCTCTGAGGAC	21	1.518	MGG_11040T0	-1.062
2DPI	AAAGGATTGGCTCTGAGGAC	20	1.622	MGG_11040T0	-1.062
2DPI	CCGGCCATCTGGGCGAGCGCC	21	1.397	MGG_15671T0	-1.154
2DPI	CCGGCCCCAAACCCGTCGGC	20	1.376	MGG_06341T0	-1.159
2DPI	TCCTCGGGCCAGACGGACAT	20	1.655	MGG_03480T0	-1.194
2DPI	ACCGCCCGTCGCTCCTACCG	20	1.255	MGG_04090T0	-1.209
2DPI	TGCCGGCCGGGGGACGGACC	20	1.662	MGG_12122T0	-1.213
2DPI	CTGAGGACTGGGCTCGGGGG	20	1.156	MGG_00755T0	-1.229
2DPI	AGGACTGGGCTCGGGGGTCC	20	1.058	MGG_01703T0	-1.232
2DPI	AGGACTGGGCTCGGGGGTCCC	21	1.090	MGG_01703T0	-1.232
2DPI	CAAGGCGTGTCCCTCGGGGC	20	1.396	MGG_06472T0	-1.265
2DPI	CGCCGCGTGCCGGCCGGGGGAC	22	1.573	MGG_01285T0	-1.323
2DPI	GCCGCGTGCCGGCCGGGGGAC	21	1.692	MGG_01285T0	-1.323
2DPI	AAGGATTGGCTCTGAGGACT	20	1.066	MGG_02928T0	-1.327
2DPI	AGTCGACGGGTTCTGAAACC	20	1.676	MGG_01982T0	-1.335
2DPI	AGTCGACGGGTTCTGAAACC	20	1.676	MGG_05675T0	-1.393
2DPI	GAGTCGACGGGTTCTGAAACC	21	2.262	MGG_05675T0	-1.393
2DPI	TGCAACGGCCTGCGGGCTCC	20	1.014	MGG_16854T0	-1.394
2DPI	TGCAACGGCCTGCGGGCTCCC	21	1.134	MGG_16854T0	-1.394
2DPI	GCAACGGCCTGCGGGCTCCC	20	1.241	MGG_16854T0	-1.394
2DPI	CTGCAACGGCCTGCGGGCTCC	21	1.321	MGG_16854T0	-1.394
2DPI	CTGCAACGGCCTGCGGGCTCCC	22	1.402	MGG_16854T0	-1.394
2DPI	CAACGGCCTGCGGGCTCCCC	20	1.880	MGG_16854T0	-1.394
2DPI	GTACACACCGCCCGTCGCTCC	21	1.431	MGG_12821T0	-1.412
2DPI	ACCAAGGAGTCTGACATGCG	20	1.340	MGG_02757T0	-1.431
2DPI	GGACCAAGGAGTCTGACATGCG	22	1.350	MGG_02757T0	-1.431
2DPI	GACCAAGGAGTCTGACATGCG	21	1.581	MGG_02757T0	-1.431
2DPI	AAGGATTGGCTCTGAGGACT	20	1.066	MGG_09767T0	-1.432
2DPI	GGAGACGCCGGCGGGGGCCTC	21	1.393	MGG_07517T0	-1.464
2DPI	TGCCGGCCGGGGGACGGACC	20	1.662	MGG_09697T0	-1.490
2DPI	GACGGACCGGGAGTCGCCCC	20	1.727	MGG_07319T0	-1.508
2DPI	ACTTGAGAGGTGTAGGATAAG	21	1.323	MGG_07312T0	-1.530
2DPI	GTACACACCGCCCGTCGCTCC	21	1.431	MGG_14773T0	-1.531
2DPI	GCGGGTCGCCGCGTGCCGGCC	21	1.098	MGG_04227T0	-1.536
2DPI	AGTCGACGGGTTCTGAAACC	20	1.676	MGG_07745T0	-1.566
2DPI	GAGCACGCCTGTCGGGACCC	20	1.888	MGG_00621T0	-1.579
2DPI	CCGGCCATCTGGGCGAGCGCC	21	1.397	MGG_02574T0	-1.585
2DPI	CGGTTAATGGGGACGGACTGTA	22	1.914	MGG_04150T0	-1.591
2DPI	CCCTGCCCTTTGTACACACC	20	1.492	MGG_07616T0	-1.616
2DPI	TACTCGACCCTTCAGCCGGCG	21	1.003	MGG_03435T0	-1.618

2DPI	GGAGCACGCCTGTCGGGACC	20	1.606	MGG_08114T0	-1.620
2DPI	TCCCTGCCCTTTGTACACACC	21	1.284	MGG_01191T0	-1.643
2DPI	CCCTGCCCTTTGTACACACC	20	1.492	MGG_01191T0	-1.643
2DPI	TGCCGGCCGGGGGACGGACC	20	1.662	MGG_06631T0	-1.666
2DPI	TCCTCAGCGACGGACCGGGC	20	1.525	MGG_00960T0	-1.716
2DPI	AGCGGGTCGCCGCGTGCCGGC	21	1.053	MGG_02224T0	-1.724
2DPI	GGAGCACGCCTGTCGGGACC	20	1.606	MGG_02774T0	-1.740
2DPI	ATGGCTTCGACGCTGGGACCT	21	#N/A	MGG_04765T0	-1.742
2DPI	GGAGACGCCGGCGGGGGCCTC	21	1.393	MGG_04241T0	-1.772
2DPI	TCCTCAGCGACGGACCGGGCCC	22	1.009	MGG_04183T0	-1.786
2DPI	TCCTCAGCGACGGACCGGGCC	21	1.149	MGG_04183T0	-1.786
2DPI	GTCCTCAGCGACGGACCGGGCC	22	1.165	MGG_04183T0	-1.786
2DPI	GTCCTCAGCGACGGACCGGGC	21	1.178	MGG_04183T0	-1.786
2DPI	AGGGTGAGAGCCCCGTCCGGCC	22	1.196	MGG_04183T0	-1.786
2DPI	CCTCAGCGACGGACCGGGCCC	21	1.322	MGG_04183T0	-1.786
2DPI	TCCTCAGCGACGGACCGGGC	20	1.525	MGG_04183T0	-1.786
2DPI	GGGCGTGGACTGTTGTCGGCC	21	1.222	MGG_03714T0	-1.796
2DPI	AGTCGACGGGTTCTGAAACC	20	1.676	MGG_12377T0	-1.808
2DPI	CGAGTCGACGGGTTCTGAAACC	22	1.783	MGG_12377T0	-1.808
2DPI	GAGTCGACGGGTTCTGAAACC	21	2.262	MGG_12377T0	-1.808
2DPI	AGCGCTGAACAGTCGACTCAG	21	1.118	MGG_11261T0	-1.852
2DPI	GACGGACCGGGAGTCGCCCC	20	1.727	MGG_04405T0	-1.879
2DPI	AAACCCGTCGGCTGTCGGCG	20	1.023	MGG_04337T0	-1.909
2DPI	TTCCGTGGGTCGGAAGCGGGGC	22	1.262	MGG_03690T0	-1.926
2DPI	CCGGCCATCTGGGCGAGCGCC	21	1.397	MGG_00501T0	-1.962
2DPI	AAAGGATTGGCTCTGAGGAC	20	1.622	MGG_14279T0	-1.967
2DPI	TTGGTAAGCAGAACTGGCGATG	22	1.017	MGG_05709T0	-2.006
2DPI	CAAACCCGTCGGCTGTCGGC	20	1.192	MGG_00698T0	-2.019
2DPI	ATGGCTTCGACGCTGGGACCT	21	#N/A	MGG_03620T0	-2.028
2DPI	GCCGCGTGCCGGCCGGGGGAC	21	1.692	MGG_09941T0	-2.113
2DPI	ACCAAGGAGTCTGACATGCG	20	1.340	MGG_00984T0	-2.135
2DPI	GACCAAGGAGTCTGACATGCG	21	1.581	MGG_00984T0	-2.135
2DPI	GGAGACGCCGGCGGGGGCCTC	21	1.393	MGG_00274T0	-2.148
2DPI	GGGCGTGGACTGTTGTCGGCC	21	1.222	MGG_01093T0	-2.165
2DPI	TGCCGGCCGGGGGACGGACC	20	1.662	MGG_04968T0	-2.193
2DPI	CGGCCCCAAACCCGTCGGCT	20	1.344	MGG_03915T0	-2.252
2DPI	TGCCGGCCGGGGGACGGACC	20	1.662	MGG_11919T0	-2.255
2DPI	CTGAGGACTGGGCTCGGGGG	20	1.156	MGG_03716T0	-2.258
2DPI	TCTGAGGACTGGGCTCGGGG	20	1.164	MGG_03716T0	-2.258
2DPI	TGCCGGCCGGGGGACGGACC	20	1.662	MGG_13935T0	-2.260
2DPI	AAGGATTGGCTCTGAGGACT	20	1.066	MGG_02253T0	-2.278
2DPI	CCGGCCATCTGGGCGAGCGCC	21	1.397	MGG_02253T0	-2.278
2DPI	AGCGGGTCGCCGCGTGCCGGC	21	1.053	MGG_00622T0	-2.285
2DPI	GGAGACGCCGGCGGGGGCCTC	21	1.393	MGG_12961T0	-2.333
2DPI	GGTGAACAGCCTCTGGCCAA	20	1.541	MGG_13192T0	-2.346
2DPI	CTGAGGACTGGGCTCGGGGG	20	1.156	MGG_09527T0	-2.352

2DPI	TCTGAGGACTGGGCTCGGGG	20	1.164	MGG_09527T0	-2.352
2DPI	AAACCCGTCGGCTGTCGGCG	20	1.023	MGG_03298T0	-2.395
2DPI	TACTCGACCCTTCAGCCGGCG	21	1.003	MGG_07110T0	-2.433
2DPI	ACCAAGGAGTCTGACATGCG	20	1.340	MGG_06612T0	-2.438
2DPI	CCGCGAACCATCGAGTCTTTG	21	1.170	MGG_08561T0	-2.444
2DPI	CCCAAACCCGTCGGCTGTCGG	21	1.216	MGG_08561T0	-2.444
2DPI	TACTCGACCCTTCAGCCGGCG	21	1.003	MGG_04967T0	-2.527
2DPI	CCGGCCCCAAACCCGTCGGC	20	1.376	MGG_17003T0	-2.538
2DPI	CCGGCCCCAAACCCGTCGGCTG	22	1.065	MGG_01229T0	-2.594
2DPI	CCGGCCCCAAACCCGTCGGCT	21	1.201	MGG_01229T0	-2.594
2DPI	CGGCCCCAAACCCGTCGGCT	20	1.344	MGG_01229T0	-2.594
2DPI	CCGGCCCCAAACCCGTCGGC	20	1.376	MGG_01229T0	-2.594
2DPI	CGGCCCCAAACCCGTCGGCTG	21	1.511	MGG_01229T0	-2.594
2DPI	ACTTGAGAGGTGTAGGATAAG	21	1.323	MGG_05478T0	-2.599
2DPI	GGTGAACAGCCTCTGGCCAA	20	1.541	MGG_01045T0	-2.752
2DPI	CGGCCTGCGGGCTCCCCATCCG	22	1.047	MGG_00633T0	-2.796
2DPI	GGAGACGCCGGCGGGGGCCTC	21	1.393	MGG_00633T0	-2.796
2DPI	ACCAAGGAGTCTGACATGCG	20	1.340	MGG_01906T0	-2.799
2DPI	GGACCAAGGAGTCTGACATGCG	22	1.350	MGG_01906T0	-2.799
2DPI	GACCAAGGAGTCTGACATGCG	21	1.581	MGG_01906T0	-2.799
2DPI	CAACGGCCTGCGGGCTCCCC	20	1.880	MGG_12396T0	-2.837
2DPI	TGCCGGCCGGGGGACGGACC	20	1.662	MGG_00261T0	-2.941
2DPI	CTGAGGACTGGGCTCGGGGG	20	1.156	MGG_08936T0	-2.941
2DPI	TCTGAGGACTGGGCTCGGGG	20	1.164	MGG_08936T0	-2.941
2DPI	CGTGCCGGCCGGGGGACGGACC	22	1.400	MGG_08936T0	-2.941
2DPI	CGCCGCGTGCCGGCCGGGGGAC	22	1.573	MGG_08936T0	-2.941
2DPI	TGCCGGCCGGGGGACGGACC	20	1.662	MGG_08936T0	-2.941
2DPI	GCCGCGTGCCGGCCGGGGGAC	21	1.692	MGG_08936T0	-2.941
2DPI	GGAGACGCCGGCGGGGGCCTC	21	1.393	MGG_09477T0	-2.983
2DPI	ATGGCTTCGACGCTGGGACCT	21	#N/A	MGG_07660T0	-3.048
2DPI	CTGAGGACTGGGCTCGGGGG	20	1.156	MGG_05261T0	-3.070
2DPI	TGCCGGCCGGGGGACGGACC	20	1.662	MGG_05261T0	-3.070
2DPI	TGCCGGCCGGGGGACGGACC	20	1.662	MGG_11534T0	-3.091
2DPI	CAAGGCGTGTCCCTCGGGGC	20	1.396	MGG_04493T0	-3.125
2DPI	TGCAACGGCCTGCGGGCTCC	20	1.014	MGG_01096T0	-3.138
2DPI	CTGCAACGGCCTGCGGGCTCC	21	1.321	MGG_01096T0	-3.138
2DPI	AGCGGGTCGCCGCGTGCCGGCC	22	1.045	MGG_06093T0	-3.159
2DPI	AGCGGGTCGCCGCGTGCCGGC	21	1.053	MGG_06093T0	-3.159
2DPI	GCGGGTCGCCGCGTGCCGGCC	21	1.098	MGG_06093T0	-3.159
2DPI	GGAGACGCCGGCGGGGGCCTC	21	1.393	MGG_01243T0	-3.160
2DPI	TGCCGGCCGGGGGACGGACC	20	1.662	MGG_09200T0	-3.162
2DPI	AGCGGGTCGCCGCGTGCCGGC	21	1.053	MGG_02072T0	-3.214
2DPI	GCGGGTCGCCGCGTGCCGGCC	21	1.098	MGG_02072T0	-3.214
2DPI	ACGGACCGGGAGTCGCCCCT	20	1.226	MGG_02072T0	-3.214
2DPI	TTCCTCGGGCCAGACGGACAT	21	1.241	MGG_01604T0	-3.221
2DPI	TCCTCGGGCCAGACGGACAT	20	1.655	MGG_01604T0	-3.221

2DPI	GGAGACGCCGGCGGGGGCCTC	21	1.393	MGG_01819T0	-3.236
2DPI	ACGGACCGGGAGTCGCCCCT	20	1.226	MGG_14713T0	-3.237
2DPI	CAAGGCGTGTCCCTCGGGGC	20	1.396	MGG_05024T0	-3.255
2DPI	CCCAAACCCGTCGGCTGTCG	20	1.091	MGG_04895T0	-3.324
2DPI	CCCAAACCCGTCGGCTGTCGG	21	1.216	MGG_04895T0	-3.324
2DPI	CCCCAAACCCGTCGGCTGTC	20	1.435	MGG_04895T0	-3.324
2DPI	CTGAGGACTGGGCTCGGGGG	20	1.156	MGG_10024T0	-3.397
2DPI	GGAGACGCCGGCGGGGGCCTC	21	1.393	MGG_06032T0	-3.400
2DPI	GGTGAACAGCCTCTGGCCAA	20	1.541	MGG_17098T0	-3.435
2DPI	GGAGCACGCCTGTCGGGACC	20	1.606	MGG_00567T0	-3.445
2DPI	CGTGCCGGCCGGGGGACGGACC	22	1.400	MGG_08374T0	-3.464
2DPI	AAAAGGATTGGCTCTGAGGAC	21	1.518	MGG_10076T0	-3.494
2DPI	AAAGGATTGGCTCTGAGGAC	20	1.622	MGG_10076T0	-3.494
2DPI	ACTTGAGAGGTGTAGGATAAG	21	1.323	MGG_06638T0	-3.499
2DPI	CAAGGCGTGTCCCTCGGGGC	20	1.396	MGG_09268T0	-3.504
2DPI	GAGCCCCGTCCGGCCCGGAC	20	1.822	MGG_09268T0	-3.504
2DPI	AGCGGGTCGCCGCGTGCCGGCC	22	1.045	MGG_05366T0	-3.512
2DPI	AGCGGGTCGCCGCGTGCCGGC	21	1.053	MGG_05366T0	-3.512
2DPI	GCGGGTCGCCGCGTGCCGGCC	21	1.098	MGG_05366T0	-3.512
2DPI	AGTCGACGGGTTCTGAAACC	20	1.676	MGG_10847T0	-3.521
2DPI	GAGTCGACGGGTTCTGAAACC	21	2.262	MGG_10847T0	-3.521
2DPI	AGGACTGGGCTCGGGGGTCC	20	1.058	MGG_10118T0	-3.536
2DPI	CAAGGCGTGTCCCTCGGGGC	20	1.396	MGG_16668T0	-3.557
2DPI	AGCACGCCTGTCGGGACCCG	20	1.152	MGG_05222T0	-3.629
2DPI	ACGGACCGGGAGTCGCCCCT	20	1.226	MGG_05222T0	-3.629
2DPI	GGAGACGCCGGCGGGGGCCTC	21	1.393	MGG_02610T0	-3.671
2DPI	CTCTGAGGACTGGGCTCGGGG	21	1.110	MGG_07639T0	-3.715
2DPI	TCTGAGGACTGGGCTCGGGG	20	1.164	MGG_07639T0	-3.715
2DPI	GGAGACGCCGGCGGGGGCCTC	21	1.393	MGG_07639T0	-3.715
2DPI	GCCGCGTGCCGGCCGGGGGAC	21	1.692	MGG_07557T0	-3.716
2DPI	CAAGGCGTGTCCCTCGGGGC	20	1.396	MGG_01486T0	-3.717
2DPI	CTGAGGACTGGGCTCGGGGG	20	1.156	MGG_07361T0	-3.727
2DPI	TCTGAGGACTGGGCTCGGGG	20	1.164	MGG_07361T0	-3.727
2DPI	ATGGCTTCGACGCTGGGACCT	21	#N/A	MGG_14703T0	-3.735
2DPI	GGAGACGCCGGCGGGGGCCTC	21	1.393	MGG_01624T0	-3.746
2DPI	CGCCGCGTGCCGGCCGGGGGAC	22	1.573	MGG_02346T0	-3.785
2DPI	GCCGCGTGCCGGCCGGGGGAC	21	1.692	MGG_02346T0	-3.785
2DPI	AGGACTGGGCTCGGGGGTCC	20	1.058	MGG_10322T0	-3.793
2DPI	AGGACTGGGCTCGGGGGTCCC	21	1.090	MGG_10322T0	-3.793
2DPI	CTGAGGACTGGGCTCGGGGG	20	1.156	MGG_10322T0	-3.793
2DPI	GAGGACTGGGCTCGGGGGTCC	21	1.161	MGG_10322T0	-3.793
2DPI	GGAGCACGCCTGTCGGGACC	20	1.606	MGG_10322T0	-3.793
2DPI	GCAACGGCCTGCGGGCTCCC	20	1.241	MGG_06402T0	-3.802
2DPI	AGGACTGGGCTCGGGGGTCC	20	1.058	MGG_03843T0	-3.817
2DPI	CCCCGGTGGCCGTCGTTGGCAC	22	1.017	MGG_15989T0	-3.850
2DPI	GCGGGTCGCCGCGTGCCGGCC	21	1.098	MGG_15989T0	-3.850

2DPI	CGGCCCCAAACCCGTCGGCT	20	1.344	MGG_06902T0	-3.890
2DPI	TTCCTCGGGCCAGACGGACAT	21	1.241	MGG_01391T0	-3.895
2DPI	GGAGACGCCGGCGGGGGCCTC	21	1.393	MGG_01391T0	-3.895
2DPI	TCCTCGGGCCAGACGGACAT	20	1.655	MGG_01391T0	-3.895
2DPI	AAACCCGTCGGCTGTCGGCG	20	1.023	MGG_00057T0	-3.927
2DPI	TCTGAGGACTGGGCTCGGGG	20	1.164	MGG_08434T0	-3.931
2DPI	AGCGGGTCGCCGCGTGCCGGC	21	1.053	MGG_09576T0	-3.960
2DPI	CAAACCCGTCGGCTGTCGGC	20	1.192	MGG_01094T0	-3.960
2DPI	AGCGGGTCGCCGCGTGCCGGC	21	1.053	MGG_13977T0	-3.968
2DPI	GCGGGTCGCCGCGTGCCGGCC	21	1.098	MGG_13977T0	-3.968
2DPI	TGCCGGCCGGGGGACGGACC	20	1.662	MGG_13977T0	-3.968
2DPI	CTGAGGACTGGGCTCGGGGG	20	1.156	MGG_00244T0	-3.989
2DPI	GCGGGTCGCCGCGTGCCGGCC	21	1.098	MGG_02330T0	-4.083
2DPI	CTGAGGACTGGGCTCGGGGG	20	1.156	MGG_03890T0	-4.160
2DPI	TGCCGGCCGGGGGACGGACC	20	1.662	MGG_03588T0	-4.216
2DPI	GGTGAACAGCCTCTGGCCAA	20	1.541	MGG_00538T0	-4.303
2DPI	AAACCCGTCGGCTGTCGGCG	20	1.023	MGG_12009T0	-4.360
2DPI	CTCGGGGCGTGGACTGTTGTCG	22	1.388	MGG_04896T0	-4.370
2DPI	GGAGACGCCGGCGGGGGCCTC	21	1.393	MGG_07232T0	-4.371
2DPI	GGGCGTGGACTGTTGTCGGCC	21	1.222	MGG_02913T0	-4.377
2DPI	GGCCCGGACCCTGTCGCCCC	20	1.343	MGG_00276T0	-4.386
2DPI	CAAGGCGTGTCCCTCGGGGC	20	1.396	MGG_08072T0	-4.403
2DPI	CAAGGCGTGTCCCTCGGGGC	20	1.396	MGG_08072T0	-4.403
2DPI	CCCCGGTGGCCGTCGTTGGCAC	22	1.017	MGG_05865T0	-4.421
2DPI	CTGAGGACTGGGCTCGGGGG	20	1.156	MGG_17879T0	-4.422
2DPI	GGCCCGGACCCTGTCGCCCC	20	1.343	MGG_14892T0	-4.444
2DPI	GAGCCCCGTCCGGCCCGGAC	20	1.822	MGG_06966T0	-4.448
2DPI	AGAGCCCCGTCCGGCCCGGAC	21	1.949	MGG_06966T0	-4.448
2DPI	AGCCCCGTCCGGCCCGGACC	20	2.058	MGG_06966T0	-4.448
2DPI	AGAGCCCCGTCCGGCCCGGACC	22	2.240	MGG_06966T0	-4.448
2DPI	GCCGCGTGCCGGCCGGGGGAC	21	1.692	MGG_03287T0	-4.449
2DPI	CCCTGCCCTTTGTACACACC	20	1.492	MGG_09388T0	-4.454
2DPI	GGAGCACGCCTGTCGGGACC	20	1.606	MGG_09388T0	-4.454
2DPI	GGAGCACGCCTGTCGGGACCC	21	1.696	MGG_09388T0	-4.454
2DPI	GAGCACGCCTGTCGGGACCC	20	1.888	MGG_09388T0	-4.454
2DPI	CGTGCCGGCCGGGGGACGGACC	22	1.400	MGG_00352T0	-4.497
2DPI	TGCCGGCCGGGGGACGGACC	20	1.662	MGG_00352T0	-4.497
2DPI	CCCCAAACCCGTCGGCTGTC	20	1.435	MGG_09292T0	-4.505
2DPI	CAAACCCGTCGGCTGTCGGC	20	1.192	MGG_13349T0	-4.559
2DPI	GAGCCCCGTCCGGCCCGGAC	20	1.822	MGG_07627T0	-4.574
2DPI	AGCCCCGTCCGGCCCGGACC	20	2.058	MGG_07627T0	-4.574
2DPI	AAACCCGTCGGCTGTCGGCG	20	1.023	MGG_01383T0	-4.590
2DPI	CAACGGCCTGCGGGCTCCCC	20	1.880	MGG_01393T0	-4.607
2DPI	CGCCGCGTGCCGGCCGGGGGAC	22	1.573	MGG_07607T0	-4.636
2DPI	GCCGCGTGCCGGCCGGGGGAC	21	1.692	MGG_07607T0	-4.636
2DPI	TTCCTCGGGCCAGACGGACAT	21	1.241	MGG_13762T0	-4.676

2DPI	TCCTCGGGCCAGACGGACAT	20	1.655	MGG_13762T0	-4.676
2DPI	TTCCTCGGGCCAGACGGACAT	21	1.241	MGG_07219T0	-4.694
2DPI	TCCTCGGGCCAGACGGACAT	20	1.655	MGG_07219T0	-4.694
2DPI	AGGACTGGGCTCGGGGGTCC	20	1.058	MGG_09460T0	-4.724
2DPI	GAGGACTGGGCTCGGGGGTCC	21	1.161	MGG_09460T0	-4.724
2DPI	AGTCGACGGGTTCTGAAACC	20	1.676	MGG_16408T0	-4.773
2DPI	GGCCCGGACCCTGTCGCCCC	20	1.343	MGG_04448T0	-4.835
2DPI	GGGCGTGGACTGTTGTCGGCC	21	1.222	MGG_01673T0	-4.847
2DPI	TCTGAGGACTGGGCTCGGGG	20	1.164	MGG_03957T0	-4.866
2DPI	ATGGCTTCGACGCTGGGACCT	21	#N/A	MGG_03662T0	-5.037
2DPI	CAAGGCGTGTCCCTCGGGGC	20	1.396	MGG_10710T0	-5.081
2DPI	GCGGGTCGCCGCGTGCCGGCC	21	1.098	MGG_05632T0	-5.085
2DPI	AGCGGGTCGCCGCGTGCCGGC	21	1.053	MGG_16392T0	-5.163
2DPI	CGGCCTGCGGGCTCCCCATCCG	22	1.047	MGG_12421T0	-5.183
2DPI	CCTACTGATGACCGTGCCGCG	21	1.260	MGG_12421T0	-5.183
2DPI	ACGGCCTGCGGGCTCCCCATCC	22	1.888	MGG_12421T0	-5.183
2DPI	ACCGCCCGTCGCTCCTACCG	20	1.255	MGG_05232T0	-5.365
2DPI	TTCCGTGGGTCGGAAGCGGGGC	22	1.262	MGG_07476T0	-5.403
2DPI	GGGCGTGGACTGTTGTCGGCC	21	1.222	MGG_13926T0	-5.633
2DPI	CGGGGCGTGGACTGTTGTCGGC	22	1.460	MGG_13926T0	-5.633
2DPI	CTCTGAGGACTGGGCTCGGGG	21	1.110	MGG_11962T0	-5.753
2DPI	CTGAGGACTGGGCTCGGGGG	20	1.156	MGG_11962T0	-5.753
2DPI	TCTGAGGACTGGGCTCGGGG	20	1.164	MGG_11962T0	-5.753
2DPI	AGCGGGTCGCCGCGTGCCGGC	21	1.053	MGG_01361T0	-5.812
2DPI	GACGGACCGGGAGTCGCCCC	20	1.727	MGG_17975T0	-5.940
2DPI	TCCTCAGCGACGGACCGGGC	20	1.525	MGG_06832T0	-6.201
2DPI	TGCAACGGCCTGCGGGCTCC	20	1.014	MGG_16853T0	-6.686
2DPI	CTGCAACGGCCTGCGGGCTCC	21	1.321	MGG_16853T0	-6.686
2DPI	GACGGACCGGGAGTCGCCCC	20	1.727	MGG_11754T0	-6.757
2DPI	GAGCACGCCTGTCGGGACCC	20	1.888	MGG_05352T0	-7.060
2DPI	GACGGACCGGGAGTCGCCCC	20	1.727	MGG_09355T0	-7.808
2DPI	AGCGGGTCGCCGCGTGCCGGC	21	1.053	MGG_06222T0	-7.920
4DPI	GCCGCCGCCGACGTCGCGAG	20	1.299	MGG_02134T0	-1.003
4DPI	CGCCGCCGCCGACGTCGCGAG	21	1.962	MGG_02134T0	-1.003
4DPI	CGCCGCCGCCGACGTCGCGA	20	#N/A	MGG_02134T0	-1.003
4DPI	CGCCGCCGCCGACGTCGCGA	20	#N/A	MGG_02134T0	-1.003
4DPI	GTGGCGGTTGACGGCGACGTTA	22	1.571	MGG_09464T0	-1.004
4DPI	TGCCGTCCGAATTGTAGTCT	20	1.749	MGG_09749T0	-1.014
4DPI	GTGCCGTCCGAATTGTAGTCT	21	#N/A	MGG_09749T0	-1.014
4DPI	GGTGTAGGATAAGTGGGAGCCT	22	1.521	MGG_00969T0	-1.014
4DPI	TCCGGTGCGCCCCCGGCGGCC	21	3.851	MGG_07182T0	-1.033
4DPI	CCGGTGCGCCCCCGGCGGCC	20	3.874	MGG_07182T0	-1.033
4DPI	TCCGGTGCGCCCCCGGCGGC	20	#N/A	MGG_07182T0	-1.033
4DPI	TCCGGTGCGCCCCCGGCGGC	20	#N/A	MGG_08293T0	-1.038
4DPI	GCCGCCGCCGACGTCGCGAG	20	1.299	MGG_16901T0	-1.044
4DPI	CGCCGCCGCCGACGTCGCGAG	21	1.962	MGG_16901T0	-1.044

4DPI	CGCCGCCGCCGACGTCGCGA	20	#N/A	MGG_16901T0	-1.044
4DPI	CGCCGCCGCCGACGTCGCGA	20	#N/A	MGG_16901T0	-1.044
4DPI	CGCCGCCGCCGACGTCGCGA	20	#N/A	MGG_16901T0	-1.044
4DPI	GGGGACGTAGCTCATATGGT	20	1.933	MGG_13798T0	-1.050
4DPI	TCCGCCGTCAAATCCCAGGGC	21	4.518	MGG_15576T0	-1.050
4DPI	CCGCCGTCAAATCCCAGGGC	20	4.707	MGG_15576T0	-1.050
4DPI	GTCCGCCGTCAAATCCCAGGGC	22	#N/A	MGG_15576T0	-1.050
4DPI	GCCGCCGCCGACGTCGCGAG	20	1.299	MGG_09346T0	-1.059
4DPI	CGCCGCCGCCGACGTCGCGAG	21	1.962	MGG_09346T0	-1.059
4DPI	CGCCGCCGCCGACGTCGCGA	20	#N/A	MGG_09346T0	-1.059
4DPI	TGCCGTCCGAATTGTAGTCT	20	1.749	MGG_04969T0	-1.063
4DPI	GTGCCGTCCGAATTGTAGTCT	21	#N/A	MGG_04969T0	-1.063
4DPI	AGGCGACGGAAGTTTGAGGC	20	1.270	MGG_17539T0	-1.068
4DPI	TCGCGTTGACTACGTCCCTGCC	22	1.083	MGG_06159T0	-1.069
4DPI	CCTCAGCGACGGACCGGGCC	20	1.653	MGG_13935T0	-1.070
4DPI	GCCGGCCGGGGGACGGACCGG	21	2.527	MGG_13935T0	-1.070
4DPI	CTGGTGTCCTAGGCGTAGAG	20	#N/A	MGG_00920T0	-1.071
4DPI	ATAGTTTGTTTGATGGTACG	20	#N/A	MGG_10140T0	-1.078
4DPI	GGGGACGTAGCTCATATGGT	20	1.933	MGG_10867T0	-1.080
4DPI	AGCCGGCGATGCGCTCCTAGCC	22	2.667	MGG_09195T0	-1.081
4DPI	GGGGGTGTAGCTCATATGGT	20	1.140	MGG_05232T0	-1.083
4DPI	GGGGATGTAGCTCAGATGGT	20	1.420	MGG_05232T0	-1.083
4DPI	TTTGGATTGAAGGGAGCTCTG	21	1.393	MGG_04422T0	-1.098
4DPI	TTTGGATTGAAGGGAGCTCT	20	2.002	MGG_04422T0	-1.098
4DPI	CCTGGGATTGGCTTTGGGCC	20	1.459	MGG_11257T0	-1.100
4DPI	CCCTGGGATTGGCTTTGGGCC	21	1.776	MGG_11257T0	-1.100
4DPI	CCCTGGGATTGGCTTTGGGC	20	1.808	MGG_11257T0	-1.100
4DPI	GCCGCCGCCGACGTCGCGAG	20	1.299	MGG_02001T0	-1.100
4DPI	CGCCGCCGCCGACGTCGCGAG	21	1.962	MGG_02001T0	-1.100
4DPI	CGCCGCCGCCGACGTCGCGA	20	#N/A	MGG_02001T0	-1.100
4DPI	TGGGCACTGTCTCGGAGAGAG	21	#N/A	MGG_05342T0	-1.102
4DPI	TGGGCACTGTCTCGGAGAGAGG	22	#N/A	MGG_05342T0	-1.102
4DPI	CCCTGGGATTGGCTTTGGGCC	21	1.776	MGG_01548T0	-1.104
4DPI	CGGCCCGGACCCTGTCGCCCC	21	1.310	MGG_01745T0	-1.104
4DPI	CGGCCCGGACCCTGTCGCCC	20	2.805	MGG_01745T0	-1.104
4DPI	CCGGCCCGGACCCTGTCGCC	20	3.313	MGG_01745T0	-1.104
4DPI	CCGCCGTCAAATCCCAGGGC	20	4.707	MGG_10493T0	-1.105
4DPI	GGAGGGCGCGGCGGCCGCTG	20	1.857	MGG_03123T0	-1.111
4DPI	GGAGGGCGCGGCGGCCGCTGC	21	#N/A	MGG_03123T0	-1.111
4DPI	CCGGTGCGCCCCCGGCGGCC	20	3.874	MGG_15018T0	-1.127
4DPI	CACCAGCTAAGGCCCCTAAATG	22	#N/A	MGG_08859T0	-1.134
4DPI	GGAGGGCGCGGCGGCCGCTG	20	1.857	MGG_08927T0	-1.136
4DPI	GGAGGGCGCGGCGGCCGCTGC	21	#N/A	MGG_08927T0	-1.136
4DPI	CGCCGCCGCCGACGTCGCGAG	21	1.962	MGG_09886T0	-1.138
4DPI	CGCCGCCGCCGACGTCGCGA	20	#N/A	MGG_09886T0	-1.138
4DPI	CCCGGTGGCCGTCGTTGGCAC	21	1.581	MGG_00104T0	-1.141

4DPI	CCCCGGTGGCCGTCGTTGGCAC	22	3.142	MGG_00104T0	-1.141
4DPI	CCGGCCCCAAACCCGTCGGC	20	2.404	MGG_04371T0	-1.144
4DPI	AGCCGGCGATGCGCTCCTAGCC	22	2.667	MGG_14154T0	-1.146
4DPI	AGGCGACGGAAGTTTGAGGC	20	1.270	MGG_03522T0	-1.157
4DPI	AGGCGACGGAAGTTTGAGGCA	21	1.493	MGG_03522T0	-1.157
4DPI	CCCTTCAGCCGGCGATGCGCTC	22	2.769	MGG_06944T0	-1.162
4DPI	CCCGGTGGCCGTCGTTGGCAC	21	1.581	MGG_11286T0	-1.166
4DPI	TCCGGAGACGCCGGCGGGGGC	21	3.779	MGG_01430T0	-1.174
4DPI	GATAAAAGGCTGACGCGGGCT	21	1.157	MGG_14872T0	-1.174
4DPI	AGCGGAGGAGAAGAAACTTAC	21	2.242	MGG_14635T0	-1.176
4DPI	TCCGGAGACGCCGGCGGGGGC	21	3.779	MGG_10733T0	-1.182
4DPI	CGCGGCGACGGGGGCGGTTCG	21	#N/A	MGG_03691T0	-1.182
4DPI	TTGGCGGCGGAGGAAGACTCG	21	3.380	MGG_00171T0	-1.187
4DPI	CCGGCCCCAAACCCGTCGGC	20	2.404	MGG_10308T0	-1.198
4DPI	TTGGCGGCGGAGGAAGACTCG	21	3.380	MGG_11611T0	-1.200
4DPI	GCCCGGGCGGAGCGGCCGTCG	21	#N/A	MGG_15954T0	-1.209
4DPI	GGAGGGCGCGGCGGCCGCTG	20	1.857	MGG_01036T0	-1.218
4DPI	GCCCGGGCGGAGCGGCCGTCG	21	#N/A	MGG_07233T0	-1.228
4DPI	CTACTCGACCCTTCAGCCGGC	21	1.004	MGG_05211T0	-1.230
4DPI	TCCGCCGTCAAATCCCAGGGC	21	4.518	MGG_05375T0	-1.242
4DPI	CCGCCGTCAAATCCCAGGGC	20	4.707	MGG_05375T0	-1.242
4DPI	AGCGGAGGAGAAGAAACTTAC	21	2.242	MGG_11317T0	-1.246
4DPI	GCTAACTAGCTATGCGGAGCC	21	1.688	MGG_09048T0	-1.246
4DPI	CTGGTGTCCTAGGCGTAGAG	20	#N/A	MGG_05323T0	-1.250
4DPI	GGGGATGTAGCTCAGATGGT	20	1.420	MGG_09991T0	-1.253
4DPI	GGGGACGTAGCTCATATGGT	20	1.933	MGG_09991T0	-1.253
4DPI	CCTGGGATTGGCTTTGGGCC	20	1.459	MGG_06920T0	-1.264
4DPI	CCCTGGGATTGGCTTTGGGCC	21	1.776	MGG_06920T0	-1.264
4DPI	CCCTGGGATTGGCTTTGGGC	20	1.808	MGG_06920T0	-1.264
4DPI	GCGCGCGACCCACACCCGGC	20	#N/A	MGG_06920T0	-1.264
4DPI	CCCGGTGGCCGTCGTTGGCAC	21	1.581	MGG_05178T0	-1.265
4DPI	CCCCGGTGGCCGTCGTTGGCAC	22	3.142	MGG_05178T0	-1.265
4DPI	GCCGCCGCCGACGTCGCGAG	20	1.299	MGG_00350T0	-1.271
4DPI	CGCCGCCGCCGACGTCGCGAG	21	1.962	MGG_00350T0	-1.271
4DPI	CGCCGCCGCCGACGTCGCGA	20	#N/A	MGG_00350T0	-1.271
4DPI	TTAATAGGGACAGTCGGGGG	20	1.441	MGG_03658T0	-1.274
4DPI	CGGCCCGGACCCTGTCGCCC	20	2.805	MGG_10800T0	-1.276
4DPI	CCGGCCCGGACCCTGTCGCC	20	3.313	MGG_10800T0	-1.276
4DPI	TCCGGTGCGCCCCCGGCGGCC	21	3.851	MGG_06056T0	-1.279
4DPI	TCCGGAGACGCCGGCGGGGGC	21	3.779	MGG_09951T0	-1.291
4DPI	CCCCGGTGGCCGTCGTTGGCAC	22	3.142	MGG_06745T0	-1.293
4DPI	GGAGGGCGCGGCGGCCGCTG	20	1.857	MGG_17617T0	-1.294
4DPI	GGTTTAAGGACACAAGGTGACC	22	#N/A	MGG_04439T0	-1.295
4DPI	CGGCGGATTGCTCGAGCTGCT	21	2.099	MGG_03896T0	-1.295
4DPI	CGGCGGATTGCTCGAGCTGC	20	#N/A	MGG_03896T0	-1.295
4DPI	GGAGGGCGCGGCGGCCGCTG	20	1.857	MGG_06083T0	-1.302

4DPI	AGATAAAAGGCTGACGCGGGCT	22	1.069	MGG_11534T0	-1.311
4DPI	GATAAAAGGCTGACGCGGGCT	21	1.157	MGG_11534T0	-1.311
4DPI	GGAGGGCGCGGCGGCCGCTG	20	1.857	MGG_11534T0	-1.311
4DPI	GCCGGCCGGGGGACGGACCGG	21	2.527	MGG_11534T0	-1.311
4DPI	CTAAATGACCGCTCAGTGAT	20	#N/A	MGG_05291T0	-1.312
4DPI	CCTAAATGACCGCTCAGTGAT	21	#N/A	MGG_05291T0	-1.312
4DPI	TGCCGTCCGAATTGTAGTCT	20	1.749	MGG_05397T0	-1.316
4DPI	GTGCCGTCCGAATTGTAGTCT	21	#N/A	MGG_05397T0	-1.316
4DPI	TTAAATAGGTAGGACGGCGC	20	#N/A	MGG_02695T0	-1.347
4DPI	CGCCGCCGCCGACGTCGCGA	20	#N/A	MGG_09465T0	-1.347
4DPI	CGGCGGATTGCTCGAGCTGC	20	#N/A	MGG_10798T0	-1.352
4DPI	TTTGGATTGAAGGGAGCTCTG	21	1.393	MGG_03621T0	-1.364
4DPI	TTTGGATTGAAGGGAGCTCT	20	2.002	MGG_03621T0	-1.364
4DPI	CCGGCCCCAAACCCGTCGGC	20	2.404	MGG_00747T0	-1.372
4DPI	CCCGGCCCCAAACCCGTCGG	20	2.721	MGG_00747T0	-1.372
4DPI	GCCGCCGCCGACGTCGCGAG	20	1.299	MGG_06934T0	-1.376
4DPI	CGCCGCCGCCGACGTCGCGAG	21	1.962	MGG_06934T0	-1.376
4DPI	CGCCGCCGCCGACGTCGCGA	20	#N/A	MGG_06934T0	-1.376
4DPI	GTGAACTATGCCTGAGCGGGG	21	1.070	MGG_11224T0	-1.378
4DPI	CGCGGCGACGGGGGCGGTTCG	21	#N/A	MGG_11224T0	-1.378
4DPI	CGCGGCGACGGGGGCGGTTCG	21	#N/A	MGG_11224T0	-1.378
4DPI	ATAGTTTGTTTGATGGTACG	20	#N/A	MGG_04564T0	-1.387
4DPI	GGGGGTGTAGCTCATATGGT	20	1.140	MGG_04935T0	-1.398
4DPI	TGCCGTCCGAATTGTAGTCT	20	1.749	MGG_04935T0	-1.398
4DPI	GCCGCCGCCGACGTCGCGAG	20	1.299	MGG_05948T0	-1.406
4DPI	CGCCGCCGCCGACGTCGCGAG	21	1.962	MGG_05948T0	-1.406
4DPI	CGCCGCCGCCGACGTCGCGA	20	#N/A	MGG_05948T0	-1.406
4DPI	CGCCGCCGCCGACGTCGCGA	20	#N/A	MGG_05948T0	-1.406
4DPI	GTTGGCCTTCGGGATCGGAGT	21	2.232	MGG_09355T0	-1.417
4DPI	CGGCGGATTGCTCGAGCTGC	20	#N/A	MGG_05170T0	-1.419
4DPI	GGGGGTGTAGCTCATATGGT	20	1.140	MGG_00722T0	-1.421
4DPI	AGGCGACGGAAGTTTGAGGC	20	1.270	MGG_00722T0	-1.421
4DPI	GGGGATGTAGCTCAGATGGT	20	1.420	MGG_00722T0	-1.421
4DPI	AGGCGACGGAAGTTTGAGGCA	21	1.493	MGG_00722T0	-1.421
4DPI	GGTGTAGGATAAGTGGGAGCCT	22	1.521	MGG_13205T0	-1.422
4DPI	CGGCGGATTGCTCGAGCTGC	20	#N/A	MGG_15354T0	-1.429
4DPI	CCTGGGATTGGCTTTGGGCC	20	1.459	MGG_17400T0	-1.435
4DPI	AGATAAAAGGCTGACGCGGGCT	22	1.069	MGG_10514T0	-1.442
4DPI	GATAAAAGGCTGACGCGGGCT	21	1.157	MGG_10514T0	-1.442
4DPI	GGGGGTGTAGCTCATATGGT	20	1.140	MGG_17699T0	-1.455
4DPI	TTCCGTGGGTCGGAAGCGGGGC	22	1.940	MGG_01470T0	-1.480
4DPI	TTTGGATTGAAGGGAGCTCTG	21	1.393	MGG_09527T0	-1.482
4DPI	TTTGGATTGAAGGGAGCTCT	20	2.002	MGG_09527T0	-1.482
4DPI	GTTGGCCTTCGGGATCGGAG	20	#N/A	MGG_04980T0	-1.500
4DPI	CCGGTGCGCCCCCGGCGGCC	20	3.874	MGG_01605T0	-1.511
4DPI	CGGCCTGCGGGCTCCCCATCCG	22	2.518	MGG_07469T0	-1.522

4DPI	GTGGCGGTTGACGGCGACGTTA	22	1.571	MGG_17453T0	-1.523
4DPI	CCTCAGCGACGGACCGGGCC	20	1.653	MGG_00500T0	-1.525
4DPI	TGTAGGCAAGGGAAGTCGGC	20	1.215	MGG_08677T0	-1.532
4DPI	AGGCGACGGAAGTTTGAGGC	20	1.270	MGG_04372T0	-1.538
4DPI	AGGCGACGGAAGTTTGAGGCAA	22	1.443	MGG_04372T0	-1.538
4DPI	AGGCGACGGAAGTTTGAGGCA	21	1.493	MGG_04372T0	-1.538
4DPI	GTTGGCCTTCGGGATCGGAG	20	#N/A	MGG_06911T0	-1.540
4DPI	AGCGGAGGAGAAGAAACTTAC	21	2.242	MGG_03905T0	-1.556
4DPI	CGCCGCCGCCGACGTCGCGA	20	#N/A	MGG_00837T0	-1.558
4DPI	TCCGGCCCGGACCCTGTCGCC	21	1.402	MGG_09649T0	-1.558
4DPI	CCGGCCCGGACCCTGTCGCC	20	3.313	MGG_09649T0	-1.558
4DPI	GGAGGGCGCGGCGGCCGCTG	20	1.857	MGG_02408T0	-1.565
4DPI	TCCGCCGTCAAATCCCAGGGC	21	4.518	MGG_02408T0	-1.565
4DPI	CCGCCGTCAAATCCCAGGGC	20	4.707	MGG_02408T0	-1.565
4DPI	GGAGGGCGCGGCGGCCGCTGC	21	#N/A	MGG_02408T0	-1.565
4DPI	TTTGGATTGAAGGGAGCTCTG	21	1.393	MGG_06677T0	-1.567
4DPI	TTTGGATTGAAGGGAGCTCT	20	2.002	MGG_06677T0	-1.567
4DPI	TTTGGATTGAAGGGAGCTCTG	21	1.393	MGG_05631T0	-1.568
4DPI	TTTGGATTGAAGGGAGCTCT	20	2.002	MGG_05631T0	-1.568
4DPI	TCCGGAGACGCCGGCGGGGGC	21	3.779	MGG_08045T0	-1.575
4DPI	GCGCGCGACCCACACCCGGC	20	#N/A	MGG_04639T0	-1.581
4DPI	GCGCGCGACCCACACCCGGCC	21	#N/A	MGG_04639T0	-1.581
4DPI	GCCGCCGCCGACGTCGCGAG	20	1.299	MGG_00277T0	-1.601
4DPI	CGCCGCCGCCGACGTCGCGAG	21	1.962	MGG_00277T0	-1.601
4DPI	CGCCGCCGCCGACGTCGCGA	20	#N/A	MGG_00277T0	-1.601
4DPI	GTTGGCCTTCGGGATCGGAGT	21	2.232	MGG_01525T0	-1.609
4DPI	GTTGGCCTTCGGGATCGGAG	20	#N/A	MGG_01525T0	-1.609
4DPI	TCTGGTGTCCTAGGCGTAGAG	21	2.532	MGG_03333T0	-1.612
4DPI	CTGGTGTCCTAGGCGTAGAG	20	#N/A	MGG_03333T0	-1.612
4DPI	TCCGGTGCGCCCCCGGCGGC	20	#N/A	MGG_05131T0	-1.613
4DPI	CTGAATACTAGATATGACCCC	21	#N/A	MGG_01222T0	-1.632
4DPI	AGGCGACGGAAGTTTGAGGC	20	1.270	MGG_01045T0	-1.637
4DPI	TCCGCCGTCAAATCCCAGGGC	21	4.518	MGG_05023T0	-1.647
4DPI	CCGCCGTCAAATCCCAGGGC	20	4.707	MGG_05023T0	-1.647
4DPI	GTCCGCCGTCAAATCCCAGGGC	22	#N/A	MGG_05023T0	-1.647
4DPI	TCCGGCCCGGACCCTGTCGCC	21	1.402	MGG_07800T0	-1.659
4DPI	TGCCGTCCGAATTGTAGTCT	20	1.749	MGG_07800T0	-1.659
4DPI	GTGCCGTCCGAATTGTAGTCT	21	#N/A	MGG_07800T0	-1.659
4DPI	GGAGGGCGCGGCGGCCGCTG	20	1.857	MGG_02739T0	-1.674
4DPI	GCGAGAGTAGTACTAGGATGGG	22	1.077	MGG_06179T0	-1.703
4DPI	AGGCGACGGAAGTTTGAGGC	20	1.270	MGG_04228T0	-1.707
4DPI	AGGCGACGGAAGTTTGAGGCA	21	1.493	MGG_04228T0	-1.707
4DPI	CGGCCCGGACCCTGTCGCCCC	21	1.310	MGG_16729T0	-1.721
4DPI	CGGCCCGGACCCTGTCGCCC	20	2.805	MGG_16729T0	-1.721
4DPI	AGCGGAGGAGAAGAAACTTAC	21	2.242	MGG_02186T0	-1.726
4DPI	AGCCGGCGATGCGCTCCTAGCC	22	2.667	MGG_07489T0	-1.754

4DPI	GCCGGCCGGGGGACGGACCGG	21	2.527	MGG_02754T0	-1.767
4DPI	GCCGCCGCCGACGTCGCGAG	20	1.299	MGG_05862T0	-1.772
4DPI	TCCGGAGACGCCGGCGGGGGC	21	3.779	MGG_09103T0	-1.781
4DPI	CGCCGCCGCCGACGTCGCGA	20	#N/A	MGG_14268T0	-1.799
4DPI	GCCGCCGCCGACGTCGCGAG	20	1.299	MGG_09833T0	-1.801
4DPI	CGCCGCCGCCGACGTCGCGAG	21	1.962	MGG_09833T0	-1.801
4DPI	CGCCGCCGCCGACGTCGCGA	20	#N/A	MGG_09833T0	-1.801
4DPI	CGGCCCGGACCCTGTCGCCC	20	2.805	MGG_03058T0	-1.808
4DPI	GCCGCCGCCGACGTCGCGAG	20	1.299	MGG_00265T0	-1.813
4DPI	GGGTAAGCCGATCCTAAGGGA	21	2.667	MGG_05366T0	-1.818
4DPI	GGGGGTGTAGCTCATATGGT	20	1.140	MGG_04938T0	-1.848
4DPI	CTGGTGTCCTAGGCGTAGAG	20	#N/A	MGG_10024T0	-1.848
4DPI	TTGGCGGCGGAGGAAGACTCG	21	3.380	MGG_05926T0	-1.859
4DPI	CTGGTGTCCTAGGCGTAGAG	20	#N/A	MGG_11713T0	-1.883
4DPI	CCCGGCCCCAAACCCGTCGG	20	2.721	MGG_09990T0	-1.901
4DPI	CGGCCCGGACCCTGTCGCCC	20	2.805	MGG_09990T0	-1.901
4DPI	CCGGCCCGGACCCTGTCGCC	20	3.313	MGG_09990T0	-1.901
4DPI	CCTGGGATTGGCTTTGGGCC	20	1.459	MGG_06144T0	-1.903
4DPI	CCCTGGGATTGGCTTTGGGCC	21	1.776	MGG_06144T0	-1.903
4DPI	CCCTGGGATTGGCTTTGGGC	20	1.808	MGG_06144T0	-1.903
4DPI	GGGGGTGTAGCTCATATGGT	20	1.140	MGG_04441T0	-1.922
4DPI	GCCGCCGCCGACGTCGCGAG	20	1.299	MGG_13276T0	-1.940
4DPI	GCCGCCGCCGACGTCGCGAG	20	1.299	MGG_13276T0	-1.940
4DPI	CGCCGCCGCCGACGTCGCGAG	21	1.962	MGG_13276T0	-1.940
4DPI	CGCCGCCGCCGACGTCGCGAG	21	1.962	MGG_13276T0	-1.940
4DPI	CGCCGCCGCCGACGTCGCGA	20	#N/A	MGG_13276T0	-1.940
4DPI	CGCCGCCGCCGACGTCGCGA	20	#N/A	MGG_13276T0	-1.940
4DPI	TGTAGGCAAGGGAAGTCGGC	20	1.215	MGG_09333T0	-1.942
4DPI	GGAGGGCGCGGCGGCCGCTGC	21	#N/A	MGG_09333T0	-1.942
4DPI	TCTGGTGTACCAGTTATCGTG	21	#N/A	MGG_03347T0	-1.997
4DPI	AGCGGAGGAGAAGAAACTTAC	21	2.242	MGG_00959T0	-2.032
4DPI	AGCGGAGTAGAGCAGTTTGGTA	22	1.092	MGG_09273T0	-2.037
4DPI	CCTGGGATTGGCTTTGGGCC	20	1.459	MGG_08279T0	-2.059
4DPI	TGCCGTCCGAATTGTAGTCT	20	1.749	MGG_09096T0	-2.070
4DPI	ATGGAACAATGTAGGCAAGGGA	22	1.421	MGG_13239T0	-2.080
4DPI	GCGCGCGACCCACACCCGGC	20	#N/A	MGG_13239T0	-2.080
4DPI	AGCGCGCGACCCACACCCGGC	21	#N/A	MGG_13239T0	-2.080
4DPI	TGTAGGCAAGGGAAGTCGGC	20	1.215	MGG_04159T0	-2.100
4DPI	GTTGGCCTTCGGGATCGGAGT	21	2.232	MGG_11168T0	-2.122
4DPI	GTTGGCCTTCGGGATCGGAG	20	#N/A	MGG_11168T0	-2.122
4DPI	TTGGCGGCGGAGGAAGACTCG	21	3.380	MGG_01861T0	-2.136
4DPI	CCGCCGCCGACGTCGCGAGAAG	22	3.021	MGG_05951T0	-2.152
4DPI	GCCCGGGCGGAGCGGCCGTCG	21	#N/A	MGG_01386T0	-2.159
4DPI	GGGGGTGTAGCTCATATGGT	20	1.140	MGG_13793T0	-2.194
4DPI	GCCGCCGCCGACGTCGCGAG	20	1.299	MGG_10409T0	-2.206
4DPI	GCCGCCGCCGACGTCGCGAG	20	1.299	MGG_10409T0	-2.206

4DPI	CGCCGCCGCCGACGTCGCGAG	21	1.962	MGG_10409T0	-2.206
4DPI	CCGCCGCCGACGTCGCGAGAAG	22	3.021	MGG_10409T0	-2.206
4DPI	CGCCGCCGCCGACGTCGCGA	20	#N/A	MGG_10409T0	-2.206
4DPI	CGCCGCCGCCGACGTCGCGA	20	#N/A	MGG_10409T0	-2.206
4DPI	ATAGTTTGTTTGATGGTACG	20	#N/A	MGG_03384T0	-2.221
4DPI	CGGCCCGGACCCTGTCGCCC	20	2.805	MGG_11754T0	-2.330
4DPI	GGGGATGTAGCTCAGATGGT	20	1.420	MGG_03002T0	-2.366
4DPI	CCCGGTGGCCGTCGTTGGCAC	21	1.581	MGG_10533T0	-2.371
4DPI	CCCCGGTGGCCGTCGTTGGCAC	22	3.142	MGG_10533T0	-2.371
4DPI	AGCGGAGGAGAAGAAACTTAC	21	2.242	MGG_02689T0	-2.400
4DPI	TTTGGATTGAAGGGAGCTCT	20	2.002	MGG_00292T0	-2.413
4DPI	AGATAAAAGGCTGACGCGGGCT	22	1.069	MGG_06203T0	-2.416
4DPI	GATAAAAGGCTGACGCGGGCT	21	1.157	MGG_06203T0	-2.416
4DPI	CTGGTGTCCTAGGCGTAGAG	20	#N/A	MGG_06203T0	-2.416
4DPI	GGGGGTGTAGCTCATATGGT	20	1.140	MGG_02101T0	-2.429
4DPI	GTTGGCCTTCGGGATCGGAG	20	#N/A	MGG_06221T0	-2.439
4DPI	GCCCGGGCGGAGCGGCCGTCG	21	#N/A	MGG_02127T0	-2.534
4DPI	GGAGGGCGCGGCGGCCGCTG	20	1.857	MGG_13116T0	-2.536
4DPI	GGAGGGCGCGGCGGCCGCTGC	21	#N/A	MGG_13116T0	-2.536
4DPI	CGCGGCGACGGGGGCGGTTCG	21	#N/A	MGG_07361T0	-2.588
4DPI	CCGGCCCCAAACCCGTCGGC	20	2.404	MGG_07367T0	-2.630
4DPI	CGGCCCGGACCCTGTCGCCC	20	2.805	MGG_07367T0	-2.630
4DPI	TGTAGGCAAGGGAAGTCGGC	20	1.215	MGG_05931T0	-2.632
4DPI	TGTAGGCAAGGGAAGTCGGC	20	1.215	MGG_06519T0	-2.649
4DPI	ATGTAGGCAAGGGAAGTCGGC	21	1.904	MGG_06519T0	-2.649
4DPI	CGGCCCGGACCCTGTCGCCC	20	2.805	MGG_06585T0	-2.694
4DPI	CCCGGTGGCCGTCGTTGGCAC	21	1.581	MGG_05530T0	-2.724
4DPI	CCTCAGCGACGGACCGGGCC	20	1.653	MGG_01701T0	-2.740
4DPI	CCCTGGGATTGGCTTTGGGC	20	1.808	MGG_17528T0	-2.757
4DPI	CTAAATGACCGCTCAGTGAT	20	#N/A	MGG_10372T0	-2.767
4DPI	GTTGGCCTTCGGGATCGGAG	20	#N/A	MGG_03963T0	-2.782
4DPI	TTAAATAGGTAGGACGGCGC	20	#N/A	MGG_03963T0	-2.782
4DPI	GATAAAAGGCTGACGCGGGCT	21	1.157	MGG_11916T0	-2.785
4DPI	TCGCGTTGACTACGTCCCTGCC	22	1.083	MGG_08458T0	-2.809
4DPI	GGGGGTGTAGCTCATATGGT	20	1.140	MGG_08458T0	-2.809
4DPI	GGGGACGTAGCTCATATGGT	20	1.933	MGG_08458T0	-2.809
4DPI	CGCCGCCGCCGACGTCGCGA	20	#N/A	MGG_10438T0	-2.818
4DPI	TCCGGTGCGCCCCCGGCGGC	20	#N/A	MGG_17103T0	-2.913
4DPI	GCGAGAGTAGTACTAGGATGG	21	1.174	MGG_09717T0	-2.922
4DPI	CCGCCGCCGACGTCGCGAGAAG	22	3.021	MGG_09717T0	-2.922
4DPI	TTAAATAGGTAGGACGGCGC	20	#N/A	MGG_09717T0	-2.922
4DPI	TTAAATAGGTAGGACGGCGC	20	#N/A	MGG_02329T0	-3.007
4DPI	CCTCAGCGACGGACCGGGCC	20	1.653	MGG_06886T0	-3.039
4DPI	TCTGGTGTCCTAGGCGTAGAG	21	2.532	MGG_06886T0	-3.039
4DPI	CTGGTGTCCTAGGCGTAGAG	20	#N/A	MGG_06886T0	-3.039
4DPI	GGAGGGCGCGGCGGCCGCTG	20	1.857	MGG_03685T0	-3.076

4DPI	GGAGGGCGCGGCGGCCGCTG	20	1.857	MGG_01358T0	-3.099
4DPI	GGAGGGCGCGGCGGCCGCTGC	21	#N/A	MGG_01358T0	-3.099
4DPI	TCCGGTGCGCCCCCGGCGGC	20	#N/A	MGG_01149T0	-3.126
4DPI	CCCGGTGGCCGTCGTTGGCAC	21	1.581	MGG_13715T0	-3.140
4DPI	GGGGGTGTAGCTCATATGGT	20	1.140	MGG_07961T0	-3.150
4DPI	CCGCCGTCAAATCCCAGGGC	20	4.707	MGG_13578T0	-3.278
4DPI	CCCGGTGGCCGTCGTTGGCAC	21	1.581	MGG_05865T0	-3.324
4DPI	CCCCGGTGGCCGTCGTTGGCAC	22	3.142	MGG_05865T0	-3.324
4DPI	TTGGCGGCGGAGGAAGACTCG	21	3.380	MGG_05865T0	-3.324
4DPI	CCTGGGATTGGCTTTGGGCC	20	1.459	MGG_16099T0	-3.345
4DPI	CCCTGGGATTGGCTTTGGGC	20	1.808	MGG_16099T0	-3.345
4DPI	CCTCAGCGACGGACCGGGCCCA	22	1.145	MGG_08735T0	-3.351
4DPI	TCCTCAGCGACGGACCGGGCCC	22	1.221	MGG_08735T0	-3.351
4DPI	CCTCAGCGACGGACCGGGCCC	21	1.662	MGG_08735T0	-3.351
4DPI	CCGGCCCGGACCCTGTCGCC	20	3.313	MGG_09341T0	-3.394
4DPI	TGCCGTCCGAATTGTAGTCT	20	1.749	MGG_02124T0	-3.433
4DPI	AGCCGGCGATGCGCTCCTAGCC	22	2.667	MGG_02124T0	-3.433
4DPI	TTGGCGGCGGAGGAAGACTCG	21	3.380	MGG_02124T0	-3.433
4DPI	GCCGCCGCCGACGTCGCGAG	20	1.299	MGG_12546T0	-3.514
4DPI	CGCCGCCGCCGACGTCGCGAG	21	1.962	MGG_12546T0	-3.514
4DPI	CGCCGCCGCCGACGTCGCGA	20	#N/A	MGG_12546T0	-3.514
4DPI	CGGCCCGGACCCTGTCGCCC	20	2.805	MGG_03403T0	-3.545
4DPI	TTGGCGGCGGAGGAAGACTCG	21	3.380	MGG_02308T0	-3.565
4DPI	GCCGCCGCCGACGTCGCGAG	20	1.299	MGG_01398T0	-3.585
4DPI	CGCCGCCGCCGACGTCGCGAG	21	1.962	MGG_01398T0	-3.585
4DPI	CGCCGCCGCCGACGTCGCGA	20	#N/A	MGG_01398T0	-3.585
4DPI	CGCCGCCGCCGACGTCGCGAG	21	1.962	MGG_05716T0	-3.591
4DPI	TCCGGCCCGGACCCTGTCGCC	21	1.402	MGG_05824T0	-3.596
4DPI	GCCGCCGCCGACGTCGCGAG	20	1.299	MGG_00634T0	-3.646
4DPI	CGCCGCCGCCGACGTCGCGAG	21	1.962	MGG_00634T0	-3.646
4DPI	CCGCCGCCGACGTCGCGAGAAG	22	3.021	MGG_00634T0	-3.646
4DPI	CGCCGCCGCCGACGTCGCGA	20	#N/A	MGG_00634T0	-3.646
4DPI	TGTAGGCAAGGGAAGTCGGC	20	1.215	MGG_08751T0	-3.703
4DPI	GCCGCCGCCGACGTCGCGAG	20	1.299	MGG_07565T0	-3.708
4DPI	CGCCGCCGCCGACGTCGCGAG	21	1.962	MGG_07565T0	-3.708
4DPI	CGCCGCCGCCGACGTCGCGA	20	#N/A	MGG_07565T0	-3.708
4DPI	GGGGGTGTAGCTCATATGGT	20	1.140	MGG_09474T0	-3.794
4DPI	GGGGATGTAGCTCAGATGGT	20	1.420	MGG_09474T0	-3.794
4DPI	GCCCGGGCGGAGCGGCCGTCG	21	#N/A	MGG_09474T0	-3.794
4DPI	CTGGTGTCCTAGGCGTAGAG	20	#N/A	MGG_12003T0	-3.795
4DPI	TCCGGTGCGCCCCCGGCGGCC	21	3.851	MGG_11537T0	-3.886
4DPI	CCGGTGCGCCCCCGGCGGCC	20	3.874	MGG_11537T0	-3.886
4DPI	TCCGGTGCGCCCCCGGCGGC	20	#N/A	MGG_11537T0	-3.886
4DPI	TCCGGAGACGCCGGCGGGGGC	21	3.779	MGG_09460T0	-3.916
4DPI	GGGGATGTAGCTCAGATGGT	20	1.420	MGG_09251T0	-3.947
4DPI	TTTGGATTGAAGGGAGCTCT	20	2.002	MGG_08370T0	-3.957

4DPI	GTGGCGGTTGACGGCGACGTTA	22	1.571	MGG_05693T0	-3.966
4DPI	TTCCGTGGGTCGGAAGCGGGGC	22	1.940	MGG_08933T0	-3.975
4DPI	CCATGAAAATCCGGAGGACCGA	22	1.408	MGG_16361T0	-3.984
4DPI	TCCGGTGCGCCCCCGGCGGCC	21	3.851	MGG_14721T0	-4.050
4DPI	CGGCCCGGACCCTGTCGCCCC	21	1.310	MGG_04448T0	-4.082
4DPI	TCCGGCCCGGACCCTGTCGCC	21	1.402	MGG_04448T0	-4.082
4DPI	CCCTTCAGCCGGCGATGCGCTC	22	2.769	MGG_04448T0	-4.082
4DPI	CGGCCCGGACCCTGTCGCCC	20	2.805	MGG_04448T0	-4.082
4DPI	CCGGCCCGGACCCTGTCGCC	20	3.313	MGG_04448T0	-4.082
4DPI	CGCGGCGACGGGGGCGGTTCG	21	#N/A	MGG_04448T0	-4.082
4DPI	GCCGCCGCCGACGTCGCGAG	20	1.299	MGG_09844T0	-4.167
4DPI	CGCCGCCGCCGACGTCGCGAG	21	1.962	MGG_09844T0	-4.167
4DPI	CGCCGCCGCCGACGTCGCGA	20	#N/A	MGG_09844T0	-4.167
4DPI	GTTGGCCTTCGGGATCGGAG	20	#N/A	MGG_10878T0	-4.244
4DPI	TGTAGGCAAGGGAAGTCGGC	20	1.215	MGG_09618T0	-4.308
4DPI	TCTGGTGTACCAGTTATCGTG	21	#N/A	MGG_00289T0	-4.441
4DPI	CCTGGGATTGGCTTTGGGCC	20	1.459	MGG_09791T0	-4.476
4DPI	CCCTGGGATTGGCTTTGGGC	20	1.808	MGG_09791T0	-4.476
4DPI	CCGGCCCGGACCCTGTCGCC	20	3.313	MGG_15534T0	-4.479
4DPI	CGCGGCGACGGGGGCGGTTCG	21	#N/A	MGG_15534T0	-4.479
4DPI	CCGGCCCCAAACCCGTCGGC	20	2.404	MGG_02885T0	-4.685
4DPI	TCCGGCCCGGACCCTGTCGCC	21	1.402	MGG_01365T0	-4.719
4DPI	CGCGGCGACGGGGGCGGTTCG	21	#N/A	MGG_01365T0	-4.719
4DPI	TTGGCGGCGGAGGAAGACTCG	21	3.380	MGG_01199T0	-4.842
4DPI	TCCGGTGCGCCCCCGGCGGCC	21	3.851	MGG_11634T0	-4.853
4DPI	TCCGGTGCGCCCCCGGCGGC	20	#N/A	MGG_11634T0	-4.853
4DPI	GGGGATGTAGCTCAGATGGT	20	1.420	MGG_13007T0	-5.265
4DPI	CCGGTGCGCCCCCGGCGGCC	20	3.874	MGG_05070T0	-5.279
4DPI	CGCCGCCGCCGACGTCGCGA	20	#N/A	MGG_16718T0	-5.472
4DPI	TATGAGCCCCGTGGACTAGC	20	#N/A	MGG_02128T0	-5.609
4DPI	TGGGCACTGTCTCGGAGAGAG	21	#N/A	MGG_05109T0	-5.741
4DPI	ATGATAACTCGACGGATCGC	20	#N/A	MGG_10050T0	-5.842
4DPI	ATGATAACTCGACGGATCGCA	21	#N/A	MGG_10050T0	-5.842
4DPI	GTTGGCCTTCGGGATCGGAG	20	#N/A	MGG_06324T0	-5.959
4DPI	TGCCGTCCGAATTGTAGTCT	20	1.749	MGG_09189T0	-5.969
4DPI	GGGGATGTAGCTCAGATGGT	20	1.420	MGG_09063T0	-6.693
4DPI	GGGGGTGTAGCTCATATGGT	20	1.140	MGG_04259T0	-6.880
4DPI	GCCGGCCGGGGGACGGACCGG	21	2.527	MGG_05761T0	-7.276
4DPI	GCCGCCGCCGACGTCGCGAG	20	1.299	MGG_02646T0	-8.703
Root	TGAACGCAAGTTGCGCCCGA	20	1.338	MGG_11785T0	-1.148
Root	CGCCGCCGCCGACGTCGCGA	20	1.064	MGG_16901T0	-1.179
Root	CGCCGCCGCCGACGTCGCGA	20	1.064	MGG_16901T0	-1.179
Root	CGCCGCCGCCGACGTCGCGA	20	1.064	MGG_16901T0	-1.179
Root	CGCCGCCGCCGACGTCGCGAG	21	1.129	MGG_16901T0	-1.179
Root	CCGTGGGTCGGAAGCGGGGC	20	1.242	MGG_16901T0	-1.179
Root	AAGGATTGGCTCTGAGGACT	20	1.207	MGG_09767T0	-1.206

Root	CGCCGCCGCCGACGTCGCGA	20	1.064	MGG_10568T0	-1.241
Root	CCGCCGCCGACGTCGCGAGA	20	1.126	MGG_10568T0	-1.241
Root	CGCCGCCGCCGACGTCGCGAG	21	1.129	MGG_10568T0	-1.241
Root	TAGGTAGGACGGCGCGGCTG	20	1.606	MGG_09927T0	-1.265
Root	CTGGGCTCGGGGGTCCCGGC	20	2.800	MGG_06203T0	-1.328
Root	CGAAGTTAAGCGTGCTTGGGC	21	1.167	MGG_06719T0	-1.347
Root	GAAGTTAAGCGTGCTTGGGC	20	1.177	MGG_06719T0	-1.347
Root	ACGCCGGCGGGGGCCTCGGG	20	1.109	MGG_05525T0	-1.396
Root	GGCTGTCGGCGGATTGCTCGAG	22	2.016	MGG_16248T0	-1.396
Root	CGCCGCCGCCGACGTCGCGA	20	1.064	MGG_07109T0	-1.431
Root	CCGCCGCCGACGTCGCGAGA	20	1.126	MGG_07109T0	-1.431
Root	CGCCGCCGCCGACGTCGCGAG	21	1.129	MGG_07109T0	-1.431
Root	GTCGCCTTCGAGAGAAGCGGG	21	1.182	MGG_06177T0	-1.542
Root	CTGGGCTCGGGGGTCCCGGC	20	2.800	MGG_00254T0	-1.633
Root	CCGGTGCGCCCCCGGCGGCCC	21	1.097	MGG_03148T0	-1.664
Root	CGGCTTTTGCTGGTCCGCCGCT	22	1.159	MGG_03148T0	-1.664
Root	CCGGTGCGCCCCCGGCGGCC	20	1.246	MGG_03148T0	-1.664
Root	AGACGCCGGCGGGGGCCTCGG	21	1.408	MGG_01790T0	-1.709
Root	ACGCCGGCGGGGGCCTCGGG	20	1.109	MGG_06371T0	-1.755
Root	CTCAGCGACGGACCGGGCCC	20	1.679	MGG_04441T0	-1.800
Root	TAGGTAGGACGGCGCGGCTG	20	1.606	MGG_02775T0	-1.833
Root	CTGGGCTCGGGGGTCCCGGC	20	2.800	MGG_02775T0	-1.833
Root	GGCTGTCGGCGGATTGCTCGAG	22	2.016	MGG_08692T0	-1.839
Root	GCCGCAAGGCGTGTCCCTCGG	21	#N/A	MGG_01752T0	-1.896
Root	CGCCGCCGCCGACGTCGCGA	20	1.064	MGG_01268T0	-1.914
Root	CGCCGCCGCCGACGTCGCGA	20	1.064	MGG_01268T0	-1.914
Root	GTCGCCTTCGAGAGAAGCGGG	21	1.182	MGG_11889T0	-1.914
Root	TCAAGAACGAAAGTTGGGGGC	21	1.834	MGG_01245T0	-1.956
Root	CGCCGCCGCCGACGTCGCGA	20	1.064	MGG_16230T0	-1.981
Root	CCGCCGCCGACGTCGCGAGA	20	1.126	MGG_16230T0	-1.981
Root	CGCCGCCGCCGACGTCGCGAG	21	1.129	MGG_16230T0	-1.981
Root	TGCTTATAGGACTCCGCCGGC	21	2.506	MGG_04114T0	-2.007
Root	GCGCTGCAACGGCCTGCGGGC	21	1.811	MGG_03653T0	-2.014
Root	ATCATTGCAATTGTTGGTCT	20	1.727	MGG_06154T0	-2.052
Root	CAACGGCCTGCGGGCTCCCC	20	1.022	MGG_10400T0	-2.108
Root	ACTGGTACGGACAAGGGGAAT	21	1.020	MGG_10504T0	-2.132
Root	CTGGTACGGACAAGGGGAAT	20	1.801	MGG_10504T0	-2.132
Root	TCCGGAGACGCCGGCGGGGGC	21	1.072	MGG_08580T0	-2.153
Root	CCGGAGACGCCGGCGGGGGC	20	1.082	MGG_08580T0	-2.153
Root	GAGGCCACCCGGTCGAGGGC	20	1.711	MGG_08580T0	-2.153
Root	GACAGACTGAGAGCTCTTTC	20	2.416	MGG_03014T0	-2.201
Root	CGGCAACGGATATCTCGGCT	20	1.733	MGG_16361T0	-2.219
Root	GGAGCACGCCTGTCGGGACC	20	1.018	MGG_04118T0	-2.220
Root	ACCCGGTCGAGGGCACGCCTG	21	1.066	MGG_04118T0	-2.220
Root	CGCTGCAACGGCCTGCGGGCTC	22	1.027	MGG_02479T0	-2.221
Root	CCGGAGACGCCGGCGGGGGC	20	1.082	MGG_02668T0	-2.222

Root	ATCATTGCAATTGTTGGTCT	20	1.727	MGG_06571T0	-2.232
Root	CGGCAACGGATATCTCGGCT	20	1.733	MGG_08584T0	-2.239
Root	AGACGCCGGCGGGGGCCTCGG	21	1.408	MGG_00289T0	-2.241
Root	GCGACCCCAGGTCAGGCGGG	20	1.482	MGG_04522T0	-2.243
Root	CCGGTGGCCGTCGTTGGCAC	20	2.133	MGG_03333T0	-2.371
Root	CCCCGGCAGATAGCGCGATC	20	1.311	MGG_06933T0	-2.373
Root	CCAAGGAGTCTGACATGCGT	20	1.277	MGG_12749T0	-2.449
Root	TTAAATAGGTAGGACGGCGC	20	1.748	MGG_02695T0	-2.464
Root	CGCACGGATTCGTCCCTCCC	20	1.866	MGG_02695T0	-2.464
Root	ACAATTGGTCATCGCGCTTGGT	22	1.815	MGG_06751T0	-2.514
Root	AAAGGATTGGCTCTGAGGAC	20	1.968	MGG_14279T0	-2.558
Root	CGCCGCCGCCGACGTCGCGA	20	1.064	MGG_05948T0	-2.583
Root	CGCCGCCGCCGACGTCGCGA	20	1.064	MGG_05948T0	-2.583
Root	CCGCCGCCGACGTCGCGAGA	20	1.126	MGG_05948T0	-2.583
Root	CGCCGCCGCCGACGTCGCGAG	21	1.129	MGG_05948T0	-2.583
Root	TAGGTAGGACGGCGCGGCTG	20	1.606	MGG_13239T0	-2.675
Root	CCCCGGCAGATAGCGCGATC	20	1.311	MGG_16853T0	-2.825
Root	TCCGGTGCGCCCCCGGCGGC	20	1.396	MGG_17103T0	-2.843
Root	TGTCCGGTGCGCCCCCGGCGGC	22	1.526	MGG_17103T0	-2.843
Root	TCCGGTGCGCCCCCGGCGGCC	21	1.133	MGG_11634T0	-3.008
Root	TCCGGTGCGCCCCCGGCGGC	20	1.396	MGG_11634T0	-3.008
Root	GGCCACCCGGTCGAGGGCAC	20	1.973	MGG_11634T0	-3.008
Root	CCCCGGTGGCCGTCGTTGGC	20	2.396	MGG_11634T0	-3.008
Root	TCCGGTGCGCCCCCGGCGGC	20	1.396	MGG_01149T0	-3.047
Root	TGTCCGGTGCGCCCCCGGCGGC	22	1.526	MGG_01149T0	-3.047
Root	AGACGCCGGCGGGGGCCTCGG	21	1.408	MGG_08146T0	-3.051
Root	CGGCAACGGATATCTCGGCT	20	1.733	MGG_00620T0	-3.118
Root	CGCCGCCGCCGACGTCGCGA	20	1.064	MGG_16718T0	-3.125
Root	CAACGGCCTGCGGGCTCCCC	20	1.022	MGG_12396T0	-3.254
Root	GAAGTTAAGCGTGCTTGGGC	20	1.177	MGG_15818T0	-3.273
Root	GCCGGCCGGGGGACGGACCG	20	1.224	MGG_15818T0	-3.273
Root	TCGGATCGCGGCGACGGGGGC	21	1.033	MGG_02308T0	-3.511
Root	TTCGGATCGCGGCGACGGGGGC	22	1.521	MGG_02308T0	-3.511
Root	CGGATCGCGGCGACGGGGGCGG	22	1.635	MGG_02308T0	-3.511
Root	GTTCGGATCGCGGCGACGGGGG	22	1.818	MGG_02308T0	-3.511
Root	GTGTTCGGATCGCGGCGACGGG	22	2.033	MGG_02308T0	-3.511
Root	AGCTCGTAGTTGGACTTTGGGC	22	1.129	MGG_05110T0	-3.568
Root	AGACGCCGGCGGGGGCCTCGG	21	1.408	MGG_00625T0	-3.634
Root	TGCTTATAGGACTCCGCCGGC	21	2.506	MGG_05181T0	-3.649
Root	GAGCACGCCTGTCGGGACCC	20	1.021	MGG_05352T0	-3.722
Root	CGAAGTTAAGCGTGCTTGGGC	21	1.167	MGG_00679T0	-3.729
Root	GAAGTTAAGCGTGCTTGGGC	20	1.177	MGG_00679T0	-3.729
Root	CCGGTGGCCGTCGTTGGCAC	20	2.133	MGG_00679T0	-3.729
Root	CCGGAGACGCCGGCGGGGGC	20	1.082	MGG_02756T0	-3.762
Root	CCCCCGGTGGCCGTCGTTGGC	21	1.385	MGG_02756T0	-3.762
Root	CCCCGGTGGCCGTCGTTGGCA	21	1.613	MGG_02756T0	-3.762

Root	CCCCGGTGGCCGTCGTTGGC	20	2.396	MGG_02756T0	-3.762
Root	CCGCCGCCGACGTCGCGAGA	20	1.126	MGG_06966T0	-3.832
Root	CCGCCGCCGACGTCGCGAGA	20	1.126	MGG_06966T0	-3.832
Root	AGCCCCGTCCGGCCCGGACC	20	1.261	MGG_06966T0	-3.832
Root	TCCCTGCCCTTTGTACACACC	21	1.426	MGG_01191T0	-3.838
Root	CCCTGCCCTTTGTACACACC	20	2.260	MGG_01191T0	-3.838
Root	ATCATTGCAATTGTTGGTCT	20	1.727	MGG_09520T0	-3.909
Root	CGCCGCCGCCGACGTCGCGA	20	1.064	MGG_17983T0	-3.959
Root	CCGGTGCGCCCCCGGCGGCCC	21	1.097	MGG_11537T0	-3.986
Root	TCCGGTGCGCCCCCGGCGGCC	21	1.133	MGG_11537T0	-3.986
Root	CCGGTGCGCCCCCGGCGGCC	20	1.246	MGG_11537T0	-3.986
Root	TCCGGTGCGCCCCCGGCGGC	20	1.396	MGG_11537T0	-3.986
Root	TGTCCGGTGCGCCCCCGGCGGC	22	1.526	MGG_11537T0	-3.986
Root	ATCATTGCAATTGTTGGTCT	20	1.727	MGG_09492T0	-4.024
Root	CCTTCAGCCGGCGATGCGCTC	21	1.926	MGG_00177T0	-4.068
Root	GAGGCCACCCGGTCGAGGGC	20	1.711	MGG_14061T0	-4.204
Root	CTGGGCTCGGGGGTCCCGGC	20	2.800	MGG_14061T0	-4.204
Root	GTGTTCGGATCGCGGCGACGGG	22	2.033	MGG_08161T0	-4.587
Root	CTGGGCTCGGGGGTCCCGGC	20	2.800	MGG_00822T0	-4.752
Root	AGCCCCGTCCGGCCCGGACCC	21	1.050	MGG_08370T0	-4.774
Root	AGCCCCGTCCGGCCCGGACCCT	22	1.068	MGG_08370T0	-4.774
Root	AGCCCCGTCCGGCCCGGACC	20	1.261	MGG_08370T0	-4.774
Root	GCCCCGTCCGGCCCGGACCCT	21	1.306	MGG_08370T0	-4.774
Root	GCCCCGTCCGGCCCGGACCC	20	1.311	MGG_08370T0	-4.774
Root	CCCCGTCCGGCCCGGACCCT	20	1.677	MGG_08370T0	-4.774
Root	GACAGACTGAGAGCTCTTTC	20	2.416	MGG_04787T0	-4.799
Root	CCGGAGACGCCGGCGGGGGC	20	1.082	MGG_02610T0	-4.974
Root	AGACGCCGGCGGGGGCCTCGGG	22	1.017	MGG_09355T0	-5.268
Root	ACGCCGGCGGGGGCCTCGGG	20	1.109	MGG_09355T0	-5.268
Root	AGCTCGTAGTTGGACTTTGGGC	22	1.129	MGG_09355T0	-5.268
Root	AGACGCCGGCGGGGGCCTCGG	21	1.408	MGG_09355T0	-5.268
Root	GACCAAGGAGTCTGACATGCG	21	1.580	MGG_01906T0	-6.447
Root	ACCAAGGAGTCTGACATGCG	20	1.588	MGG_01906T0	-6.447
Root	GGACCAAGGAGTCTGACATGCG	22	1.835	MGG_01906T0	-6.447
Root	ACGGATATCTCGGCTCTCGC	20	1.127	MGG_05761T0	-6.621
Root	GCCGGCCGGGGGACGGACCGG	21	1.257	MGG_05761T0	-6.621